Final Technical Report:

Improved Die Casting Process to Preserve the Life of the Inserts
Award number: DE-FC36-04GO14230

Project Period: (January 2004 – June 2012)

David Schwam, PI
(216) 368-6499
dxs11@case.edu
Department of Materials Science and Engineering
10900 Euclid Ave.
Cleveland, OH 44106

Contributor:
Xuejun Zhu, Sr. Research Associate

September 30, 2012

Acknowledgement/Disclaimer

Disclaimer: Any opinions, findings, and conclusions or recommendations expressed in this material are those of the author and do not necessarily reflect the views of the Department of Energy.

Proprietary Data Notice: This report does not contain any proprietary data.

Document Availability: Reports are available free via the U.S. Department of Energy (DOE) Information Bridge Website: http://www.osti.gov/bridge

Reports are available to DOE employees, DOE contractors, Energy Technology Data Exchange (ETDE) representatives, and Informational Nuclear Information System (INIS) representatives from the following source:

> Office of Scientific and Technical Information
> P.O. Box 62
> Oak Ridge, TN 37831
> Tel: (865) 576-8401
> FAX: (865) 576-5728
> E-mail: reports@osti.gov
> Website: http://www.osti.gov/contract.html

Table of Contents

List of Figures

List of Tables

Executive Summary

The goal of this project was to study the combined effects of die design, proper internal cooling and efficient die lubricants on die life. The project targeted improvements in die casting insert life by:

- *__Optimized die design for reduced surface temperature__*. The life of die casting dies is significantly shorter when the die is exposed to elevated temperature for significant periods of time. Any die operated under conditions leading to surface temperature in excess of $1050^{o}F$ undergoes structural changes that reduce its strength. Optimized die design can improve die life significantly. This improvement can be accomplished by means of cooling lines, baffles and bubblers in the die. Use of one or more of these devices can maintain low die temperatures during processing and substantially improve die life in the process. The distance of the cooling lines from the surface is a critical variable. Presently, the industry is using an old "rule of thumb" stating cooling lines should not be drilled closer than ¾" from the surface. Cooling line drilled closer to the surface would presumably cause cracking of the die due to excessive thermal gradients and thermal shock. This rule limits the extraction of the heat. Recent improvements in the quality of H13 and new, tougher die steels i.e. Uddeholm Dievar, Thyrotherm E38K and Ellwood ExELL Tuf-Die should allow drilling cooling lines closer to the surface, thus providing more effective cooling. A key objective of the project was to establish criteria for the minimal distance of the cooling lines from the surface. This effort was supported with alloys and machining by BohlerUddeholm, Dunn Steel, HH Stark and Rex Buckeye. In plant testing and evaluation was conducted as in-kind cost share at St. Clair Die Casting. The Uddeholm Dievar steel evaluated in this program showed superior resistance to thermal fatigue resistance. Based on the experimental evidence, cooling lines could be placed as close as 0.5" from the surface.

- *__Die life extension by optimized die lubrication.__* The life of die casting dies is affected by additions made to its surface with the proper lubricants. These lubricants will protect the surface from the considerable temperature peaks that occur when the molten melt enters the die. Dies will reach a significantly higher temperature without this lubricant being applied. The amount and type of the lubricant are critical variables in the die casting process. However, these lubricants must not corrode the die surface. This effort was supported with alloys and machining by BohlerUddeholm, Dunn Steel, HH Stark and Rex Buckeye. In plant testing and evaluation was conducted as in-kind cost share at St. Clair Die Casting. Chem-Trend participated in the program with die lubricants and technical support. Experiments conducted with these lubricants demonstrated good protection of the substrate steel. Graphite and boron nitride used as benchmarks are capable of completely eliminating soldering and washout. However, because of cost and environmental considerations these materials are not widely used in industry. The best water-based die lubricants evaluated in this program were capable of providing similar protection from soldering and washout.

In addition to improved part quality and higher production rates, improving die casting processes to preserve the life of the inserts will result in energy savings and a reduction in environmental wastes. Improving die life by means of optimized cooling line placement, baffles and bubblers in the die will allow for reduced die temperatures during processing, saving energy associated with production. The utilization of optimized die lubricants will also reduce heat requirements in addition to reducing waste associated with soldering and washout. This new technology was predicted to result in an average energy savings of 1.1 trillion BTU's/year over a 10 year period.

Current (2012) annual energy saving estimates, based on commercial introduction in 2010, a market penetration of 70% by 2020 is 1.26 trillion BTU's/year. Along with these energy savings, reduction of scrap and improvement in casting yield will result in a reduction of the environmental emissions associated with the melting and pouring of the metal which will be saved as a result of this technology. The average annual estimate of CO_2 reduction per year through 2020 is 0.025 Million Metric Tons of Carbon Equivalent (MM TCE).

1. Introduction and Background

Die casting is a process of choice for numerous components used in many manufacturing industries - automotive, hardware, electrical and electronics, computers and many others. It produces aluminum, zinc and magnesium alloy components with satisfactory properties at competitive prices. The main advantages of die casting are [1,2]:

- Die casting is able to provide complex shapes within close tolerances;
- High rates of production with little or no machining required;
- Die cast parts are durable, dimensionally stable, and have a good appearance;
- Die castings are monolithic; they combine many functions in one complex shaped part;

During the aluminum die casting process, some parts of the die are subjected to very severe conditions of temperature and stress. Generally, these are thin sections, cores, corners and slides surrounded by molten metal. In many of these cases the heat transfer is two-dimensional. Consequently, these sections of the die must absorb much more heat than the rest of the die. Often these are the sections that fail prematurely either by soldering or heat checking. A high production rate is always desirable since it has a major impact on profitability. Sometimes this consideration overrides die life concerns. Under these circumstances, it becomes critical to create conditions for rapid heat extraction from the surface, dissipation inside the material, or rapid heat transfer to a "heat conveyor" such as a cooling line. The application of the die lubricant becomes an important variable in the process. The design of the cooling lines, i.e. location, size and distance from the cavity are critical parameters. High heat diffusivity die materials can contribute to rapid transfer of the heat away from the casting. However, any material selected for these applications must withstand the harsh conditions of the die casting process without failing prematurely. A sound understanding of the failure causes of dies is important in design of the dies and the die casting process.

1.1. Die Failure Mechanism

The durability of materials in molten aluminum is a great concern in die casting, containment of liquid metals and semi-solid processing [3]. The main failure modes identified for aluminum die casting dies are physical erosion (wash-out), chemical attack (corrosion), gross-cracking (cleavage cracking) and thermal fatigue cracking (heat checking) [1,2,4,5]. Erosion occurs when there is a fast flow of molten metal relative to the surface of the die; it becomes more severe in the presence of hard particles (such as primary solid silicon in 390 alloys or SiC particles in metal matrix composites. Chemical corrosion refers to penetration and dissolution of materials by the melt as well as the formation of interphase layers, when relative motion between the solid materials and the melt is negligible [3]. Gross cracking is usually catastrophic and may result in complete cracking of the die. Cracking and fracture of die occurs when the die material is stressed beyond its fracture strength. This can occur even when the mechanical stress applied on the die is below the yield stress. It results from a combination of residual stresses, thermal and

mechanical stresses [6]. This type of failure is related to the inherent resistance of the die material to brittle fracture termed "fracture toughness".

1.2 Thermal Fatigue Failure in Die Casting Dies

The life of dies used at elevated temperatures is often determined by their thermal fatigue properties [7]. The fatigue failure produced by fluctuating thermal stresses is known as thermal fatigue. Thermal stresses occur when the expansion or contraction of a part as a result of a temperature change is restrained [8]. The constraint may be internal or external [9]. External constraints produce forces that act on a component that is alternately heated and cooled. Internal constraints may result from temperature gradients across the section (simply because heat is not able to flow quickly enough in response to the external changes), structural anisotropy and different coefficients of expansion in adjacent phases or grains [10]. Thermal fatigue resulting from the action of internal constraints can also be defined as thermal cycling damage.

Temperature gradients form as a result of heating and cooling of the surface during injecting the molten metal, ejection and the lubricant spraying stages of the die casting cycle [4, 11]. When molten aluminum is injected, the die surface heats up, creating a steep temperature gradient between the surface and the cooler underlying mass of the die. As a result, the surface wants to expand more than the interior. Because the interior is more massive, it prevents the surface layer from expanding. As a result of this internal restraint, the surface is placed under compression. As heat is conducted into the underlying layers, the surface temperature decreases rapidly. When the casting is ejected, the surface of the die cools down. The spray of die lubricant further decreases the surface temperature [12]. The surface cools faster than the interior, the compression stresses are relieved and tensile stresses may be created.

The temperature gradient and the coefficient of the thermal expansion of the material determine the magnitude of the surface stress. For the simple case of a bar with fixed end supports, the thermal stress generated by a temperature change ΔT is:

$$\sigma = \alpha E \Delta T \qquad (1\text{-}1)$$

where α is the linear thermal coefficient of expansion and E is the elastic modulus [8].

For a biaxial condition, the stress is given by:

$$\sigma = \alpha E \Delta T / (1-\nu) \qquad (1\text{-}2)$$

where ν is Poisson's ratio. The thermal stresses never fully develop because α, E, ν and the thermal conductivity all change with temperature [13].

The fatigue damage in metallic materials can be subdivided into the stages of crack initiation, subcritical crack propagation, and final unstable fracture [14]. Crack initiation usually occurs at stress concentration sites originating from component geometry, machining irregularities or surface imperfections [15]. During the compressive part of the cycle, the increase in temperature lowers the yield strength of material, and the compressive strain may become plastic when the substrate prevents deformation. During the tension part of the cycle, if the concentrated thermal stress is larger than the yield strength of the material, reversed plastic deformation may occur. After sufficient number of cycles, the localized plastic deformation will cause a fatigue crack. Once a crack has initiated, propagation occurs along a plane perpendicular to the maximum tensile stress. Fatigue cracks in steels can deviate noticeably from the expected plane of propagation when large prior austenite grain boundaries are present or when another crack is in

close proximity [15]. The influence of other cracks on crack propagation is explained by the interaction of the highly stressed regions at the tips of the cracks. When the crack tips are close enough, this interaction changes the general state of stress. This provides an attraction of cracks to each other until the cracks are joined by reversed crack branching or forking. When the side branches join, they produce the classical craze-cracking pattern [16]. Several opinions exist about the driving force for crack propagation. One opinion is that cracks widen and deepen by the wedging action of the molten metal or oxide that is forced into them in each shot [17]. Another is that crack propagation occurs only by the thermal fatigue mechanism. In this event, propagation has to occur during the cooling cycle, since that provides the tensile stress necessary for crack propagation. Once a fatigue crack is formed, it will continue to grow because of the stress concentration effect even when the tensile stress is low [18].

The damage caused by thermal cycling can be separated into stages [14]:

- crack initiation at the surface;
- crack linking at the surface;
- growing of small cracks in depth direction from the crack net;
- growing of the largest crack to the complete failure.

The generation and evolution of thermal stress have been explained based on the type of thermal transients that occur during the service of a die subjected to thermal shock-thermal fatigue [10]. Suppose a heavy section at low temperature is suddenly brought in contact with a hot molten metal. As explained before, the surface tends to expand against the remaining material and goes into compression, yielding along OQ (Figure 1). Because of the heat transfer towards the core, the temperature gradient decreases and the system expands, taking the surface into tension at R. The residual tension is responsible for intergranular cracking. When the material is further subjected to rapid cooling this series of events is reversed. The surface now goes into tension, as it tends to contract, with a tension peak at point S that promotes transgranular cracking since the corresponding strain rate is high and the temperature decreases. Later, when the die cools, the yielded section at A goes into compression. The compression stress at P (at the original strain level) is not particularly damaging, but when many cycles are repeated, the system goes into a hysteresis loop at the surface (PQRS), leading to thermal fatigue cracking due to the reversed deformation.
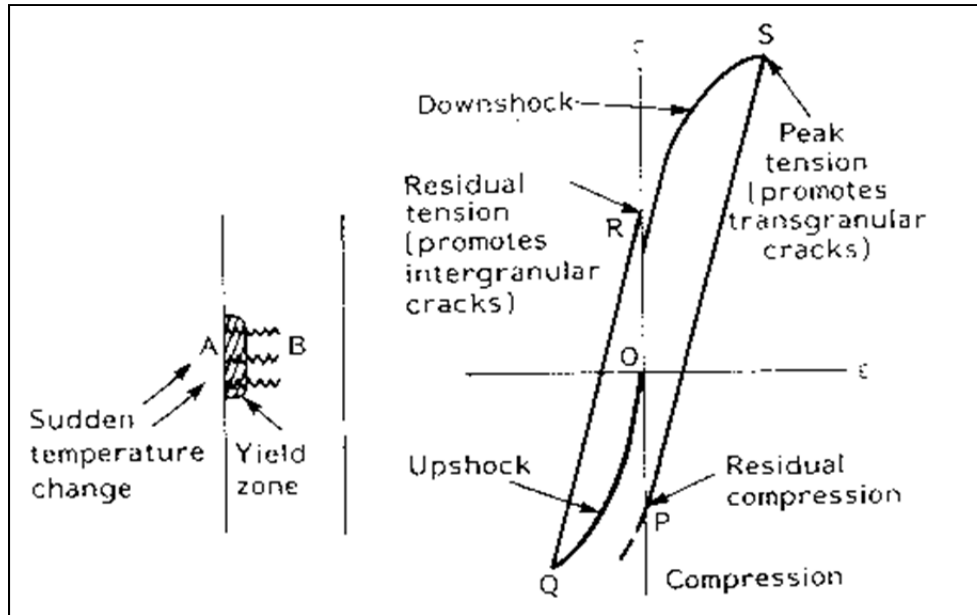
Figure 1 Hysteresis Loop at the Surface of a Material Subjected to Cyclic Heating and Cooling [10].

1.3 Thermal Shock and Thermal Fatigue Resistance - Materials Evaluation Criteria

A common measure of thermal shock resistance is the maximum sudden increase in the surface temperature that a material can sustain without cracking [19]. The thermal shock resistance and thermal fatigue resistance depend on a number of material properties. These include the thermal expansion coefficient α, thermal conductivity k, thermal diffusivity K, elastic modulus E, fracture toughness K_{Ic}, tensile (fracture) strength σ_f and upon the additional parameters of heat transfer coefficient h, specimen size and duration of thermal shock [4,19,20,21].

A commonly used thermal shock - thermal fatigue resistance parameter is the merit index of $R=\sigma_f/E\alpha$ or $R'=k\sigma_f/E\alpha$ [4,19,21]. For large values of Biot number ($\beta = bh/k$), i.e. large heat transfer coefficient h, radius or thickness r or b, respectively, and small thermal conductivity k, or when thermal strains are the result of the material being mechanically constrained, the thermal shock resistance is determined by R. For very small Biot numbers, i.e. small heat-transfer coefficients, small radius or thickness, and large conductivity, or when thermal strains are a consequence of thermal gradients resulting from rapid heating or cooling, the thermal shock resistance is determined by R'. If we consider the thermal fatigue as a series of repeated thermal shocks, these parameters can be used to describe the thermal fatigue resistance and for ranking of materials.

In this respect, the effect of elements incorporated into the chemistry of an alloy should be considered based on their contribution to [22]:

a) Thermal properties of the material: coefficient of thermal expansion, specific heat, and thermal conductivity

b) Material strengthening through carbide formation, solid solution strengthening with consequent increase in the capacity for withstanding repeated strains and with improved creep performance.

c) Microstructural stability and oxidation resistance.

11

1.3.1 Thermal Conductivity

The thermal conductivity is the quantity of heat transmitted, due to unit temperature gradient, in unit time under steady conditions in the direction of the temperature gradient. This condition occurs when the heat transfer is dependent only on the temperature gradient [23]. Under the conditions described above, higher thermal conductivity will reduce thermal fatigue by establishing a lower thermal gradient between the surface and the underlying layer. Equations (1-1) and (1-2) indicate that a lower temperature gradient will decrease the stress in the material. The successful use of molybdenum inserts in pressure die casting dies results to a large extent from the high value of the thermal conductivity. However, because of its variation with temperature, the influence of this parameter may diminish under operating conditions. For instance, ferritic steels have generally higher values of thermal conductivity than austenitic steels, but at high temperature, say at $1073^{o}K$, their thermal conductivities become similar [22].

1.3.2. Thermal Expansion Coefficient

The coefficient of linear thermal expansion is the ratio of the change in length per degree K to the length at 273 K. The coefficient of volume expansion is about three times the linear coefficient. The combination of the temperature gradient and the coefficient of thermal expansion determines the magnitude of strain, as shown by equation (1-3). The expansion in the axial direction of an element subjected to a temperature T_x will be, according to Duhamel's analogy [20]:

$$\varepsilon = \alpha T_x \qquad (1-3)$$

and the compressive stress induced by bringing the element back to its initial dimension, will be:

$$\sigma = -E\alpha T_x \qquad (1-4).$$

Among metals, refractory metals have the lowest thermal expansion coefficients [22]. Consequently, refractory alloys have superior resistance to thermal fatigue.

1.3.3. Elastic Modulus and Strength

The elastic modulus is a measure of the stiffness of the material. It is defined as the ratio of the stress and strain in the elastic deformation range:

$$E = \sigma/\varepsilon \qquad (1-5)$$

For a given strain, a lower modulus results in lower stress. Some metallic, but especially structural ceramic materials are susceptible to failure when thermally shocked due to a high Young's modulus, combined with relatively high thermal expansion coefficient, low strength and low thermal conductivity [22].

In general, a material with a low Young's modulus and a high value of yield strength is desirable, as the elastic component of the strain is large and the plastic component is small during a typical thermal cycle. The best combination of properties is a high strength-high ductility (high toughness) material. Unfortunately high strength is often associated with a low value of ductility.

A very important issue related to thermal fatigue resistance of materials is the hot hardness and the variation of strength with temperature. At high temperatures, the surface loses strength and hardness, especially in steels. This fact will lower the thermal fatigue resistance. The parameters R and R' will therefore not change their values much with temperature because of variation in

Eα, which is roughly constant with temperature [10]. The change is primarily due to the drop in strength at higher temperature that cannot be compensated by the rise in thermal conductivity.

1.3.4. The Effect of Thermal Cycling on the Microstructure

The prolonged exposure to elevated, cyclic temperatures and thermal stresses can cause marked changes in the microstructure [22]. These changes in the metallurgical structure contribute to failure by reducing the strength and are referred to as microstructural instabilities. Sources of instabilities include transgranular-intergranular fracture transition, recrystallization, aging or overaging, phase precipitation decomposition and coarsening of carbides. Borides or nitrides, intermetallic phase precipitation, delayed transformation to equilibrium phase, order-disorder transition, general oxidation, intergranular corrosion, stress-corrosion cracking, slag-enhanced corrosion, and contamination by some trace elements may also cause microstructural instabilities [5].

1.4. Soldering and Washout damage

Washout involves removal of die material by the impinging jet of an incoming molten metal stream. Washout in aluminum die-casting dies is accompanied by corrosive wear, erosive wear and soldering. Excessive washout results in the damage of the die surface and finally leads to the failure of the die. Corrosive wear is defined as the dissolution of die material in the molten aluminum and the formation of intermetallic layers. Corrosion is caused by the following facts:

- Iron and most of the alloying elements in the die steel are more or less soluble in liquid aluminum.
- The high die temperatures may cause oxidation of the die surface.
- Intermetallic layers may form at die surface.

Erosive wear is defined as the gradual removal of material from the die with every liquid aluminum impingement. This takes place as a result of the motion of the aluminum melt, which can reach velocities within the range of 20 to 60 m/s in gate area. The main erosion mechanisms are:

- Liquid-impingement erosion that creates pits on the eroded sample surfaces.
- Cavitation, which is the result of the formation and collapse of bubbles (cavities) in a fluid due to local pressure fluctuations.
- Solid erosion, which is caused by the impact of solidified particles (primary Si particles, oxide particles and impurities or intermetallic particles) during filling.

Soldering is defined as the adhesion of the cast metal to the die or core surface. Chemical and mechanical reactions occur during the filling and solidification stage due to the affinity of the aluminum alloy and die substrate. The chemical reactions often result in the formation of intermetallic layers at the die substrate/aluminum alloy interface. Mechanical interlocking will also result in aluminum buildup on the die surface when the molten aluminum penetrates into cracks in die surface. The consequent buildup of the aluminum alloy that occurs at the interface is called soldering. Soldering will cause sticking problems when the casting is ejected and it can also give rise to adhesive wear when the casting is separated from the die.

Die materials for aluminum die-casting should be resistant to heat checking, resistance to washout and to soldering in a fast flow of molten aluminum. To resist heat checking, die materials should have a low coefficient of thermal expansion, high thermal conductivity, high

hot yield strength, good temper softening resistance, high creep strength, and adequate ductility. To resist the washout and soldering, die materials should have high hot hardness, good temper resistance, low solubility in molten aluminum and good oxidation resistance. It is difficult for one material to satisfy with all above requirements. In practice, H13 steel is the most popular material for aluminum die casting dies. The design of the dies, and the die casting process have to factor in the capabilities of the die material to withstand the demanding temperatures and thermal stresses. It is imperative that cooling lines are placed in an optimized manner to extract heat efficiently while not exceeding the allowable thermal stresses. Also, appropriate die lubricants need to be used to prevent soldering and washout.

1.5 Cooling of Die Inserts

In die casting applications, the highest temperature will occur in thin or overheated sections where the material capacity to absorb and transfer the heat from the surface is very different [23]. So, cores and slides should be water-cooled whenever possible [24]. Water is commonly used as the cooling medium. Often, water cooling needs to have access to localized die areas including long cores which are often "hot spot" areas. Typical water passage systems for these applications are termed "fountains", "cascades" or "bubblers", as shown in Figure 2 [25]. Bubblers are ideal for cooling die casting dies where drilled waterlines through the insert are not possible due to interface with ejector pins, core pins, pull-down inserts, etc.[26]. A flow of water is directed locally behind a core or die and its return is confined to an outer sleeve, the whole unit taking up little space and being conveniently threaded for use in assembly [25].

(a) Illustration of Bubblers   (b) Illustration of Baffles

Figure 2 Illustrations of Bubblers and Baffles

Brass plug baffles, as shown in Figure 2, provide another water passage system for these applications. They are available in both straight and spiral styles, constructed entirely of high quality brass with blades brazed to the plugs for long, dependable service. They provide a high pressure seal through a deliberate difference of taper between the plug and the tapped hole. The function of the baffle is to split the drilled waterline into two equal channels. As the heating or cooling medium enters, the baffle diverts the flow to travel up to and over the end of the baffle and down the other side. Spiral baffles improve cooling balance by creating turbulent action in the channel, reducing laminar or straight-layered flow patterns and providing efficient coolant movement. Clearance must be provided between the end of the baffle and the end of the drilled channel to provide adequate flow [26].

Recently a device known as a heat pipe has been introduced for very small cores. This is not as effective as a water circuit but does give some assistance to cooling. A sealed passage or inserted tube inside the core contains liquid under vacuum. The liquid vaporizes under heat at the impression end of the core and, after being condensed by a cooling system at the other end, recirculates via a capillary wick at high frequency circles [27].

1.6 Heat Transfer in Die Cooling System

1.6.1 Heat Transfer through Boundary Layer

When a fluid flows over a surface, a stagnant film adheres to the surface and acts as a heat insulator. Experiments have shown the actual existence of such a film. In the study of heat transfer it may be visualized as a barrier to the flow of heat. Heat is presumed to be conducted through this film, and its thickness has been found to be dependent upon its viscosity and density and upon the velocity of fluid stream [28]. Under steady state condition, the boundary layer heat transfer coefficient h is:

$$h = k/\delta \qquad (1-6)$$

where k is the thermal conductivity of the liquid in the boundary layer and δ is the boundary layer thickness. The boundary layer thickness varies approximately as the square root of the shear velocity of the liquid outside the boundary layer [29]. The circulation of fluids through channels in dies varies greatly in heat transfer characteristics. Velocity, volume, and turbulence are important factors in the rate of heat transfer. It has been found advisable to introduce devices to increase turbulence in some channels to increase the heat transfer rate. An increase in velocity of a stream causes the heat transfer rate to be improved. [30].

1.6.2 Brief Review of the Heat Transfer of Forced Convection

The transfer of heat to or from a fluid flowing over a surface of a hotter or colder body is by the process known as convection. When circulation is made positive by some mechanical means, such as a pump or fan, convection is termed forced convection. If the size and shape of the stream are expressed in terms of the diameter, the heat transfer coefficient of convention may be stated in equation form as [28]:

$$h = f(D, V, \mu, \rho, c_p, k) \qquad (1-7)$$

where h is the heat transfer coefficient of convection; D is the diameter of fluid stream; V is the velocity; μ is viscosity; ρ is density; c_p is the specific heat at constant pressure; k is thermal conductivity. By the method of dimensional analysis, for most practical applications, the equation form is well expressed by the equation:

$$\frac{hD}{k} = C\left(\frac{DV}{\nu}\right)^b \left(\frac{c_p\mu}{k}\right)^d \qquad (1-8)$$

The three fractions within the brackets are known as follows: $\dfrac{hD}{k}$ is Nusselt number (Nu), $\dfrac{DV}{\nu}$ is Reynolds number (Re), and $\dfrac{c_p\mu}{k}$ is Prandtl number (Pr). It has been concluded that a fair

correlation for the heating and cooling of various fluids in turbulent flow in horizontal circular tubes is shown by the equation:

$$Nu = 0.023 \, \mathrm{Re}^{0.8} \, \mathrm{Pr}^{0.4} \qquad (1\text{-}9)$$

This equation applies where the Reynolds number is within the range of 10,000 to 120,000, the Prandtl number is between 0.7 and 120.

Equation (1-9) can also be used to predict heat transfer for turbulent flow in noncircular smooth ducts, provided that the tube diameter D is replaced by equivalent diameter D_{eq} defined as:

$$D_{eq} = \frac{4 \times (\text{cross - sectional area for flow})}{\text{wetted perimeter}} \qquad (1\text{-}10)$$

1.6.3 Heat Transfer through Vapor Blanket

For an upward flow of a liquid in a vertical channel with heated walls, when the heat flux from the heating surfaces is increased above a certain value, the convective heat transfer is not strong enough to prevent the wall temperature from rising above the saturation temperature of the coolant. The elevated wall temperature superheats the liquid in contact with the wall and activates the nucleation sites, generating bubbles to producing incipience of boiling [29]. The heat transfer mechanism of a vapor-liquid mixture in which the critical heat flux has been exceeded can be classified as partial or stable film boiling. The difference between the two lies in the magnitude of the surface temperature [30]. The repetitive vapor blanketing occurs within the cooling line [31]. An insulating vapor film covers the surface through which the heat must pass. The heat transfer coefficient is orders of magnitude lower than in the corresponding region before the critical heat flux was exceeded, due mainly to the lower thermal conductivity of the vapor [32]. This implies that the thin, continuous, vapor sublayer governs the heat transfer process. The film boiling model indicates a special forced convection-induced change, where an increased coolant velocity and subcooling lead to a sudden decrease in the vapor film thickness. It can be seen that the predicted increase in heat flux, as caused by the increased coolant velocity and a sudden decrease in the predicted vapor film thickness, is present in the experimental data for film boiling [33]. Of critical importance is the velocity of the interface between the vapor and fluid, then the velocity would then be determined by the critical Reynolds number for the system under consideration. Unfortunately, the values of this quantity available in the literature show very wide variations so it is difficult to predict the velocity in these circumstances and experimental measurements are lacking [34].

1.6.4 Heat Transfer of Bayonet Tube

The bayonet tube has a similar configuration with the bubbler/core; therefore, the theoretical and experimental studies on the bayonet tube are helpful to understand heat transfer of a bubbler system in a core. The bayonet tube is a refluent heat exchanger commonly used in operations where the medium to be heated or cooled is either too large to be treated or is readily accessible from one side only. It consists of two concentric tubes, one end of the inner tube reaching close to the sealed end of the outer tube. The fluid entering through the open end of the inner tube is therefore constrained to return along the annulus between the two tubes [35]. For a case when the fluid (air) enters the central tube and returns through the annulus while hot gas is flowing on the outside, the temperature distribution of the tube wall and fluid without radiation heat transfer is shown in Figure 3 [36,37]. In another study, results have been obtained using three different

fluids: namely, air (Pr=0.7), water (Pr=2.61), and ethylene glycol (Pr=40.36). Figure 4 shows a Nusselt number comparison for air, water, and ethylene glycol at different mass flow rates. The heat transfer rate is clearly dependent on flow rate and shows a marked improvement with an increase in Reynolds number. Furthermore, the shape of the curve changes as Reynolds number increases. For ethylene glycol and water, the curve exhibits an inflexion point in the lower range of the transitional regime [35]. It should be noted that the heat transferred from the bottom of the outer tube is negligible in the research of bayonet tube heat exchanger.
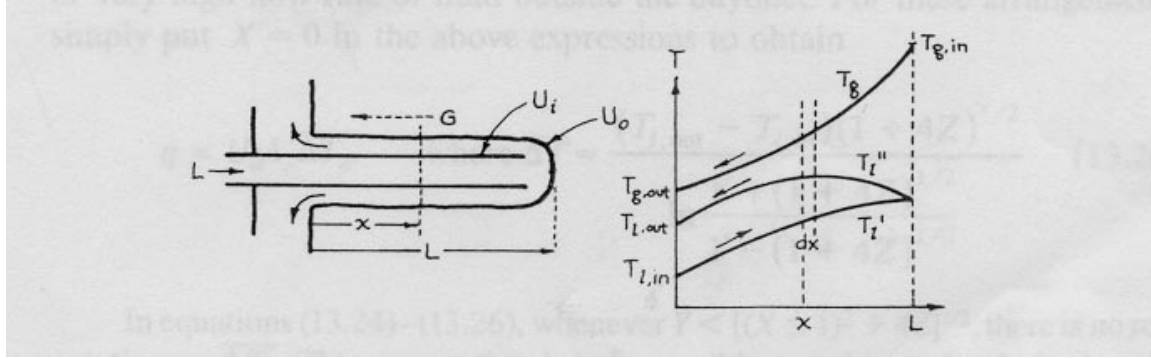
G: Hot Gas Flowing on the Outside; L: Length of Bayonet Tube $T_{l,in}$: Inlet Coolant Temperature [K]
$T_{l,out}$: Outlet Coolant Temperature [K] T_l': Temperature in the Inner Tube [K]
T_l'': Temperature in the Annulus [K] T_g: Temperature of Hot Gas Flowing on the Outside [K]

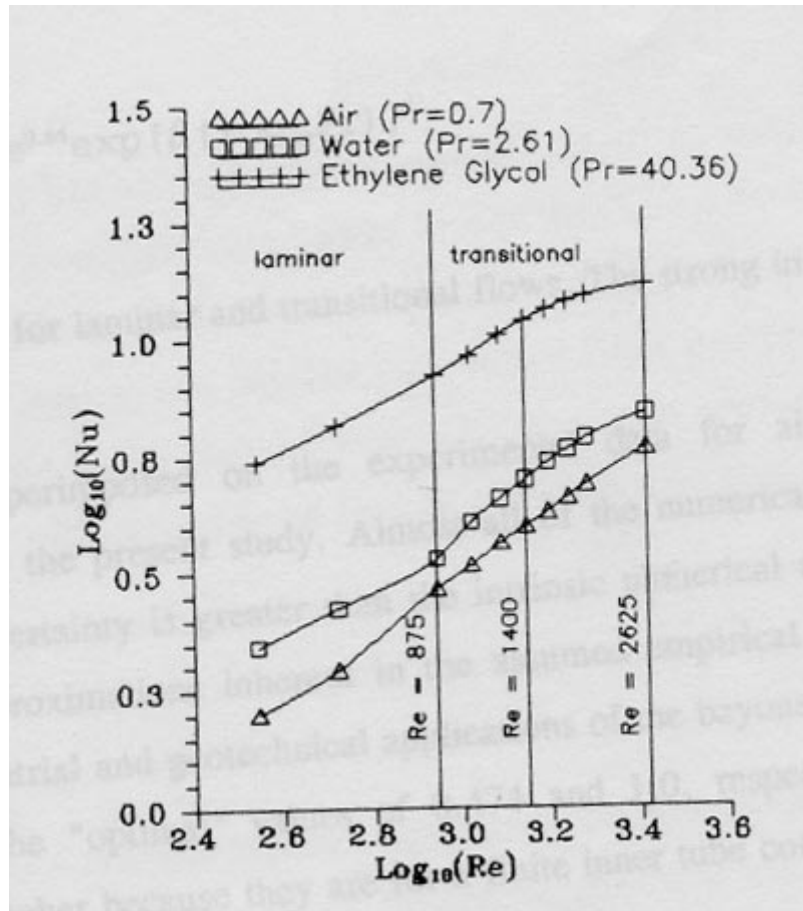**Figure 3 Temperature Distribution in the Bayonet Exchanger**

Figure 4 Effect of Reynolds Number on Nusselt Number for Bayonet Tube

17

1.6.5 Heat Transfer between Impinging Jet Flow and Objective

For forced convection heat transfer, a simplified form representing the heat transfer coefficient is usually used:

$$Nu = f \text{ (Re, Pr, generic shape)} \qquad (1\text{-}11)$$

where the functional relation is a power law, Nu is the Nusselt number, Re is the Reynolds number, and Pr is the coolant Prandtl number. In the case of a jet impinging on a surface (see Figure 5) the heat transfer coefficient, h, depends also on other parameters: normalized jet nozzle-to-plane spacing L/D; jet inclination angle, α_j; displacement of the stagnation point from the geometric center of the jet on the impingement surface, E; normalized distance from the stagnation point to a point considered on the impingement surface, r/D; jet Renolds number Re_j; and the jet velocity at the exit plane of the nozzle. Considering water as coolant, a correlation equation was proposed for the local Nusselt number in the form:

$$Nu = 1.122 A \cdot Pr^{\frac{1}{3}} \cdot Re^{0.7} \cdot \exp\left[-\left(B + C \cos\phi \right)\left(r/D \right)^m \right] \qquad (1\text{-}12)$$

where D is the diameter of the jet nozzle, and r and ϕ are cylindrical coordinates for correlation of contours of constant Nu. For two-dimensional problems, r is the distance from the stagnation point on the cooled surface, whilst ϕ is determined according to:

$$0, \text{ along the side of surface with } \alpha_j < \pi/2$$

$$\pi, \text{ along the side of surface with } \alpha_j > \pi/2 \qquad (1\text{-}13)$$

The coefficients of the relationship, A, B, C are determined by α_j and L/D [35].
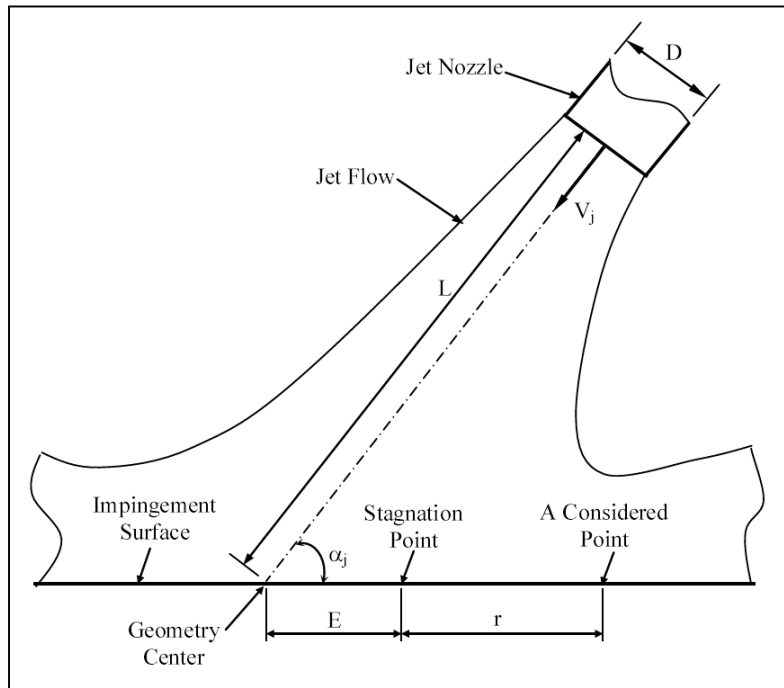

Figure 5 Jet Flow Impinging on a Flat Surface (Schematically)

1.6.6 Flow Pattern in Bayonet Tube

See Figure 6 as the reference to the structure of the tip of a bayonet. A vortex exists at the tip of the bayonet tube [36]. The flow field of the fluid at the tip of a bayonet tube is dependent on the geometry parameters as following:

(1) Relative height: h/D;

(2) Ratio of section area: m ($m=F_w/F_n$, where F_w is the annulus section area and F_n is the inner section area of inner tube);

(3) Configuration factor: b/a.

The generation of the big scale vortex depends on the value of m [37]. When m has a higher value (e.g. smaller I.D. of inner tube), the eject flow of fluid impinges the bottom of the outer tube with a high velocity. There is a small-scaled vortex area exiting at the stagnant point under the tip of inner tube, see Figure 6. While m has a lower value (e.g. bigger I.D. of inner tube), when h/D is higher than a certain value, it is found that a big scaled vortex area existing, and sometimes the vortex rotates faster, sometimes slower. When the vortex rotates faster, the scale of the vortex becomes larger. In engineering application, it is recommended to select the bayonet tube with a relatively higher value of m [36].
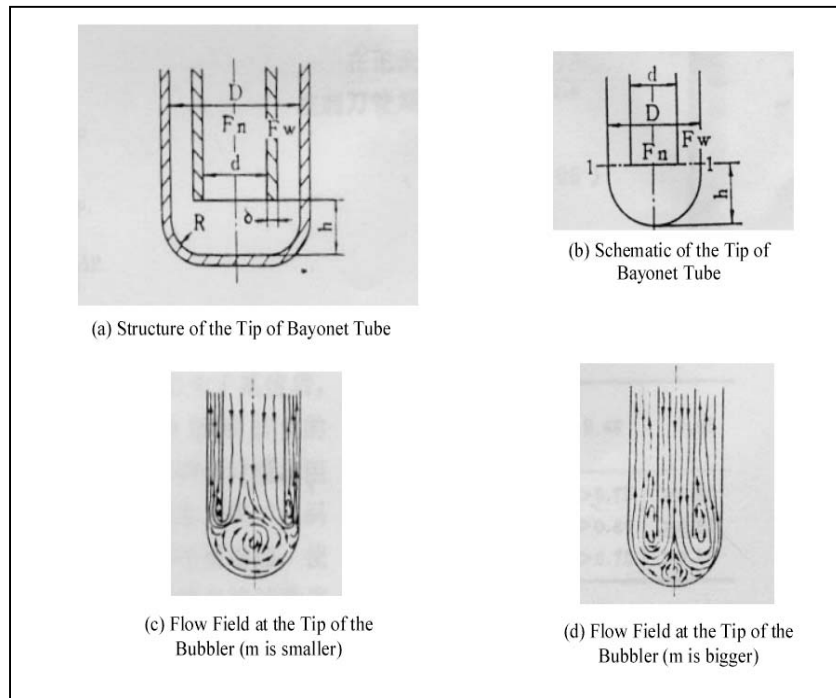

(a) Structure of the Tip of Bayonet Tube

(b) Schematic of the Tip of Bayonet Tube

(c) Flow Field at the Tip of the Bubbler (m is smaller)

(d) Flow Field at the Tip of the Bubbler (m is bigger)

Figure 6 Flow Field and Schematic of the Tip of Bayonet Tube

2. Experimental Procedures

2.1 Effect of Superheating to Die Steel: H13

2.1.1 Material

The material chosen for the work was the Premium Grade H13 steel, since it is the preferred die steel for the aluminum die casting industry. The following heat treatment procedure was chosen in order to obtain the strength and toughness combination required by the aluminum industry.

The original H13 steel bar (ϕ1"×20") was austenitized at 1875°F, oil-quenched, and then double tempered at 1130°F for 2 hours. Such a procedure with double tempering will tend to eliminate the residual austenite, and lead to a predominantly tempered martensitic structure with a hardness of 44-46 Rc, high strength and good toughness.

2.1.2 Specimen and Experimental Procedure

The oil-quenched and double tempered H13 steel bar was cut into short specimens for ϕ1"×0.5" each. In order to avoid the variation of microstructure during cutting, the steel bar was water cooled at the cutting region while the cutting was being operated. In order to reduce the thickness of decarburization layer, the specimens were wrapped in stainless steel foil and then were heated in a heat treatment. The furnace temperature rose up to the set temperature by approximately 50 ^{o}F per minute. After the holding time, the specimen was taken out of the furnace and air-cooled, and then ground and polished. The hardness was measured at the middle of the polished surface, and the distance between any two indentations is kept no less than 0.25". The polished specimens were etched with 4% Nital solution. A Hitachi-4500 Scanning Electron Microscope (SEM) was used to study the microstructure of the specimen.

2.2 Cooling Effect Evaluation Experiment in Air Furnace

2.2.1 Specimen

The material selected for the specimen was H13 steel, which is widely used for aluminum die-casting die inserts. The specimen design selected was a ϕ1.5"×10" cylinder, with water inlet, water outlet and a ϕ9/16" blind channel drilled for water-cooling. The detail of the design is shown in Figure 7. The specimen was designed as a cylinder for the purpose of simplifying the analysis of the heat transfer into the specimen, which as a result is a two-dimensional process. Since the surface temperature is a significant consideration in thermal fatigue testing, a small hole (ϕ0.075") was drilled for a thermocouple at the bottom of the specimen. The distance between the center line of the tiny hole and the bottom surface is 0.06". The temperature measured there was used as the criteria to evaluate the cooling efficiency of bubblers and baffles.
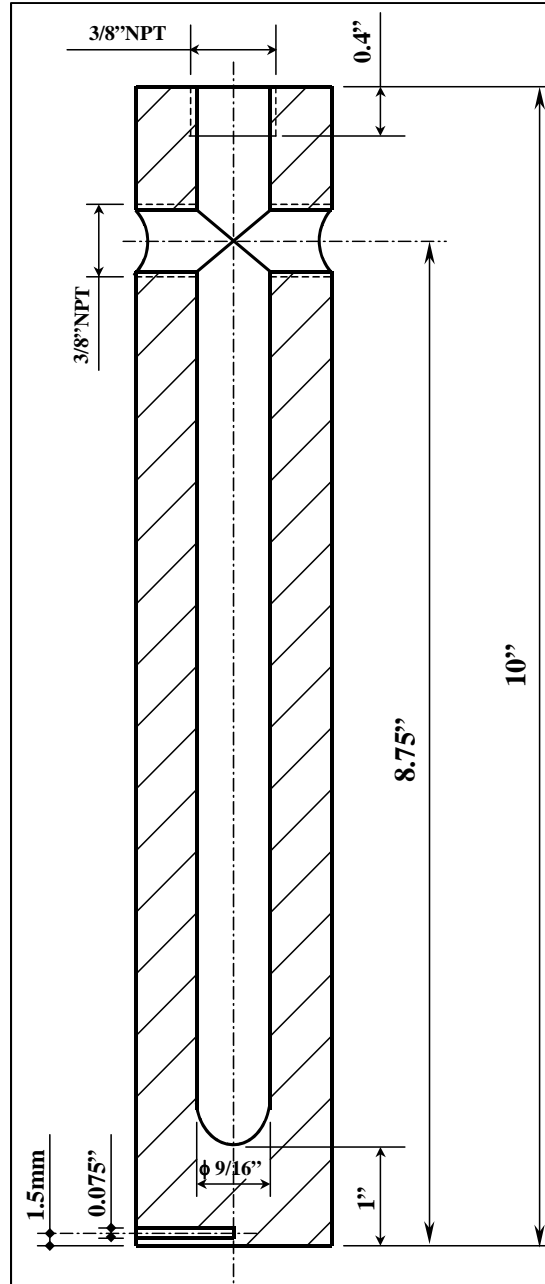
Figure 7 Specimen used in Air Furnace

2.2.2 Bubbler and Baffle

The commercially available bubblers and baffles, shown in Figure 8, were used in the experiment to represent different cooling methods currently used in die casting dies. The brass bubbler and baffle have the rigidity to maintain uniform spacing inside the water channel and are threaded into body for firm support. The inner diameters of the bubblers used in the experiment were 0.17", 0.214" and 0.307" respectively. The configuration and geometry details are shown in Figure 9.
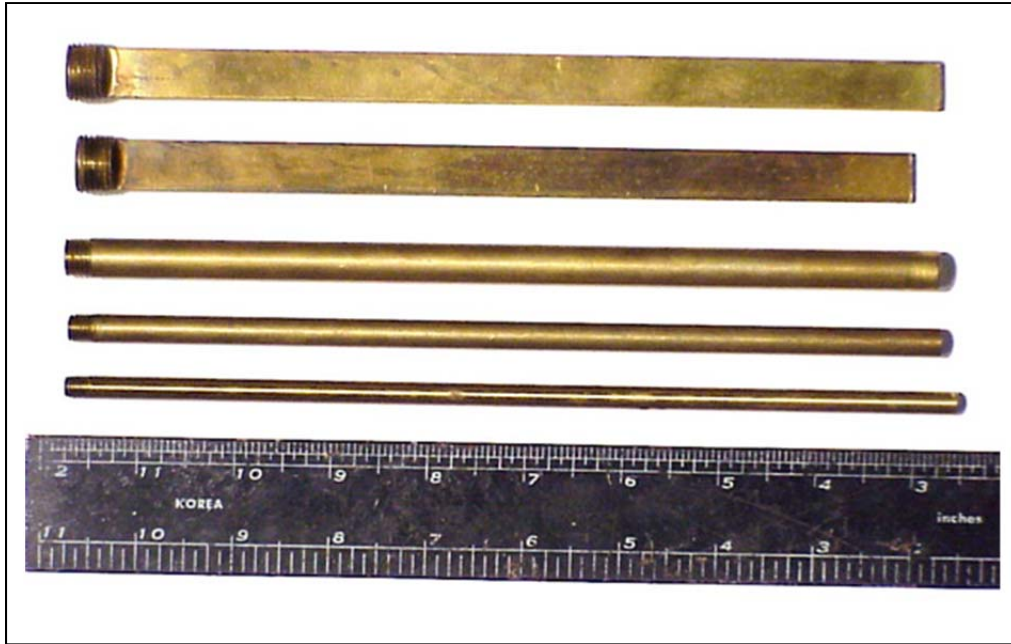
Figure 8 Bubblers and Baffles Used in Experiments
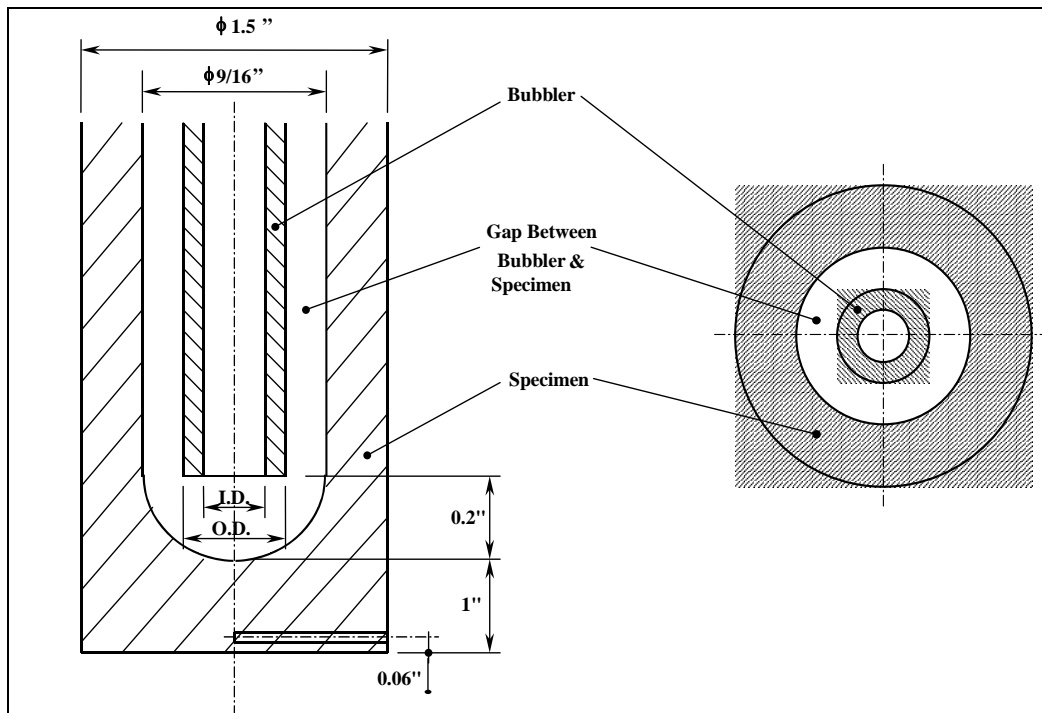
Figure 9 Configuration Details of Bubbler/Specimen

2.2.3 Air Furnace and Cooling Water

The furnace was cylindrical in shape, with a removable cover. A drilled hole in the cover allowed for the specimen insertion. Heating was performed by a resistance type heating element located in the sidewall. At normal working conditions, the furnace is capable of extended use at temperatures of up to 1200^oF /2192^oF. The controlling thermocouple was located 0.5" away from the inner wall of the chamber. The cooling water used in the experiment was untreated city water.

2.2.4 Experimental Procedure

During the experiment, the temperature of the furnace was kept at $950^{o}F/1742^{o}F$. The specimen was immersed and heated in the furnace. Meanwhile, the cooling water was going through the cooling line and being directed by bubbler or baffle in order to cool the specimen. The experimental rig is shown in Figure 10. For bubblers, at steady state, the specimen bottom temperatures at different cooling water flow rates were measured as the cooling efficiency evaluation criteria with respect to different inner diameters of bubblers. For baffles, at steady state, bottom temperatures of the specimen at different cooling water flow rates were measured as the cooling efficiency evaluation criteria with respect to different gap areas. The different gap areas were formed by cutting the tip of the baffle little by little, as shown in Figure 11.
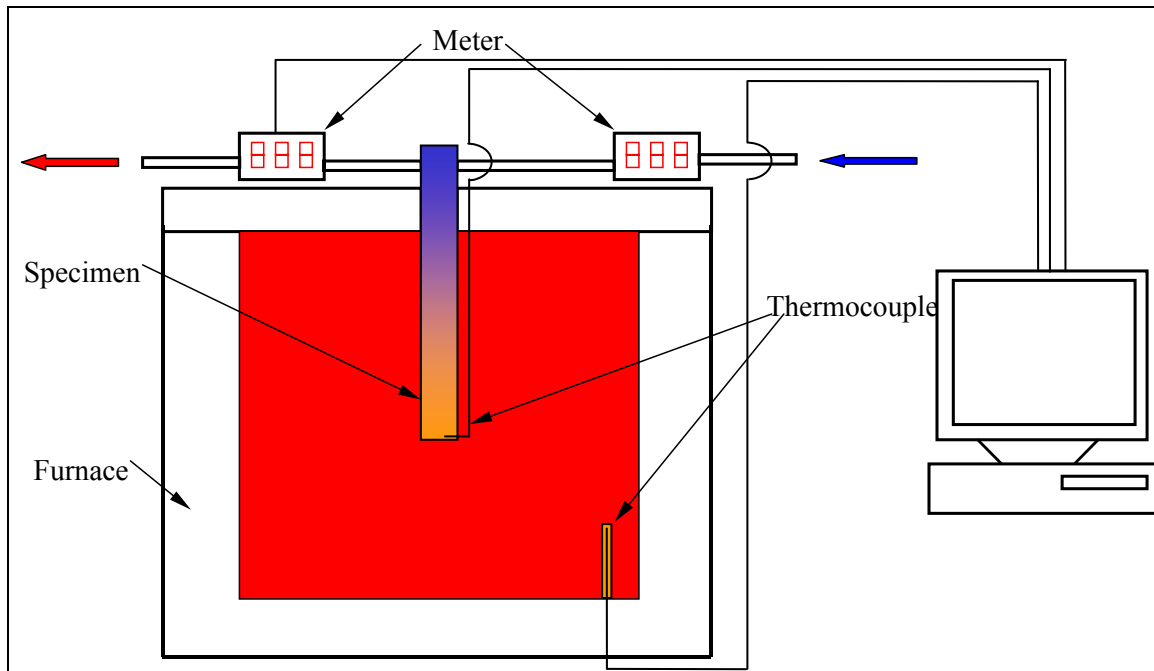
Figure 10 Schematic of Cooling Evaluation Experiment in Air Furnace
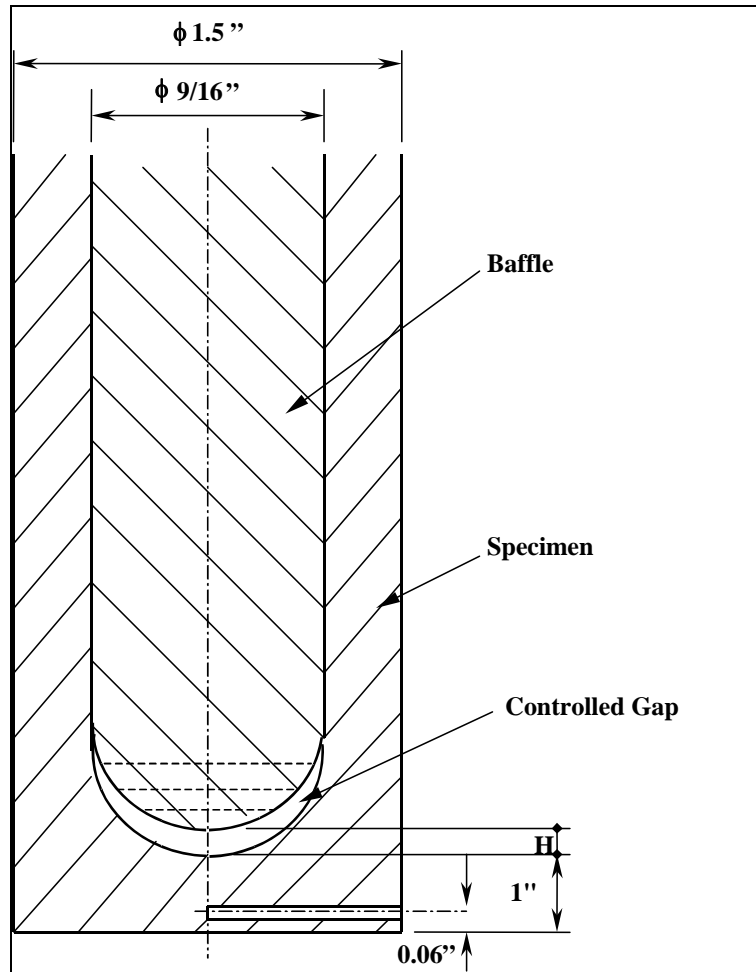
Figure 11 Illustration of Gap of Baffle/Specimen

The inlet cooling water temperature and the outlet cooling water temperature were measured at the same time. Then the temperature difference could be measured for different flow rates, which could be used to calculate the amount of heat that was extracted by the cooling water from the specimen. It should be noted that, at a given flow rate, the criterion for steady state was that the bottom thermocouple temperature and the outlet cooling water temperature were kept unchanged with respected to time.

2.3 Dip In/Out Experiment in Molten Aluminum

Although the cooling efficiency evaluation experiment run in the air furnace has some advantages, such as easy control, accurate temperature measurement and safe operation, the experiment conditions are far away from the working conditions in the die casting industry. The results from the experiment can only provide a general trend for heat transfer between cooling water and specimen, which are not directly applicable to the die casting industry. The reason is that the thermal shock and heat transfer in die casting dies are transient processes and the heat transfer coefficients of molten metal with dies are orders higher than those of air with specimens at natural convection.

To simulate the working conditions of die casting dies, it is preferable to use liquid aluminum instead of air as the heating medium in studying the heat transfer process. In order to simulate cyclic thermal shock that a die casting die suffers, the specimen was dipped and kept in the

molten aluminum (AL356, 732°F /1350°F) for a given time, then pulled out of the molten aluminum and kept in air for another given time. First, the specimen was tested without cooling water and the bottom temperature was measured as a reference at the quasi-steady-state. Then the cooling water flowed into the cooling line and was directed by bubbler or baffle to cool the specimen internally, while the specimen was dipped into and out of the molten aluminum. The cycle was repeated many times, and measurements were taken for the specimen bottom temperature at the quasi-steady-state for a given flow rate of cooling water. This procedure was repeated for different flow rates. The schematic of the experiment rig is shown in Figure 12. The cycle time was 50 seconds, with 25 seconds in the molten aluminum and 25 seconds in air for each cycle.
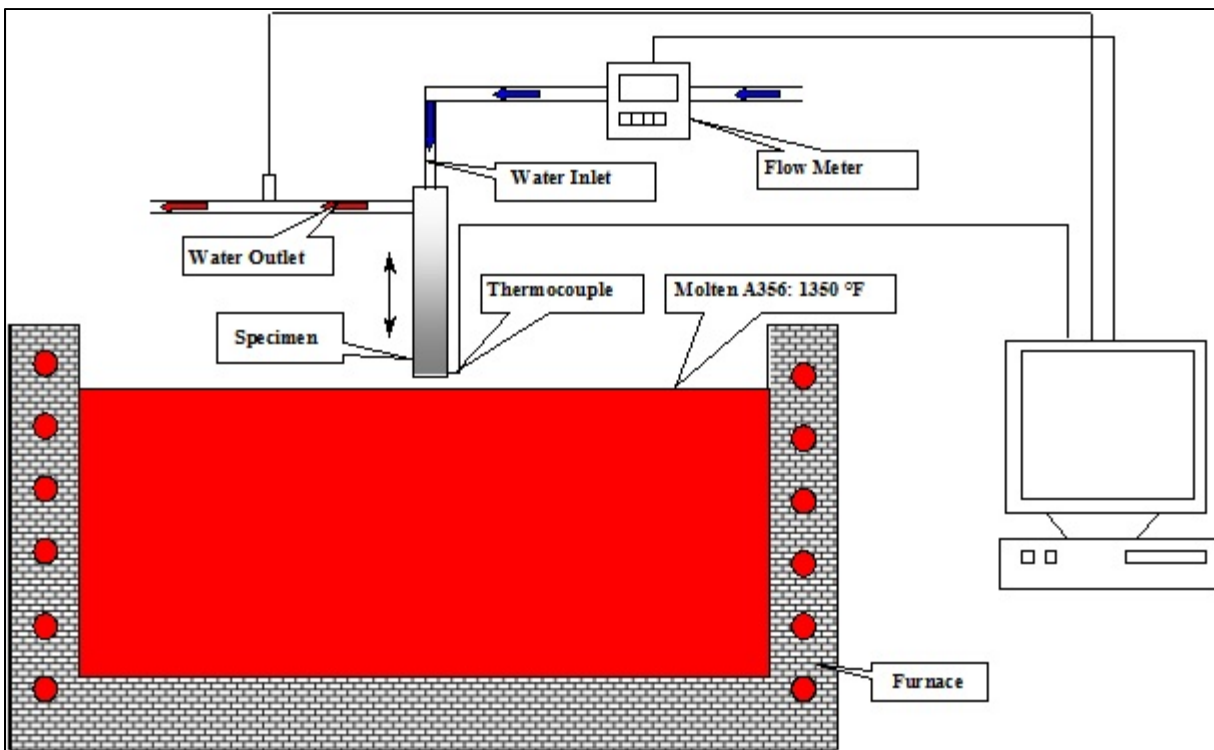
Figure 12 Schematic of Dip In/Out Experiment in Molten Aluminum

2.3.1 Dip In/Out Experiment for 1" Immersion Depth

The configuration details of the specimen used in the experiment are shown in Figure 13. The specimen material is H13 steel. It should be noted that the distance between the specimen bottom surface and the bottom of the water line is 3/8", instead of 1" like the specimen used in the air furnace.
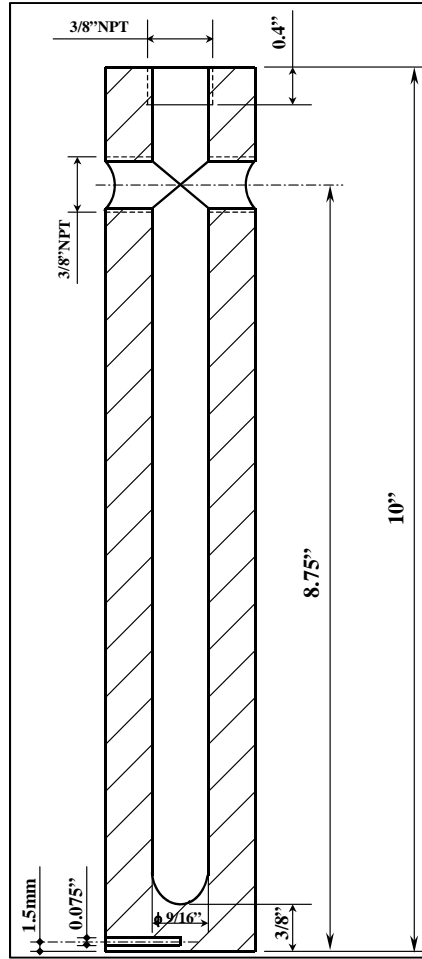
Figure 13 Specimen Used in Dip In/Out Experiment

The temperature measured from the bottom of the specimen shows a wavy relationship with respect to time, which reflects the periodic temperature variation of the die cavity surface. As it is valuable to show the highest temperature at which the die suffers from the thermal shock, the peak temperatures for each cycle at the quasi-steady-state were recorded. Then the mathematical average value of the peak temperatures, which is the criterion to evaluate the cooling effect, was calculated for each flow rate, as shown in Figure 14.
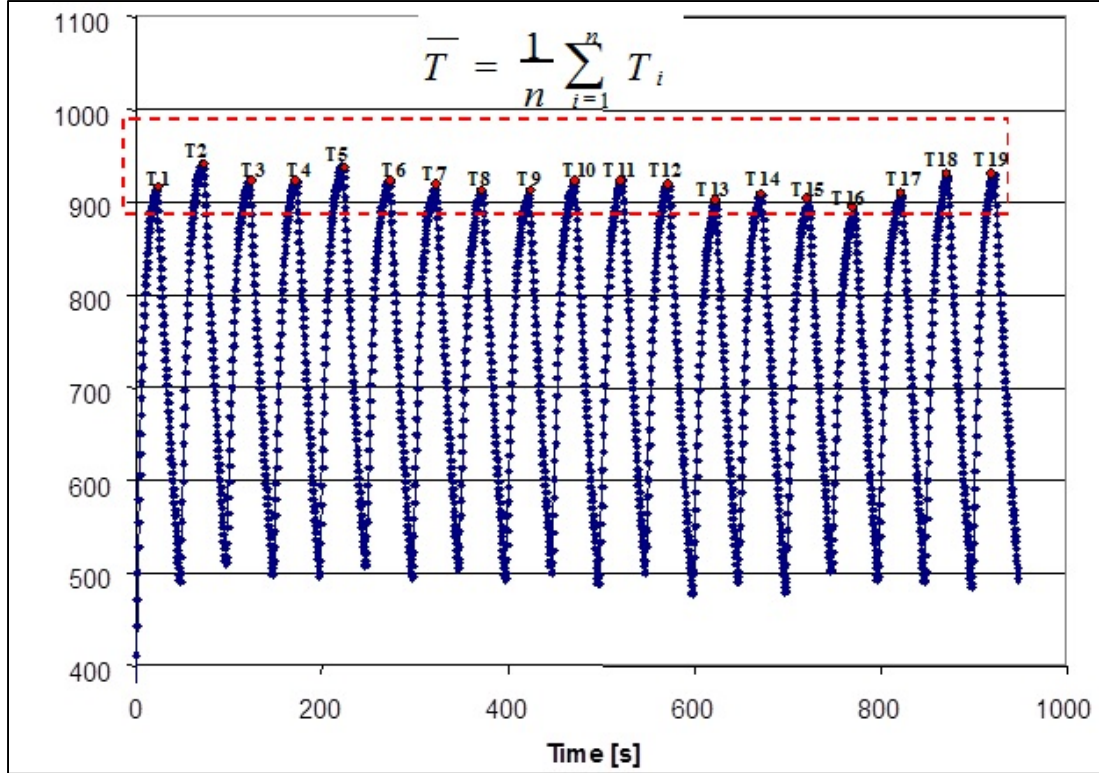
Figure 14 Typical Temperature Cycle and Mean Peak Temperature of Dip In/Out Experiment

2.3.2 Dip In/Out Experiment for 4.5" Immersion Depth

Die casting dies have different surfaces to be cooled, in addition to the "hot spot," due to different configurations and sizes of die castings. In order to evaluate the cooling effect of bubbler and baffle on a certain surface, the specimen was tested in the dip in/out experiment with an immersion depth of 4.5", while the bubbler (I.D.=0.17") or the baffle was used to cool the specimen internally. Temperatures were measured at three different points in the specimen. The two points used for measurement were located on the halfway of the sidewall where there was the cooling water inlet for the baffle. Experimental parameters and data processing methods were kept the same as those of the dip in/out experiments mentioned above, except that the immersion depth was 4.5" instead of 1".

3. Results and Discussion

3.1. Softening During Thermal Cycling and Thermal Fatigue Resistance

During the aluminum die casting process, some parts of the die are subjected to very severe conditions of temperature and consequently, stress. Generally, these are thin sections, fingers and corners, where the heat transfer is two-dimensional and the amount of energy that the material must absorb is much higher than the average for the rest of the die. Often these are the sections that fail first. It becomes critical to create conditions for rapid heat extraction from the surface, dissipation inside the material, or transfer towards a "heat conveyor" such as a cooling line.

The main mechanism and the most frequent manifestation of die failure is thermal fatigue cracking. It has been shown in previous investigations [15] that the strength is very important in controlling crack initiation. It is also known that the mechanical properties are directly related to the hardness of the material (Figure 15).
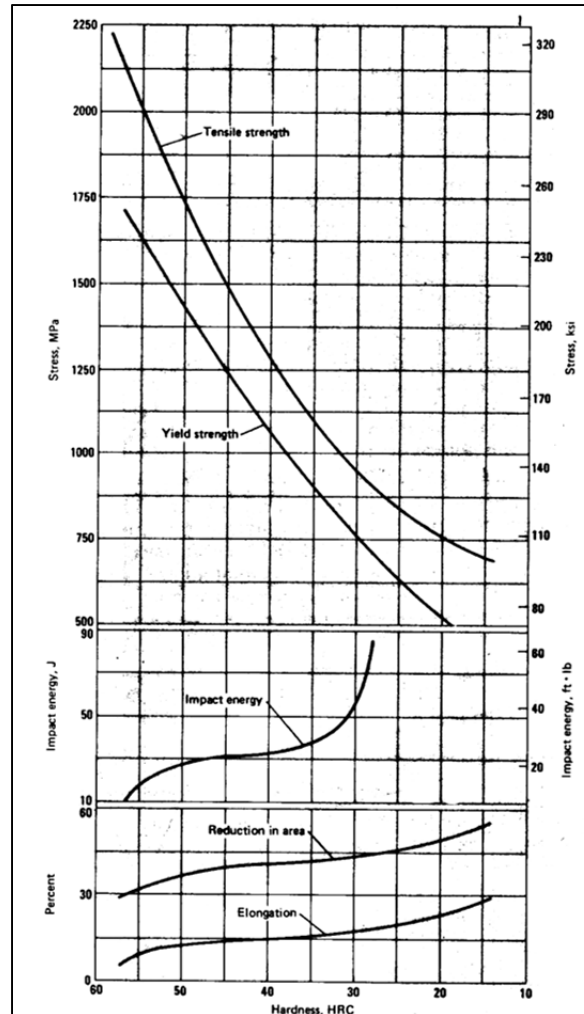
Figure 15 Relationship between Tensile Properties and Hardness for H13 Steel [45, Reprinted with permission of American Society of Materials]

The capability of a steel to preserve good mechanical properties during cycling at temperatures above the tempering temperature, is essential in establishing a satisfactory level of performance to be expected. This assertion leads directly to the interest in the phenomenon of softening during thermal cycling of die casting dies. This subject will be considered and analyzed in this work. Hot-work tool steels like H13 are used in quenched and tempered condition.

In this work, the extent of softening and the means to minimize it were evaluated. The effect of immersion time and diameter of the cooling line on the temperature and softening of the surface were studied. In both cases, there are differences regarding the heat supply and extraction to and from the surface. In the case of different immersion times, the amount of heat supplied to the surface of the specimen is limited by the time spent in contact with molten aluminum. The heat extraction capacity is determined by the size of the cooling line. If the immersion time is constant, a constant amount of heat is supplied to the surface. However, a larger cooling line diameter will enhance the capacity of heat extraction. In production, it is very difficult to control the time spent by the casting in the die. The cycle length is limited by solidification time, especially for large parts. Under these conditions, designing the die with cooling lines closer to the surface may be the only feasible solution. One must be cautious and consider the limits set by

28

the hoop stresses, which are increasing with the temperature gradient. Nevertheless, varying immersion time is very useful for the proposed study due to the ability to simulate extreme conditions that may occur during the die life.

3.1.1. The Influence of Immersion Time on Softening and Thermal Fatigue Cracking

The experiment involved testing of three specimens for which the immersion time in the molten aluminum was the only variable. The maximum and minimum temperatures reached at the corner and the temperature distribution inside the specimen (toward the cooling line) varied as a function of the time spent in the molten metal bath. Thermal fatigue behavior of the three specimens was compared with the reference 9 seconds immersion time specimen. The results are presented as the Total Crack Area and the Average Maximum Crack Length for each immersion time (Figure 16 and Figure 17). The hardness measured at the corner of the specimens after 15,000 cycles is shown in Figure 18.
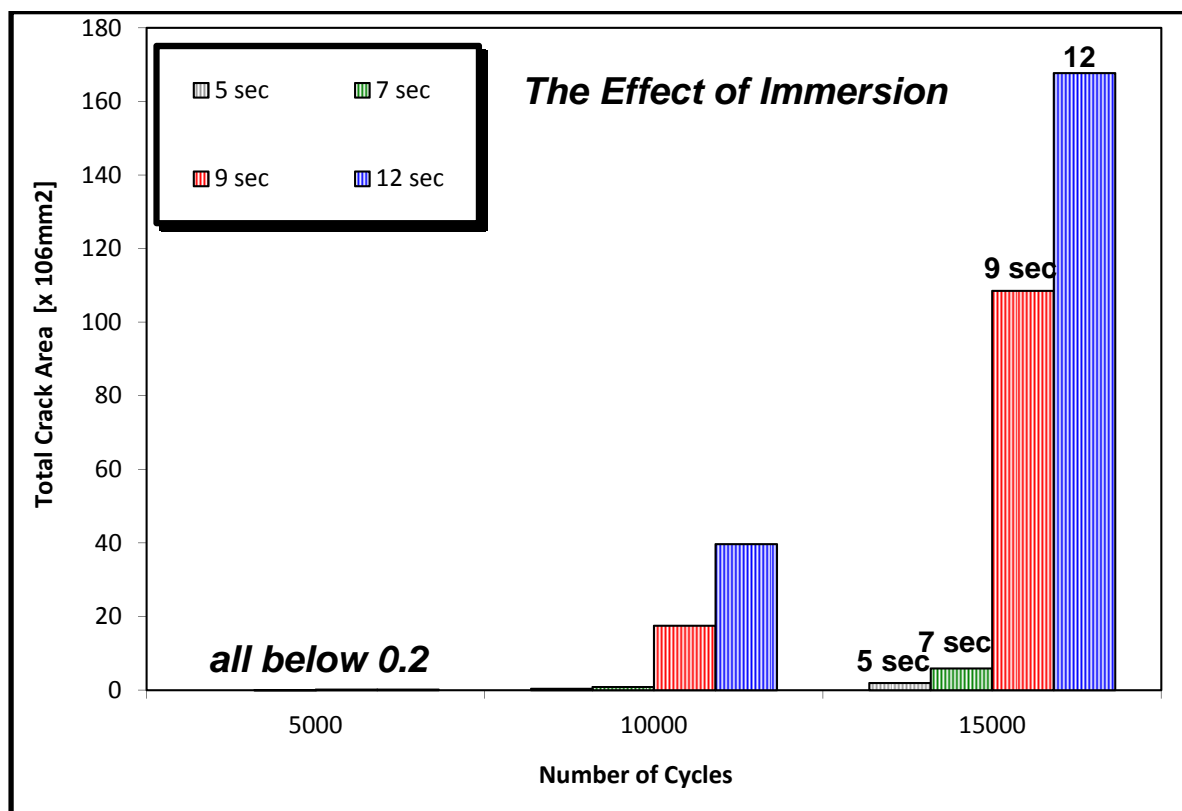
Figure 16 The Effect of Thermal Cycling on Crack Area - Different Immersion Times
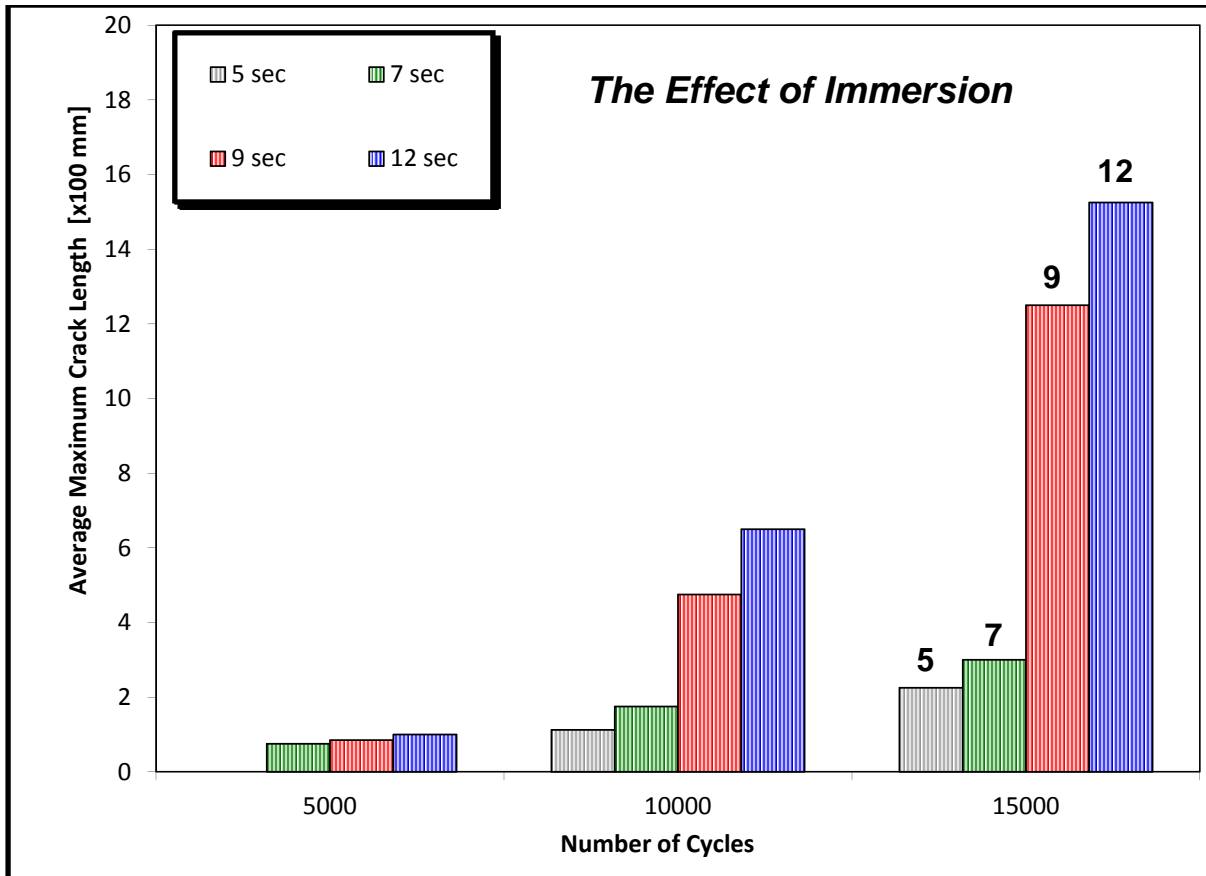
Figure 17 The Effect of Thermal Cycling on Crack Length - Different Immersion Times
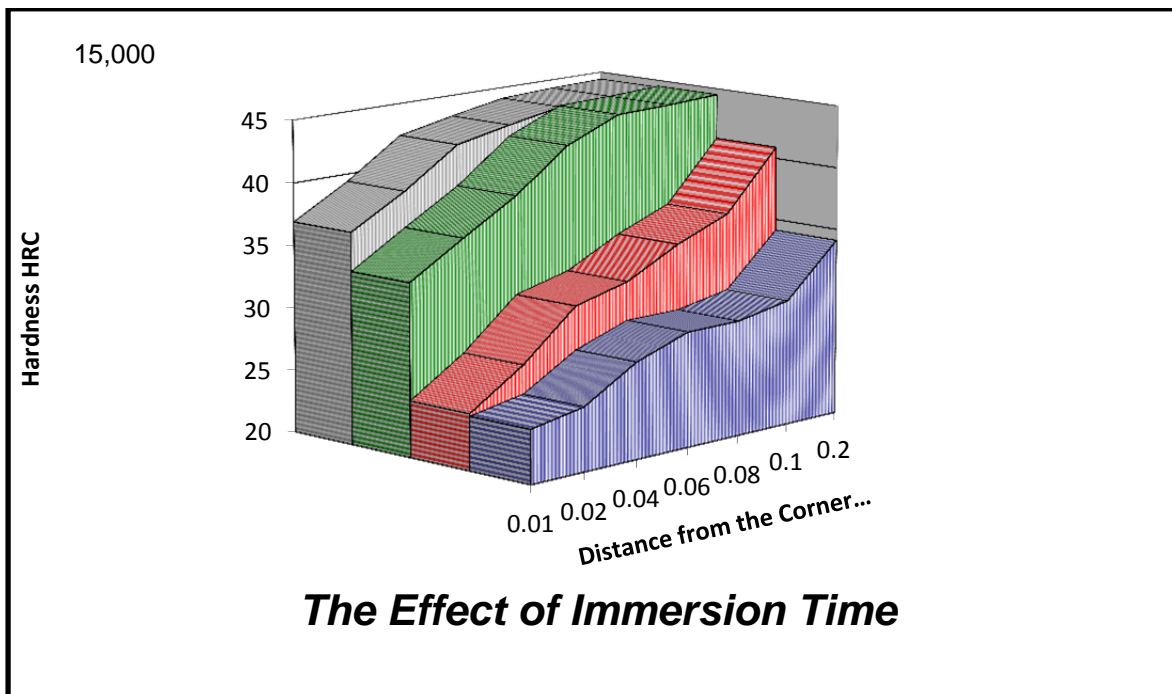
Figure 18 The Effect of Thermal Cycling on Microhardness Distribution Across the Surface - Different Immersion Times

There is a clear trend for the thermal fatigue cracking parameters (i.e. Total Crack Area and Average Maximum Crack Length) to increase with immersion time. This observation points at the main cause of thermal fatigue damage, which is the temperature variation during cycling. One of the direct effects of the temperature, in particular the maximum temperature reached at the corner, is the softening of the steel. The extent of softening during tempering is generally evaluated by a master parameter, known as Hollomon-Jaffe parameter. This value represents the combined effect of temperature and time. Since the temperature and time are interdependent variables in the thermally activated process of tempering, a trade-off of temperature for time or vice-versa is based upon a simple equation:

$$P = T(C + \log t) \times 10^{-3} \qquad (3\text{-}1)$$

where P is the Hollomon-Jaffe parameter
T is the absolute temperature [K]
t represents the time [hours]
C is a material constant

This equation yields a reasonably accurate prediction of hardness for carbon and alloy steels containing 0.2-0.85% carbon and less than 5% total alloying elements, irrespective of initial structure. It is not the scope of this work to investigate the hardness of steel as a function of temperature-time. The hypothesis is however that the temperature is the main factor that causes hardness loss. The dependency of thermal fatigue cracking on the level of hardness is investigated in detail.

The dependency of Total Crack Area and Maximum Crack Length on the maximum temperature at the corner of the specimen for different immersion times is presented in Figures 19 and 20. The results demonstrate that the higher the temperature, the more thermal fatigue damage will occur. As previously discussed, a higher temperature will produce a more severe and deeper softening of the surface and within the section of the specimen. Initially, the surface deformation (strain) is within the elastic capabilities of the die steel. The surface of the specimen has irregularities in the forms of corrosion pits or surface scratches. These sites serve as stress concentrations. Plastic deformation can therefore occur at stresses well below the yield strength of the parent material (it must be also noted that the strength of the material drops at high temperature, see Figure 21), and initiate fatigue cracks. In addition to the stress concentrations caused by surface imperfections, tempering weakens the surface material. A cumulative fatigue process occurs in the material, since plastic strain gradually increases during the test as a result of lower yield strength of the material. The compressive stress will eventually exceed the elastic limit of the steel and plastic deformation will take place after the initial elastic strain has occurred. Under these conditions, it is therefore necessary for the material to drop below of certain strength level characterized by a lower hardness value in order for the crack to initiate.
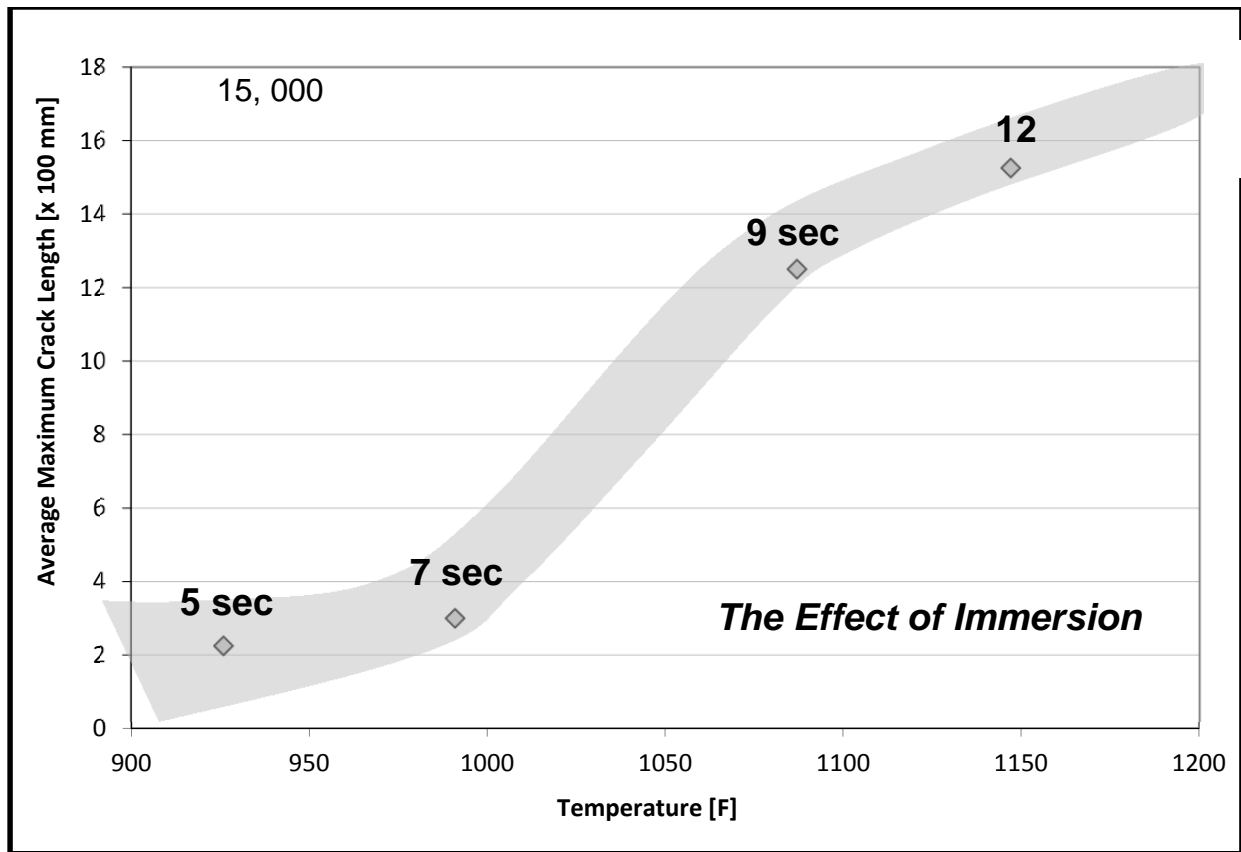
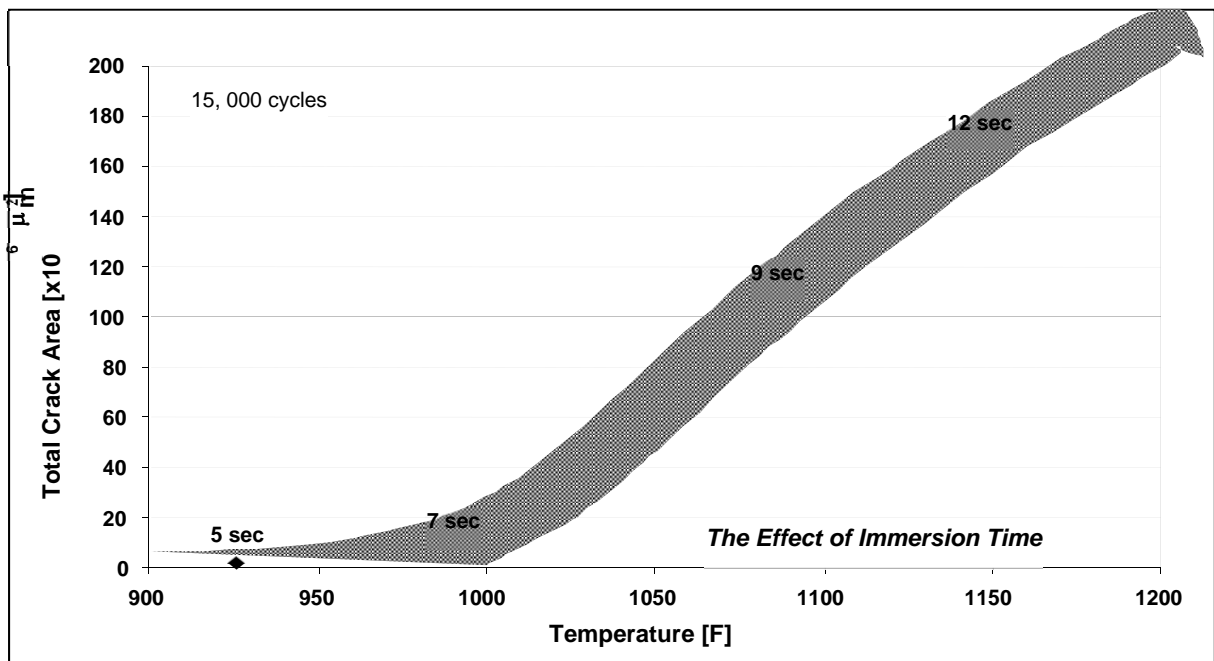**Figure 19 The Effect of Temperature on Crack Area**

Figure 20 The Effect of Temperature on Crack Length - Different Immersion Times
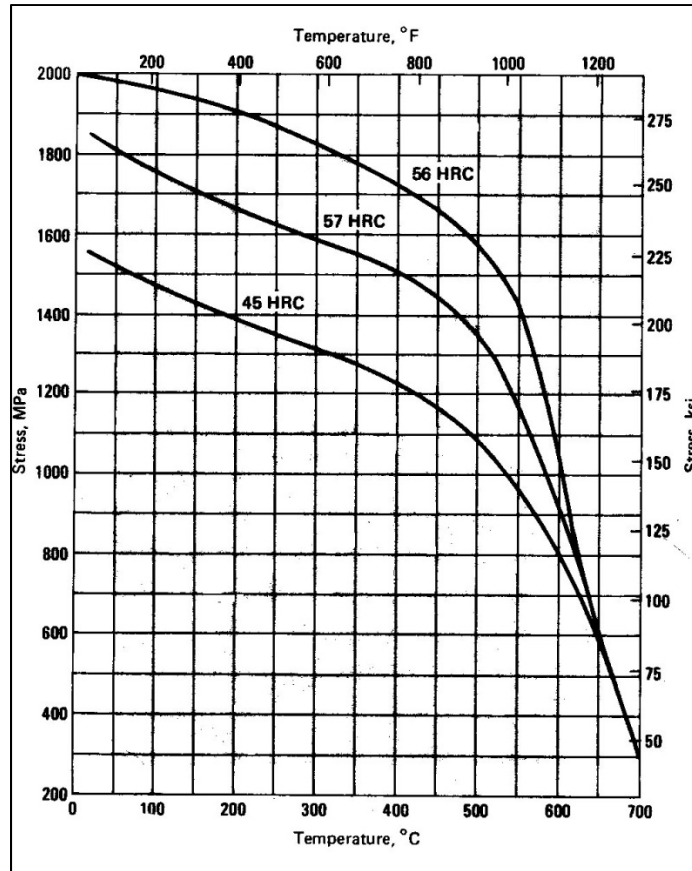
Figure 21 Effect of Elevated Temperature on Tensile Strength [45, Reprinted with permission of American Society of Materials]

It has been experimentally demonstrated that if the strength properties of the material are reclaimed before the cracks initiated, the thermal fatigue behavior can be markedly improved. The experiment consisted of cycling a H13 steel specimen for 2,500 cycles and then re-heat-treating it to the original hardness value. The results compared to regular 51 HRC and 46 HRC H13 specimens are presented in the Figure 22. It is clearly shown that the re-heat treated specimen to 51 HRC after every 2,500 cycles exhibited better resistance against heat checking. The cyclic heat treatment reclaimed the strength of the material and its resistance against cracking, impeding crack initiation, as well as the propagation of the existent cracks. Based on this evidence, it is believed that for a certain combination of temperature/stress the crack initiation will occur at a correspondent value of hardness. Therefore, it is expected that in a specimen subjected to a higher maximum temperature the hardness will drop faster. The higher drop in strength during immersion will thus cause cracks to initiate earlier. The cracks have then more time to grow, and the Average Maximum Crack Length will presumably be higher. The relationship between Average Maximum Crack Length and Total Crack Area is presented in Table 1 and Figure 23. Longer cracks correspond to a higher value of Total Crack Area. In addition, more cracks may initiate at the weakened surface, grow faster, and contribute to a higher Total Crack Area.
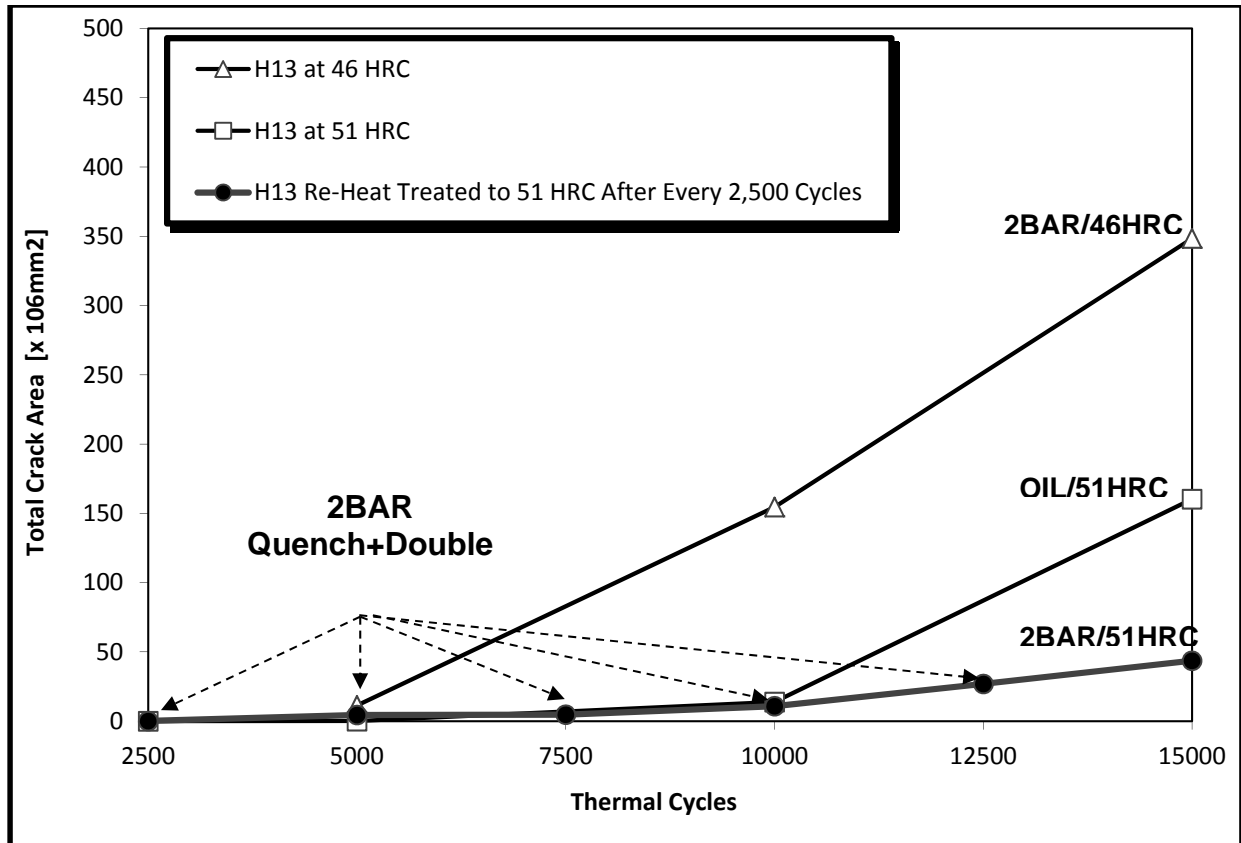
Figure 22 The Effect of Hardness Recovery on Thermal Fatigue Cracking

Table 1 Measurement Data For Different Immersion Times

Immersion Time	5 sec	7 sec	9 sec	12 sec
Maximum Temperature [F]	926	991	1087	1147
Minimum Temperature [F]	322	346	399	460
Total Crack Area [x 10^6 m^2] After 15,000 Cycles	1.97	5.9	108.56	167.72
Average Maximum Crack Length After 15,000 Cycles [x 100 m]	2.25	3	12.5	15.25
Hardness at the Average Maximum Crack Length [HRC] After 15,000 Cycles	36.9	33.8	31.6	29.2
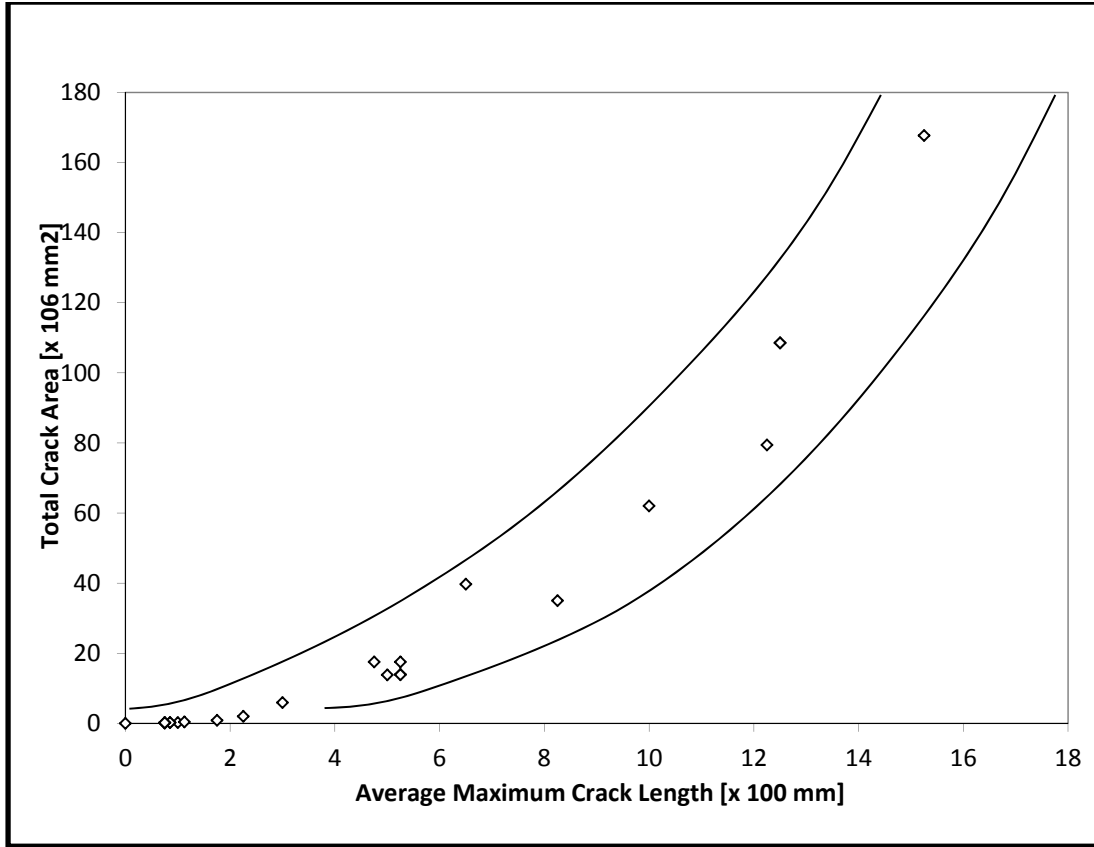
Figure 23 Relationship Between Total Crack Area and Average Maximum Crack Length

At the same time, the behavior of the propagating crack is influenced by the characteristics of the material at the crack tip, and hence by the ability to resist plastic deformation. A parameter was chosen, which could provide information about the properties ahead the crack tip/front, namely the microhardness at a distance equal to the Average Maximum Crack Length (Figure 24). It is asserted that this distance characterizes well the propagation of cracks inside the specimen. The dependency of this new parameter on the temperature measured at the corner is presented in Figure 25 and appears to have a linear trend. The relationship between the cracking parameters and the microhardness measured at the distance equal to the Average.
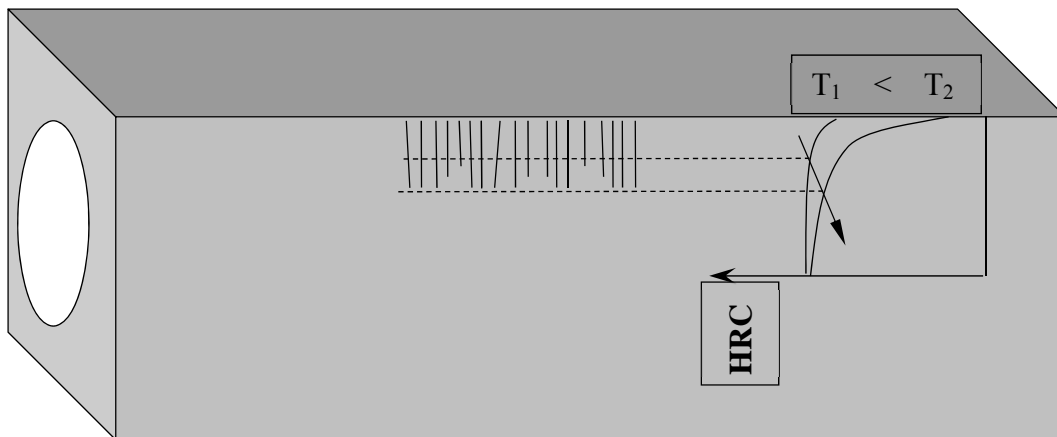
Figure 24 The Relationship Between Maximum Crack Length and Microhardness at Maximum Crack Length
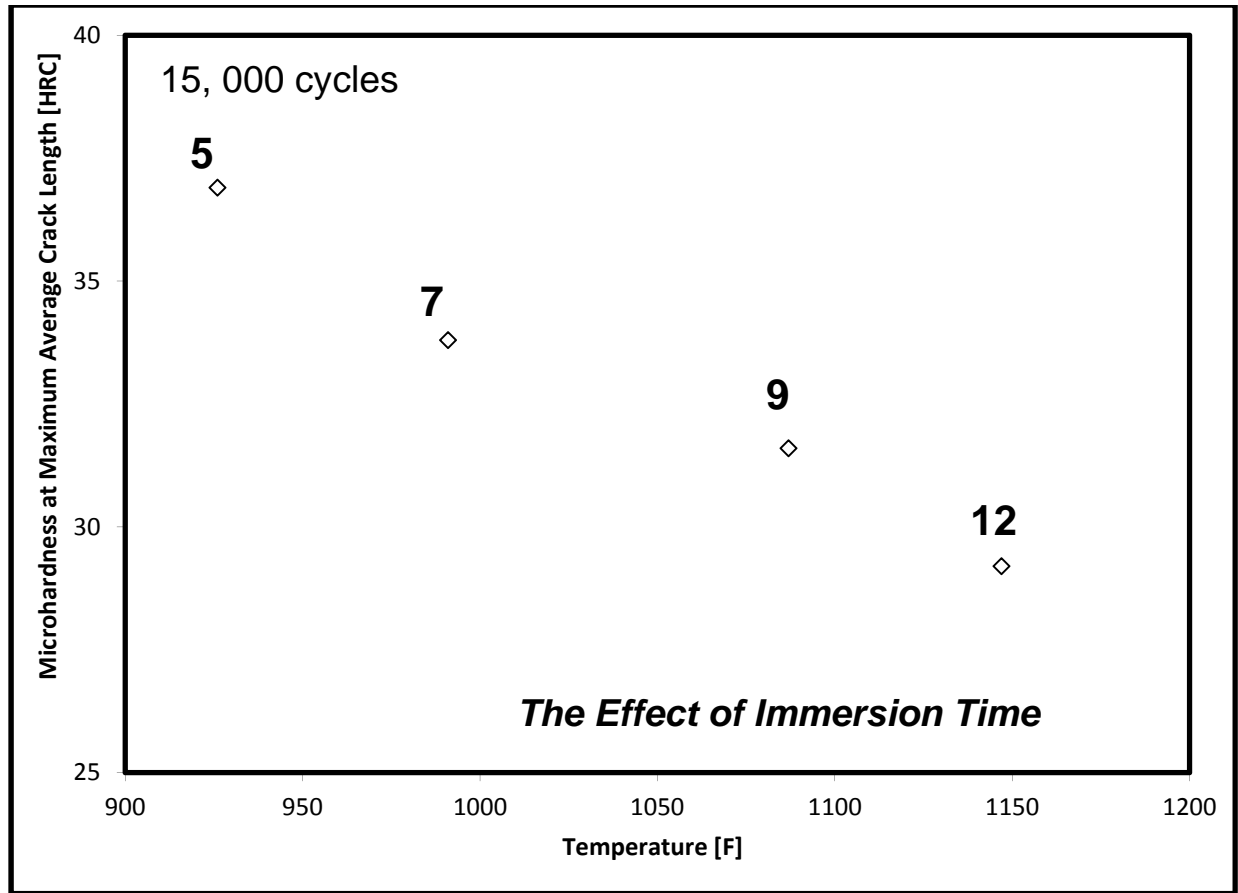
Figure 25 The Effect of Temperature on Microhardness - Different Immersion Times

The Maximum Crack Length is described in Table 2, Figure 26 and Figure 27.

Table 2 Immersion Time Effect on Hardness Variation Across the Surface

Distance From the Corner [in]	5 sec	7 sec	9 sec	12 sec
0.01	36.9	33.8	24.5	24.3
0.02	39.4	36.5	27.4	25.1
0.04	42.4	39.1	31.2	27.7
0.06	43.3	42.4	32.3	29.2
0.08	44.1	44.2	34.5	29.2
0.1	44.3	44.3	36.2	30
0.2	44.4	44.5	40.9	34.1
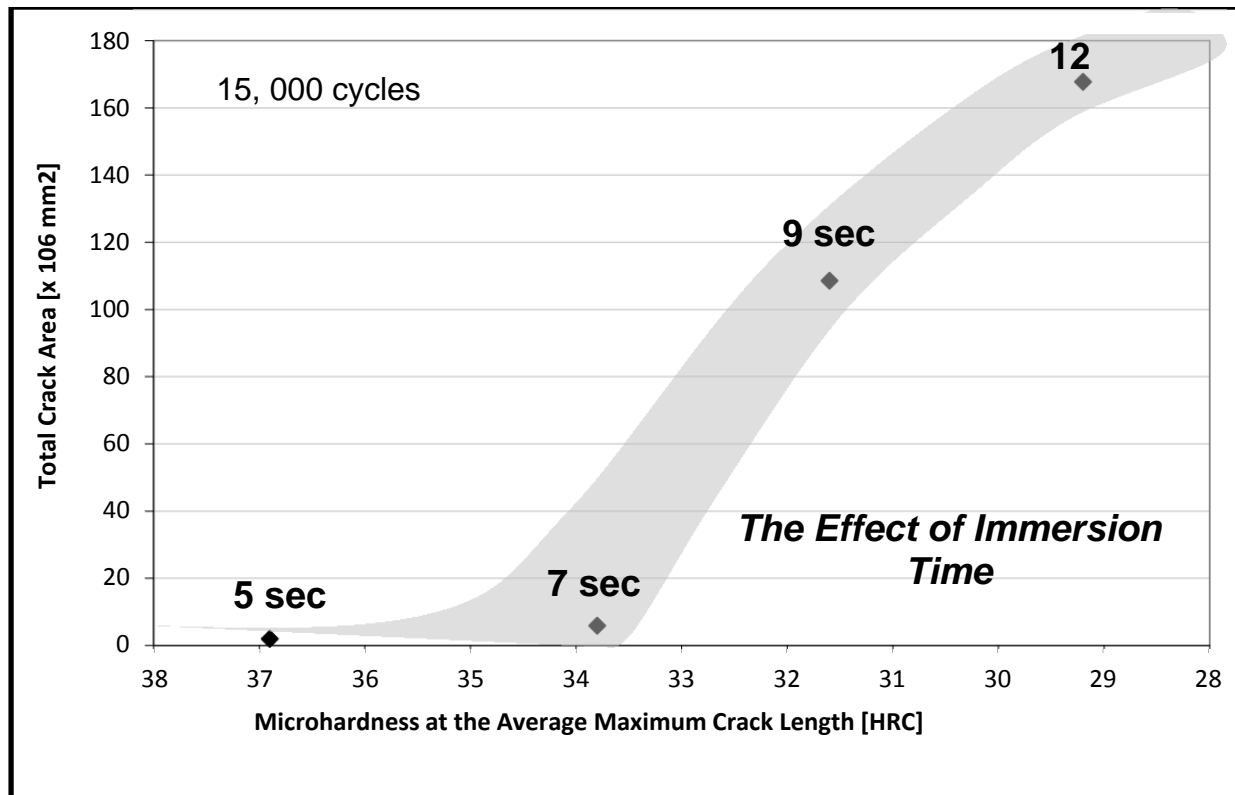
Figure 26 The Effect of Microhardness at Average Maximum Crack Length on Crack Area - Different Immersion Times
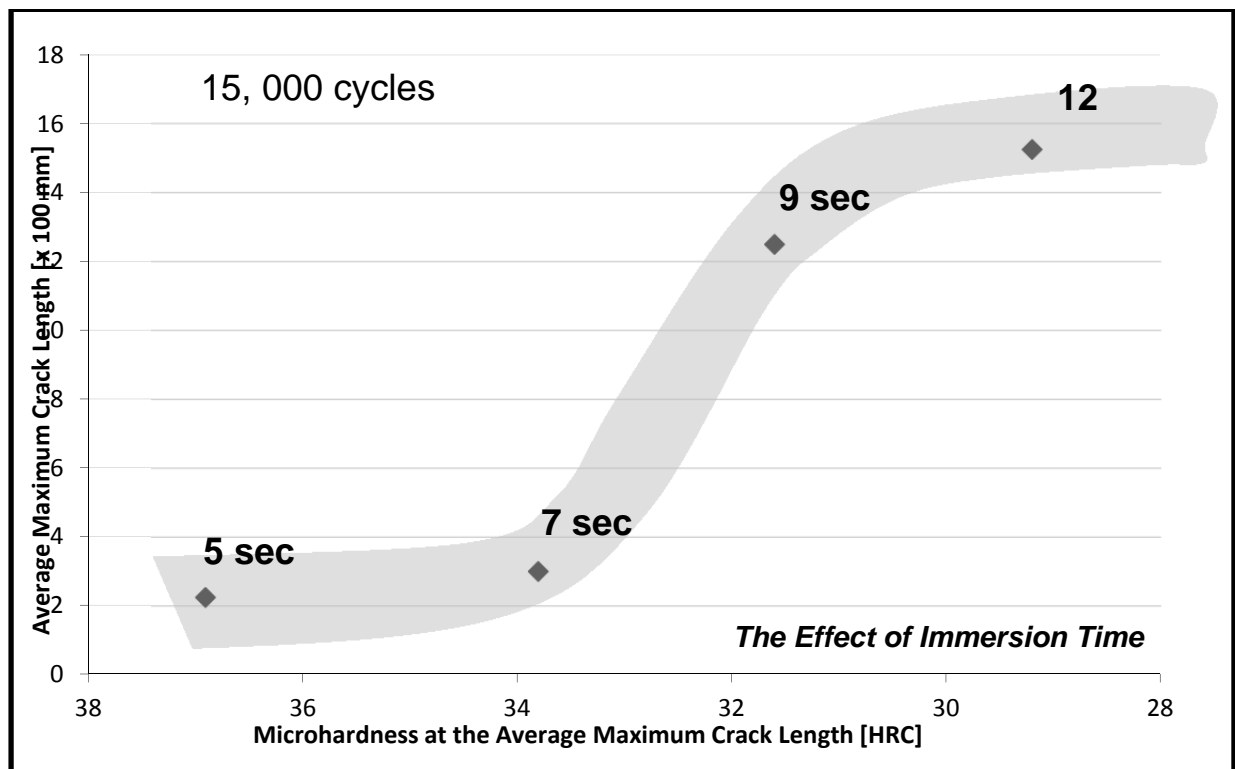
Figure 27 The Effect of Microhardness at Average Maximum Crack Length on Crack Length - Different Immersion Times

It can be concluded that a higher maximum temperature will accelerate the loss in hardness at the corner of the specimen. The crack will extend to a longer distance, as it will have more time to propagate. The hardness loss will be also more severe further inside the material. It appears that the longer the crack is, i.e. the higher the temperature at the surface, the lower the hardness ahead of it. A possible explanation of this phenomenon is that the thermal stresses decrease from the surface towards the interior as the temperature gradient drops, mainly due to the decrease in the maximum temperature. In order for the crack to advance, the strength of the material must decrease even more. However, in this particular configuration, the cooling line does not allow a very deep softening and the crack may eventually stop before it attains a critical length that will lead to instability.

In addition to the surface microhardness evaluation, internal hardness measurements were taken on a center section of the 1.5" cooling line diameter and 12 seconds immersion time specimen. This specimen was under to the most severe test conditions among all the specimens used. The sample was sectioned at the center (about 3.5" from the both ends). The Rockwell hardness profiles obtained from these HV microhardness values are shown in Figure 28.
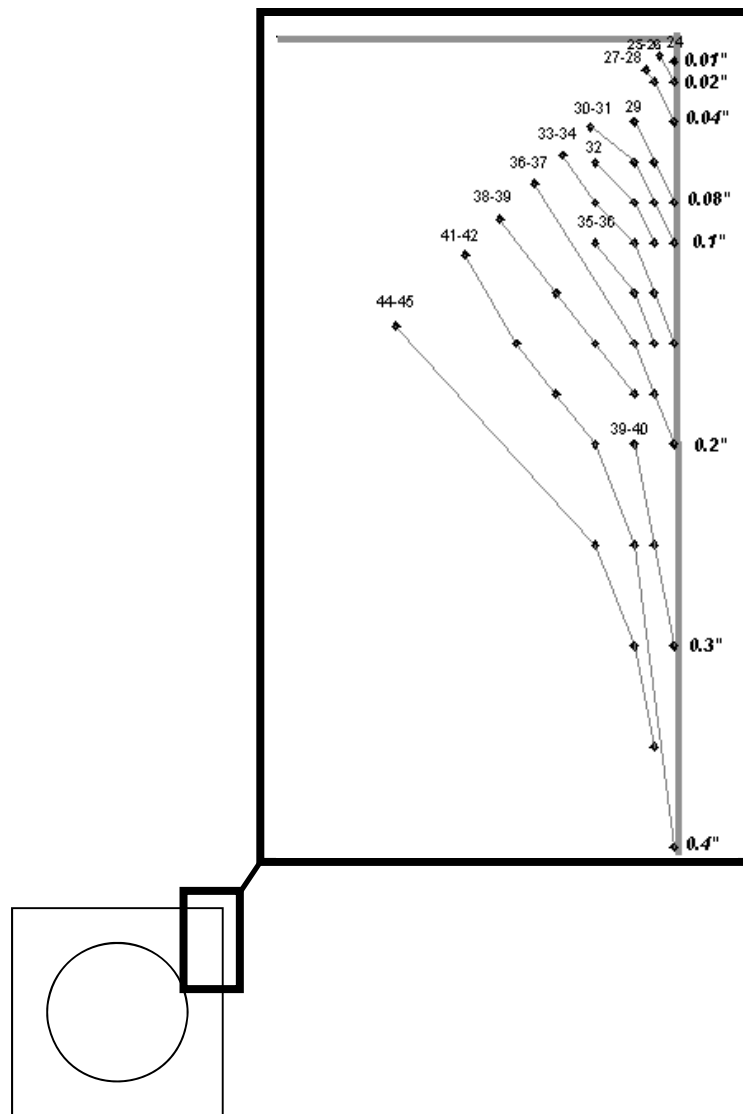
Figure 28 Microhardness Profile at the Corner of 12 Seconds Immersed Specimen

The hardness distribution plots indicate that the softening near the edge is significantly higher than inside the sample, which is predictable due to the higher temperature and heat transfer conditions. However, the degree of softening exceeds the typical tempering curve, shown in the Figure 29. The temperature measured at about 0.06" from the corner of the specimen is almost 1150°F. The temperature cycle at this location has a minimum at 460°F and a maximum at 1147°F. If the peak portion of the thermal cycle is separated (from the cycle presented in Figure 30), it will show that the specimen resided a total of 5.5 sec x 15,000 cycles = 82,500 seconds ~ 23 hours, at a temperature between 1100°F and 1150°F. The value of the hardness at 0.06" from the corner was measured to be 30.6 HRC. According to the tempering curve of the steel (from Figure 18), such a drop in hardness from 45 to around 30 HRC would be produced after about 23 hours at 1150°F. It is concluded that another mechanism contributed to the softening, presumably cyclic stress softening.
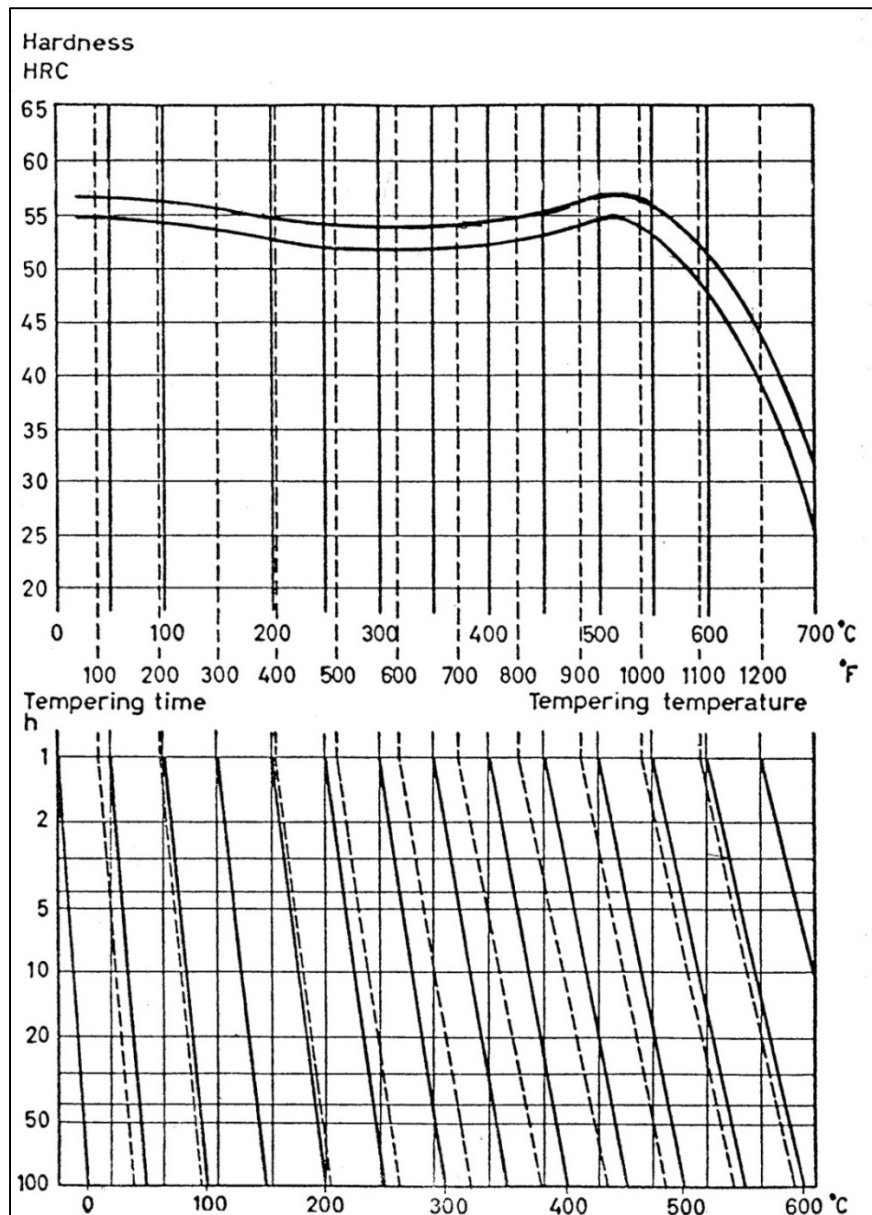
Figure 29 Tempering Curve for H13
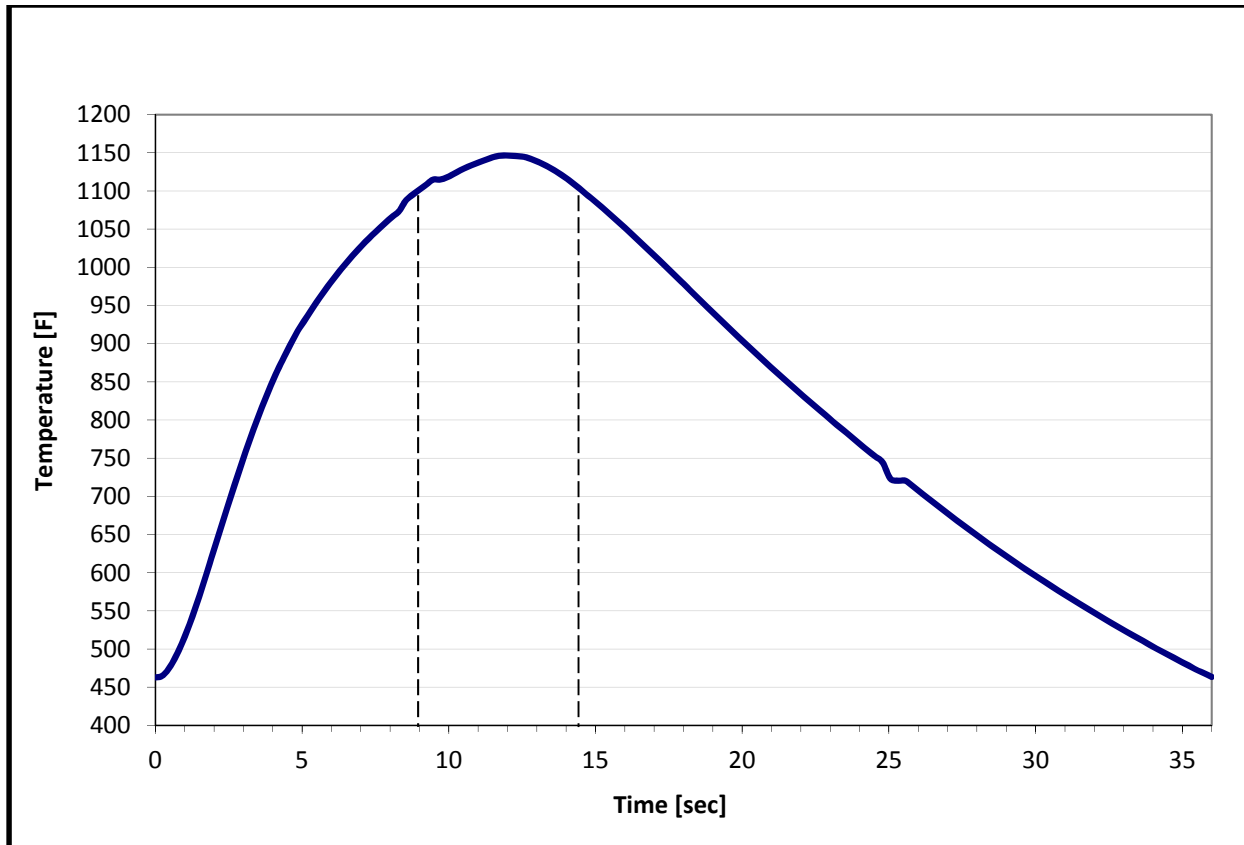
Figure 30 Maximum Temperature Cycle for 1.5" Cooling Line Specimen After 12 Seconds Immersion Time

3.1.2. The Influence of Cooling Line Diameter on Softening and Thermal Fatigue Cracking

Frequently, critical sections (usually thin parts or complicated shape sections subjected to multidirectional heat transfer) occur within a die-casting die. These sections are under high temperature and severe stress conditions. The importance of the maximum temperature and its influence on softening, and hence on thermal fatigue cracking was discussed in the previous section.

In this experiment the maximum and the range of temperature reached at the corner and the variation inside the specimen was investigated as a function only of the cooling line diameter. A larger cooling line will actually bring down the maximum temperature at the surface, and at the same time will keep the temperature range almost the same, since the minimum temperature drops as well, because of a higher heat extraction capability.

The thermal fatigue behavior of three specimens with different cooling line diameters, 1.6", 1.7" and 1.8", was compared with the reference 9 seconds immersion time - 1.5" cooling line diameter specimen. The results are presented as the Total Crack Area and the Average Maximum Crack Length for each cooling line diameter (Figures 31 and 32). The evaluation of softening or hardness loss at the corner of the specimens after 15,000 cycles is shown in Figure 33. The same trend as in the previous experiment was observed for the thermal fatigue cracking parameters. The values of Total Crack Area and Average Maximum Crack Length decrease with the increase in the maximum temperature.
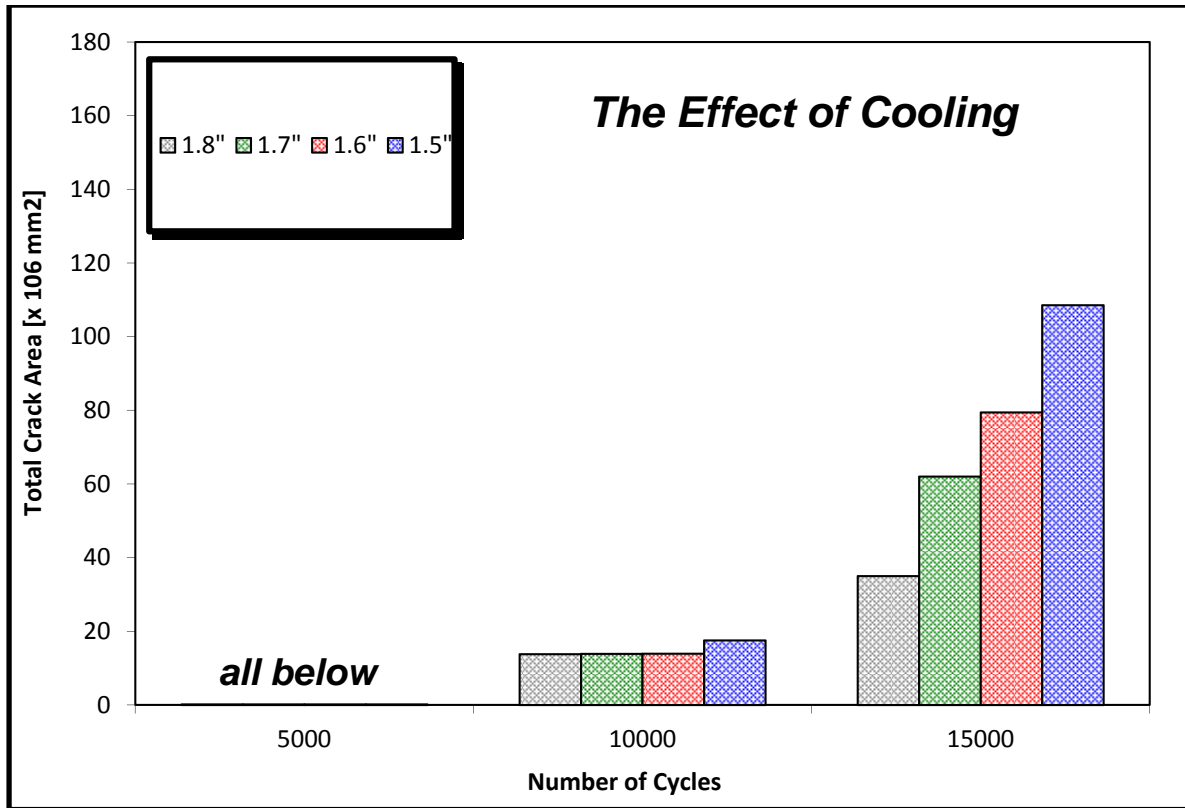
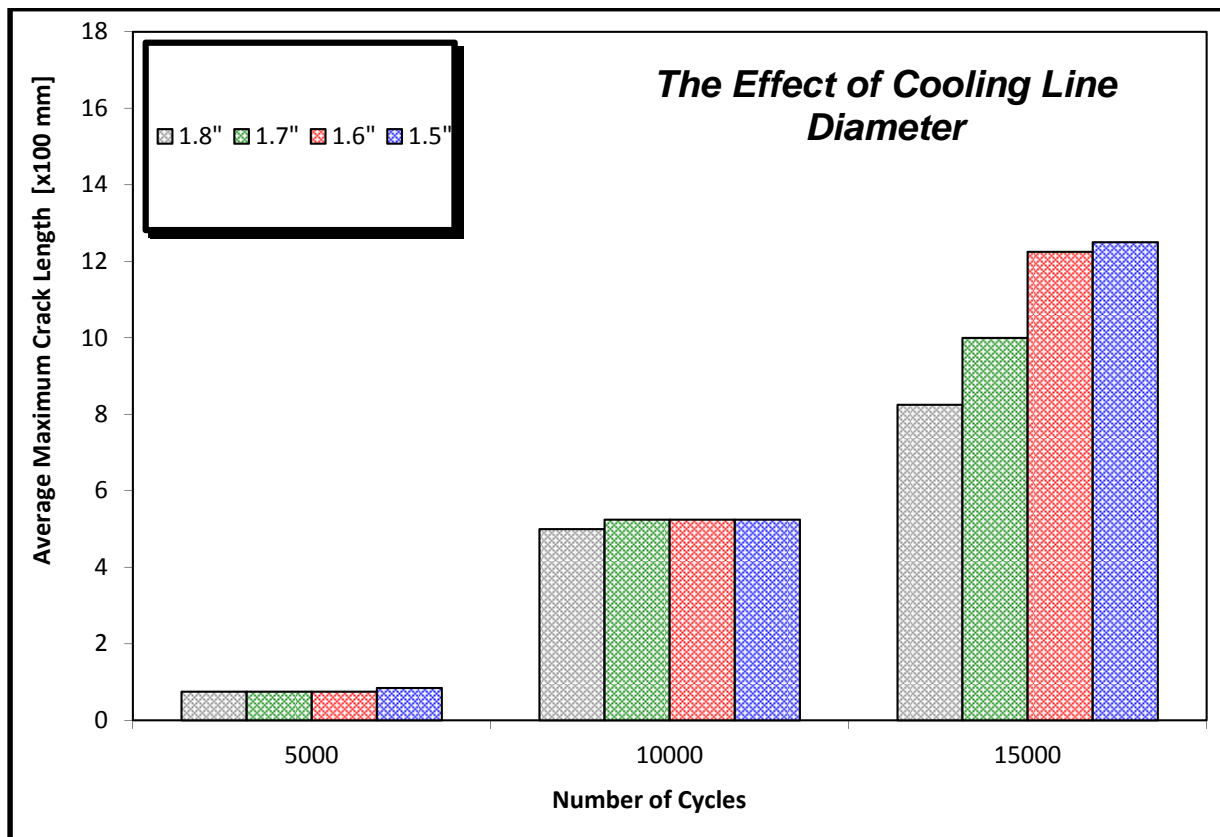**Figure 31 The Effect of Thermal Cycling on Crack Area - Different Cooling Line Diameters**

Figure 32 The Effect of Thermal Cycling on Crack Length - Different Cooling Line Diameters
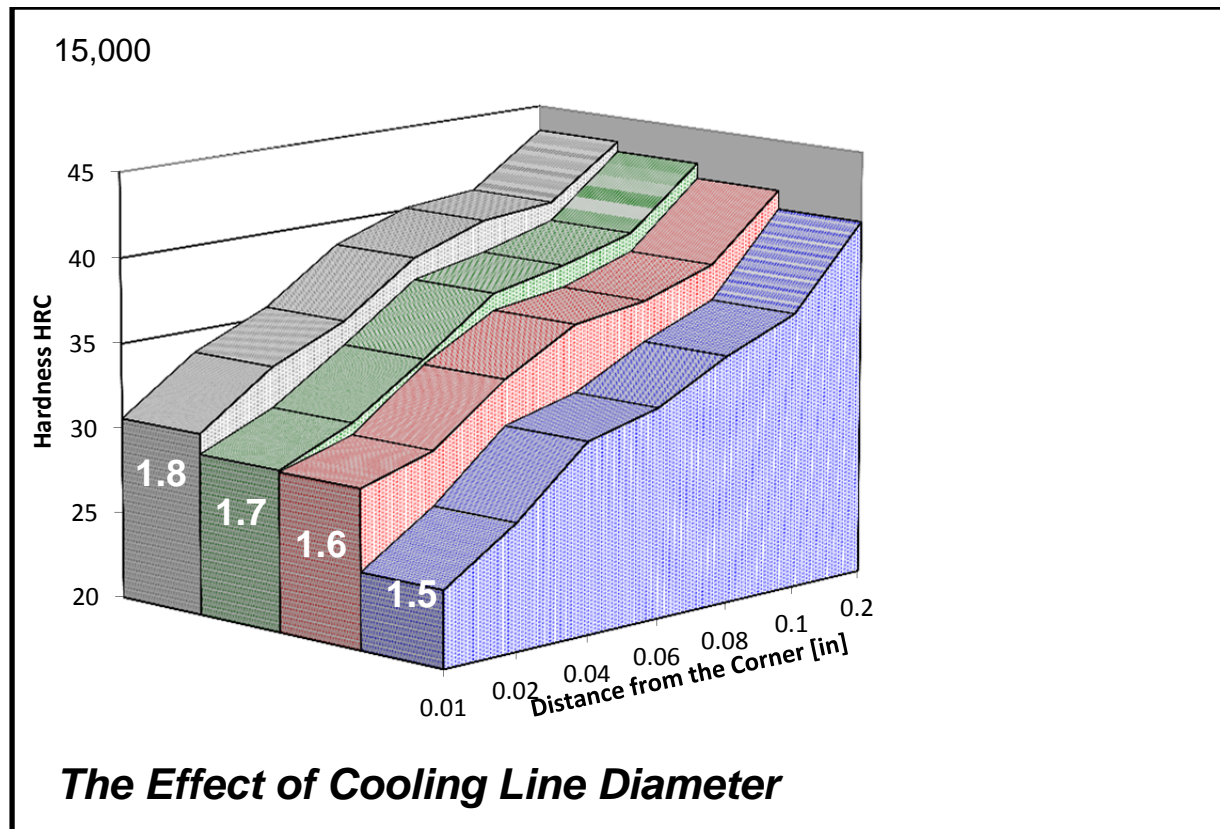
41

Figure 33 The Effect of Thermal Cycling on Microhardness Distribution Across the Surface - Different Cooling Line Diameters

The effect of different cooling line diameter on Total Crack Area and Average Maximum Crack Length as a function of maximum temperature at the corner of the specimen is presented in Table 3 and in Figures 34 and 35. The curve seems to reach a plateau as the cooling line diameter becomes smaller. If the curves are compared with those obtained for varying immersion times, it will be noticed that the tendency of the curve to level around a certain maximum temperature is common for both situations. The variation of microhardness measured at the Average Maximum Crack Length is shown in Table 4 and in Figure 36. The dependency of the thermal fatigue cracking on the microhardness measured at the Average Maximum Crack Length is presented in Figures 37 and 38.The relationship between the cracking parameter and the microhardness measured at the distance equal to the Average Maximum Crack Length follows the temperature trend, confirming the observation made for different immersion times. The longer the crack is, because of the higher temperature at the surface, the lower the hardness ahead the crack.

Table 3 Measurement Data For Different Cooling Line Diameters

Cooling Line Diameter [in]	1.8"	1.7"	1.6"	1.5"
Maximum Temperature [F]	909	939	1002	1087
Minimum Temperature [F]	197	237	326	399
Total Crack Area [x 10^6 m^2] After 15,000 Cycles	35	62.05	79.44	108.56
Average Maximum Crack Length After 15,000 Cycles [x 100 m]	8.25	10	12.25	12.5
Hardness at the Average Maximum Crack Length [HRC] after 15,000 Cycles	35.1	34.6	34.1	31.6
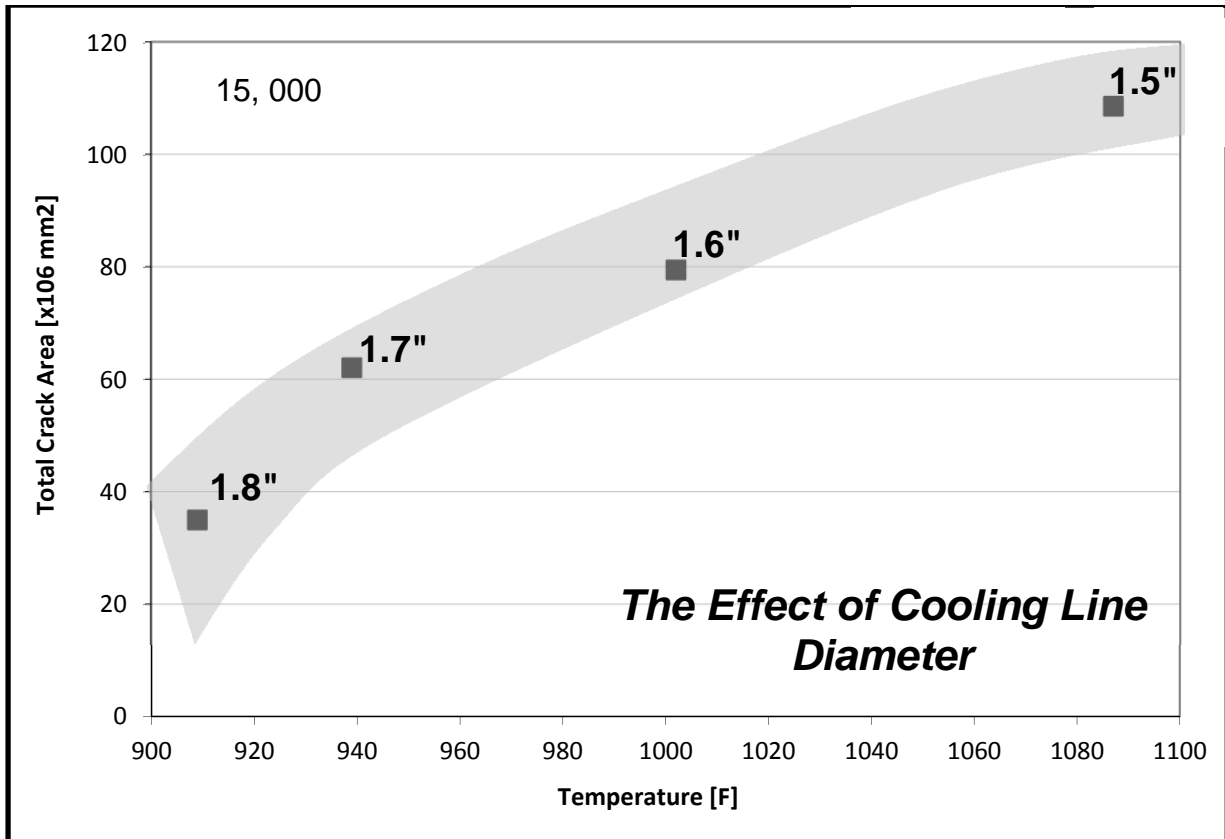
Figure 34 The Effect of Temperature on Crack Area - Different Cooling Line Diameters
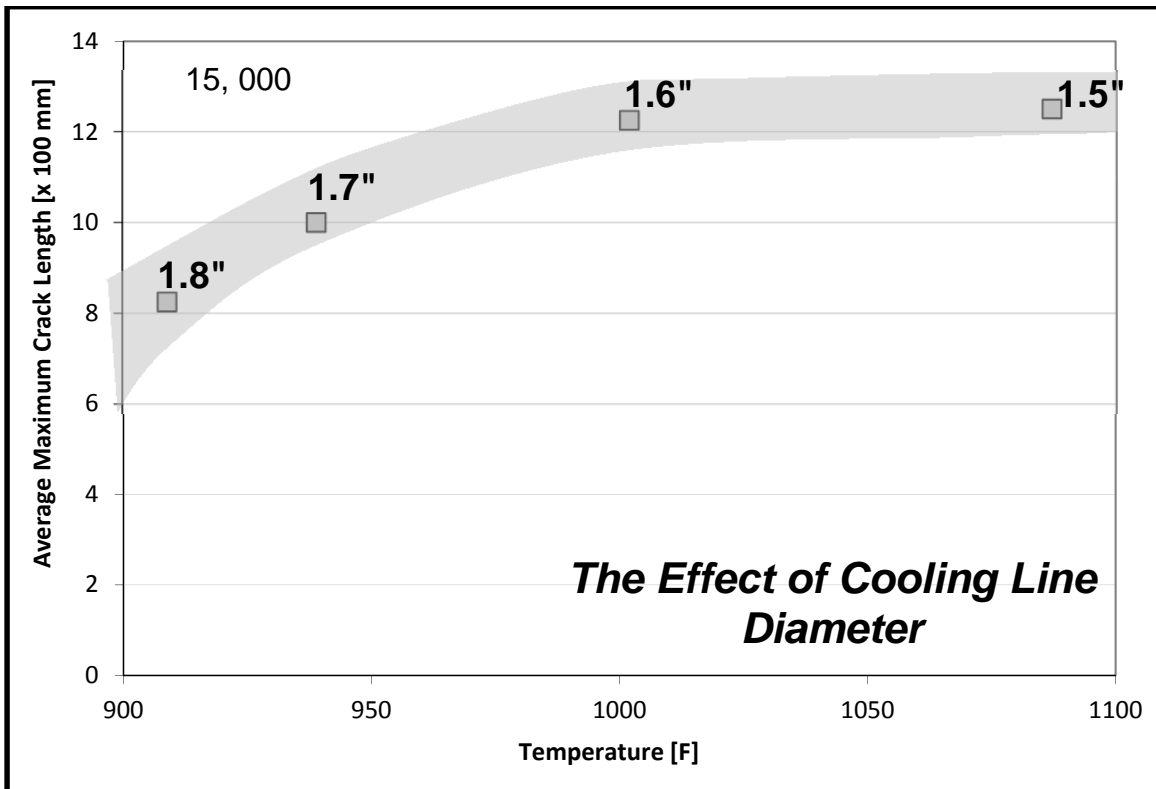

Figure 35 The Effect of Temperature on Crack Length - Different Cooling Line Diameters

Table 4 Cooling Line Diameter Effect on Hardness Variation Across the Surface

Distance From the Corner [in]	1.8"	1.7"	1.6"	1.5"
0.01	30.6	29.4	29.3	24.3
0.02	33.7	31.3	30.6	25.1
0.04	35.6	34.2	33.9	27.7
0.06	38.6	37.3	36.3	29.2
0.08	40.1	38.2	36.9	29.2
0.1	40.5	39.4	38.3	30
0.2	43.5	42.9	42	34.1
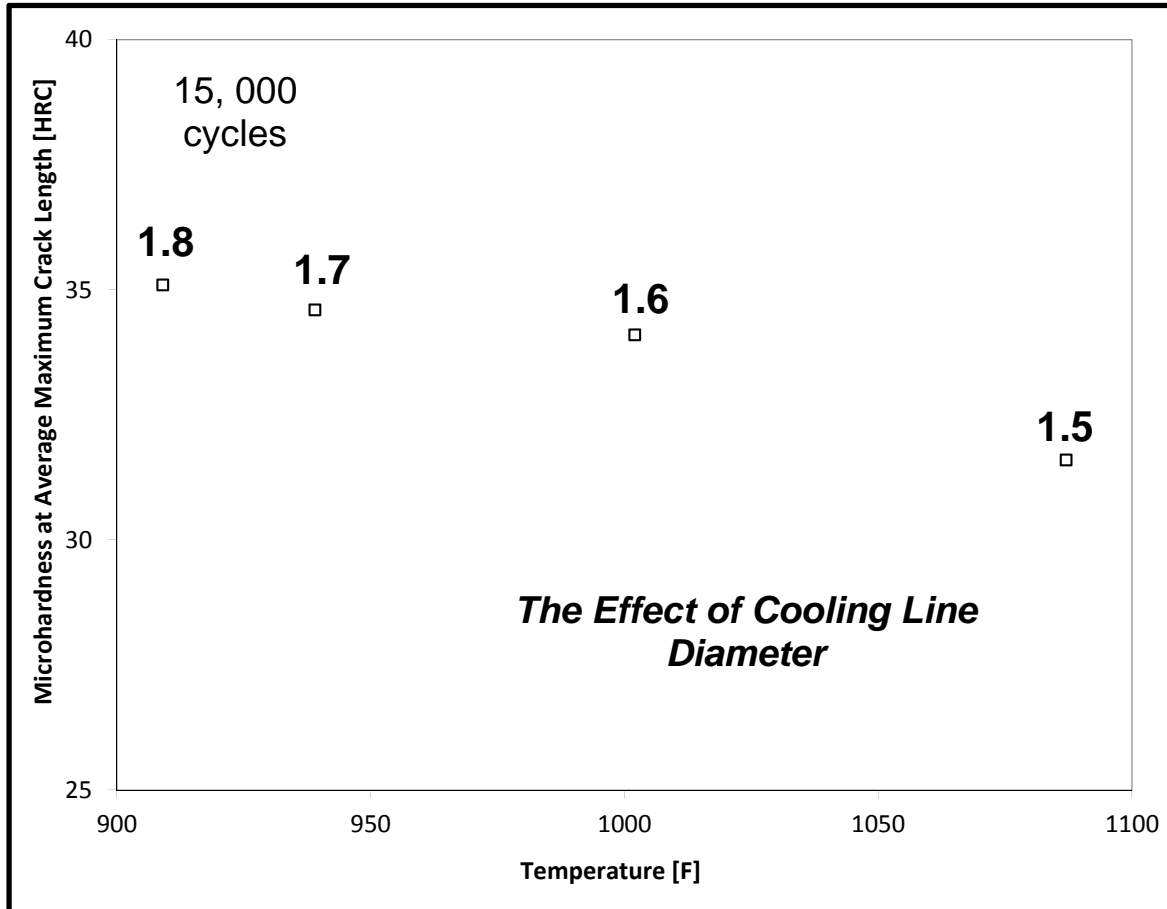
Figure 36 The Effect of Temperature on Microhardness - Different Cooling Line Diameters
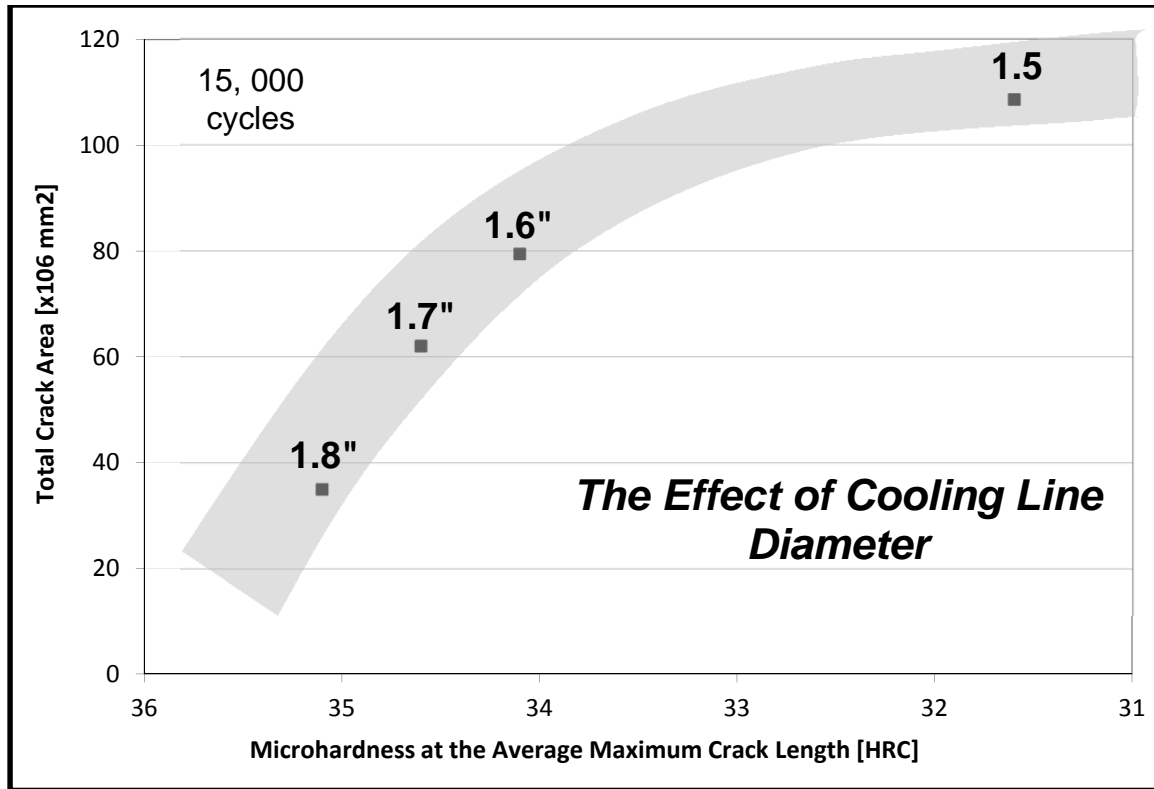
Figure 37 The Effect of Microhardness at Average Maximum Crack Length on Crack Area
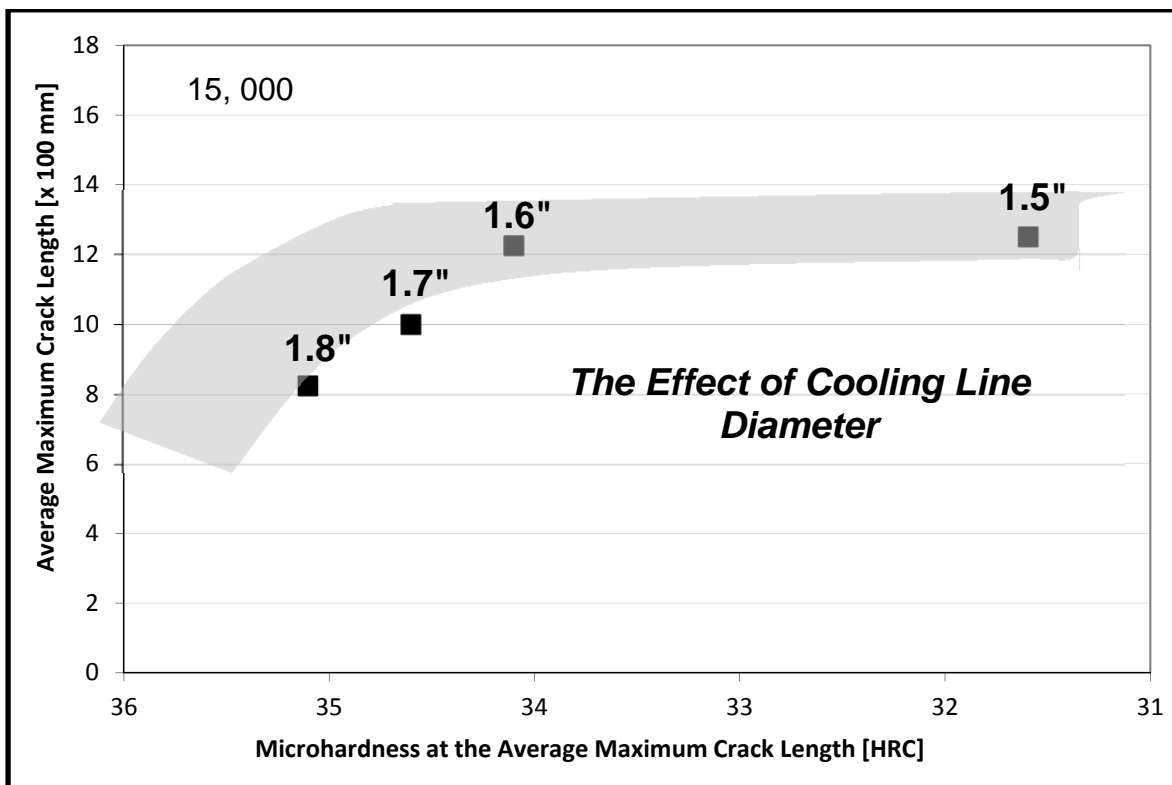
Figure 38 The Effect of Microhardness at Average Maximum Crack Length on Crack Length - Different Cooling Line Diameters

3.2. Stress Analysis at the Specimen Surface and Around the Cooling Line

The stresses developed at the surface are responsible for initiation and subsequent crack propagation. The required hardness loss for crack initiation and propagation varies function of the level of induced stress. These thermal stresses are generated by the difference between the maximum and minimum temperature (temperature gradient). Different testing or production conditions will result in different temperature and stress distributions. The effect of immersion time and cooling line diameter on maximum, minimum and range of temperature are presented in Figures 39 and 40. More severe conditions (longer immersion time or smaller diameter of the cooling line) will not raise only the maximum temperature but also the minimum temperature, so that the temperature gradient (range, in the plots) will not increase too much. Consequently, a larger cooling line or a shorter immersion time will shift the overall cycle towards lower values, keeping the stress in about the same range. This observation is extremely important, because of the implications resulting from the capacity of a larger cooling line diameter to promote a lower softening-causing maximum temperature without a major increase in the stress level.
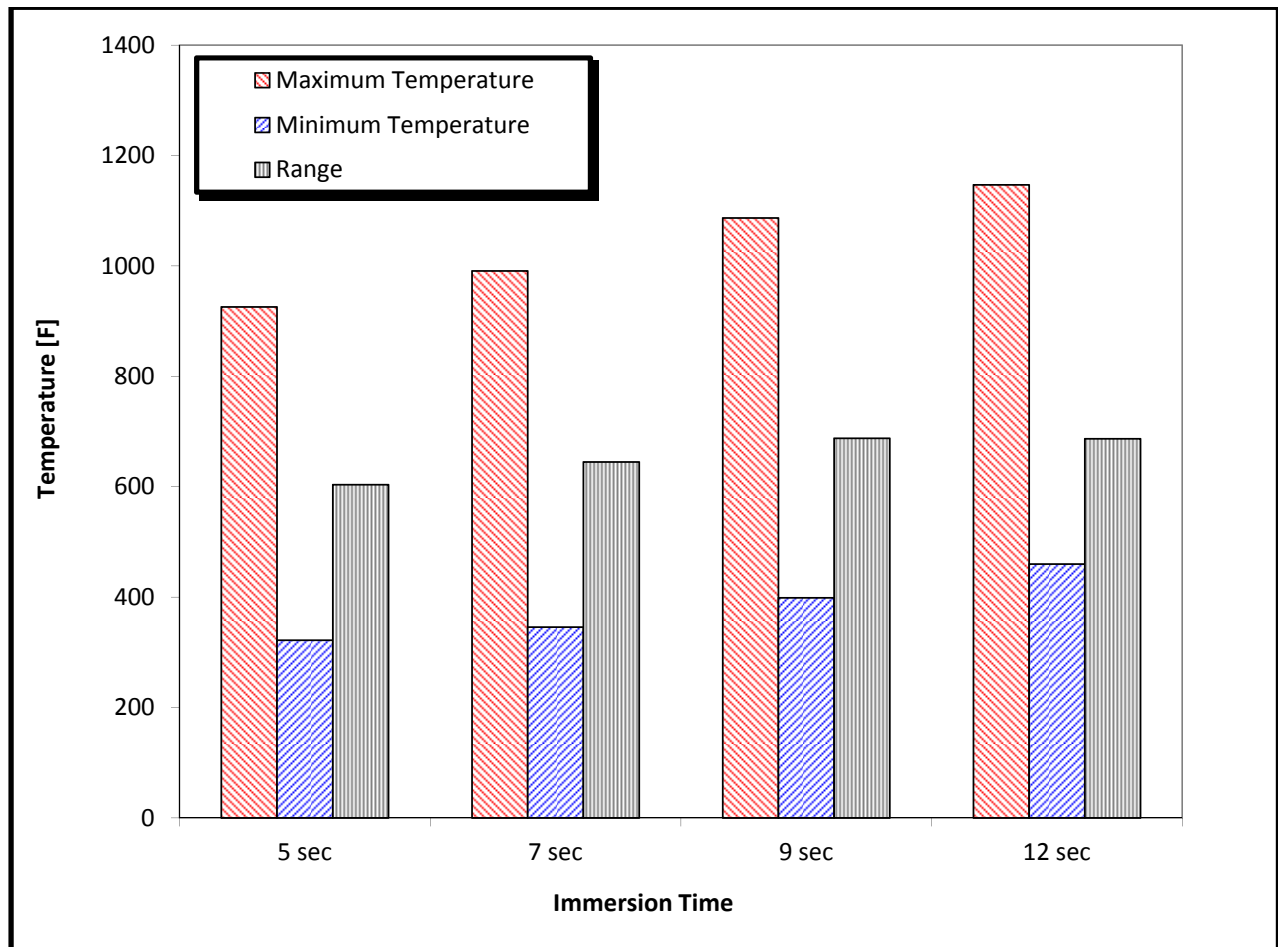
Figure 39 The Effect of Immersion Time on Temperature
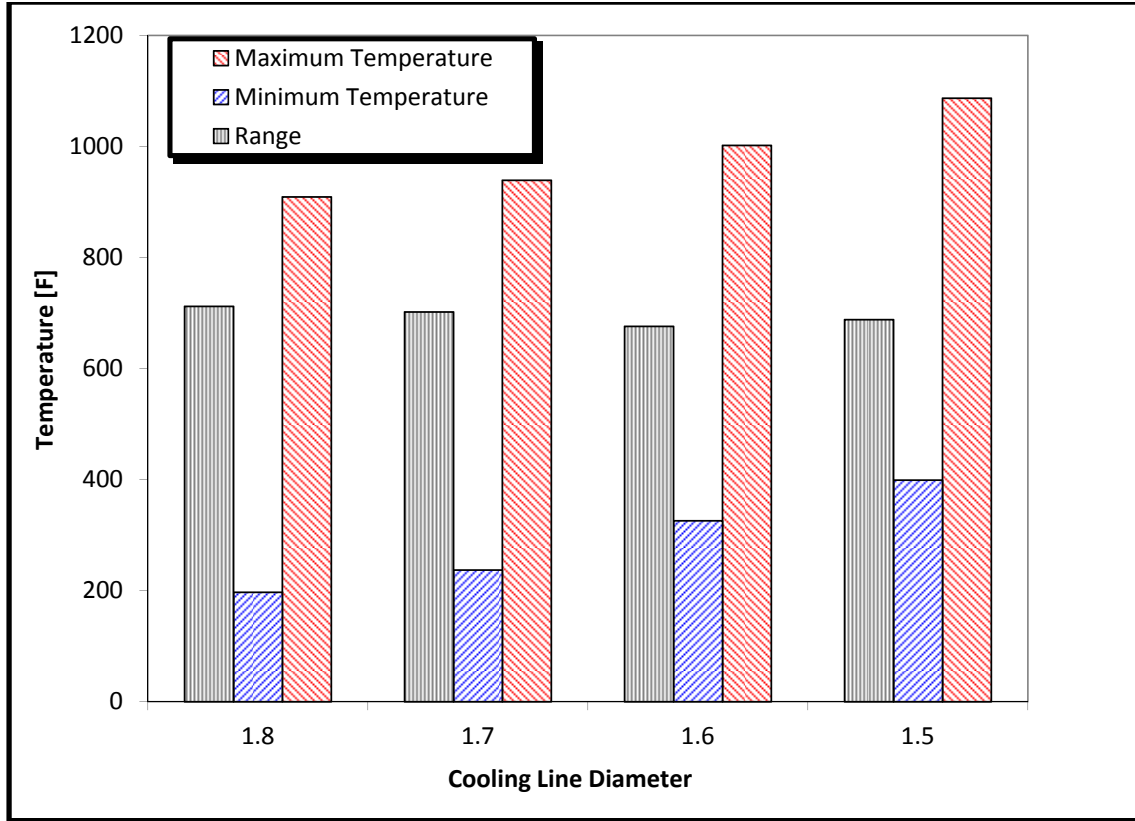
Figure 40 The Effect of Cooling Line Diameter on Temperature

The stresses in the thermal fatigue specimen are complex. The cracks initiate not only at the corner of the specimen, where softening favors the plastic strain accumulation (Figure 41), but also at the cooling line, due to high hoop tensile stresses created during immersion. The latter formation is promoted by the existence of severe stress concentrators caused by cooling water corrosive action. In extreme conditions, the cracks initiated at the cooling line can cause failure of the specimen, mainly because they initiate and grow faster in the thinnest section of the specimen or die as a consequence of high tensile hoop stress induced by the extreme temperature gradient (Figure 42). The axial stress range at the corner for 12 seconds immersion and 1.5" cooling line diameter specimen can be estimated as:

$$\alpha E \Delta T = 6.9 \text{ in/in}°F * 30,500 \text{ ksi} * 687 °F = \sim 145 \text{ ksi. (3-2)}$$

where α is the coefficient of thermal expansion, E represents the elastic modulus and ΔT is the temperature gradient. This estimation agrees relatively well with the value of stress range obtained by computer modeling (Figure 43). The computer modeling for the 1.5" cooling line diameter specimen and 12 seconds immersion time shows that during immersion in molten aluminum the compressive axial stress at the corner attains a high value. High compressive stress and low yield strength may generate plastic strain. The result is a residual tensile stress, which is well below the yield strength, but high enough to initiate fatigue cracks at stress concentrators. The axial stress at the cooling line is tensile. Because the temperature at the wall of the cooling line is low, the axial stress is tolerated. However, the hoop stress developed is markedly higher. In the presence of stress concentrators like machining marks and corrosion pits, cracks can initiate and propagate from the cooling line.
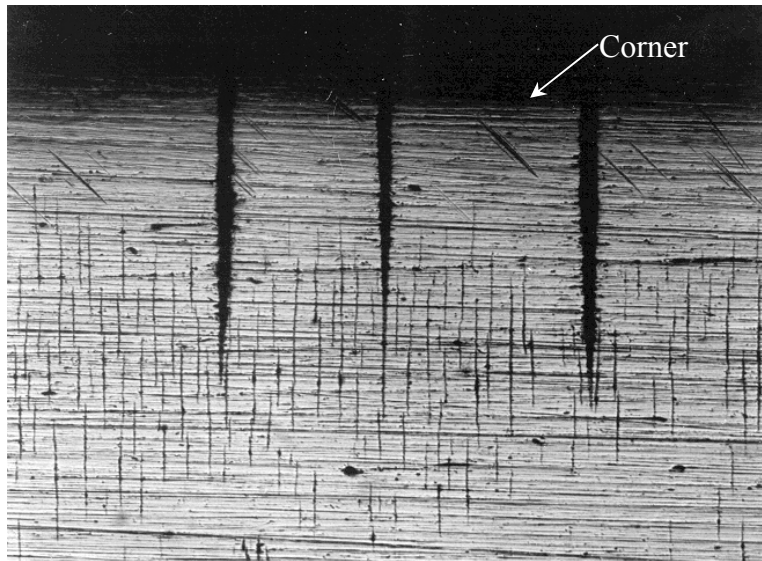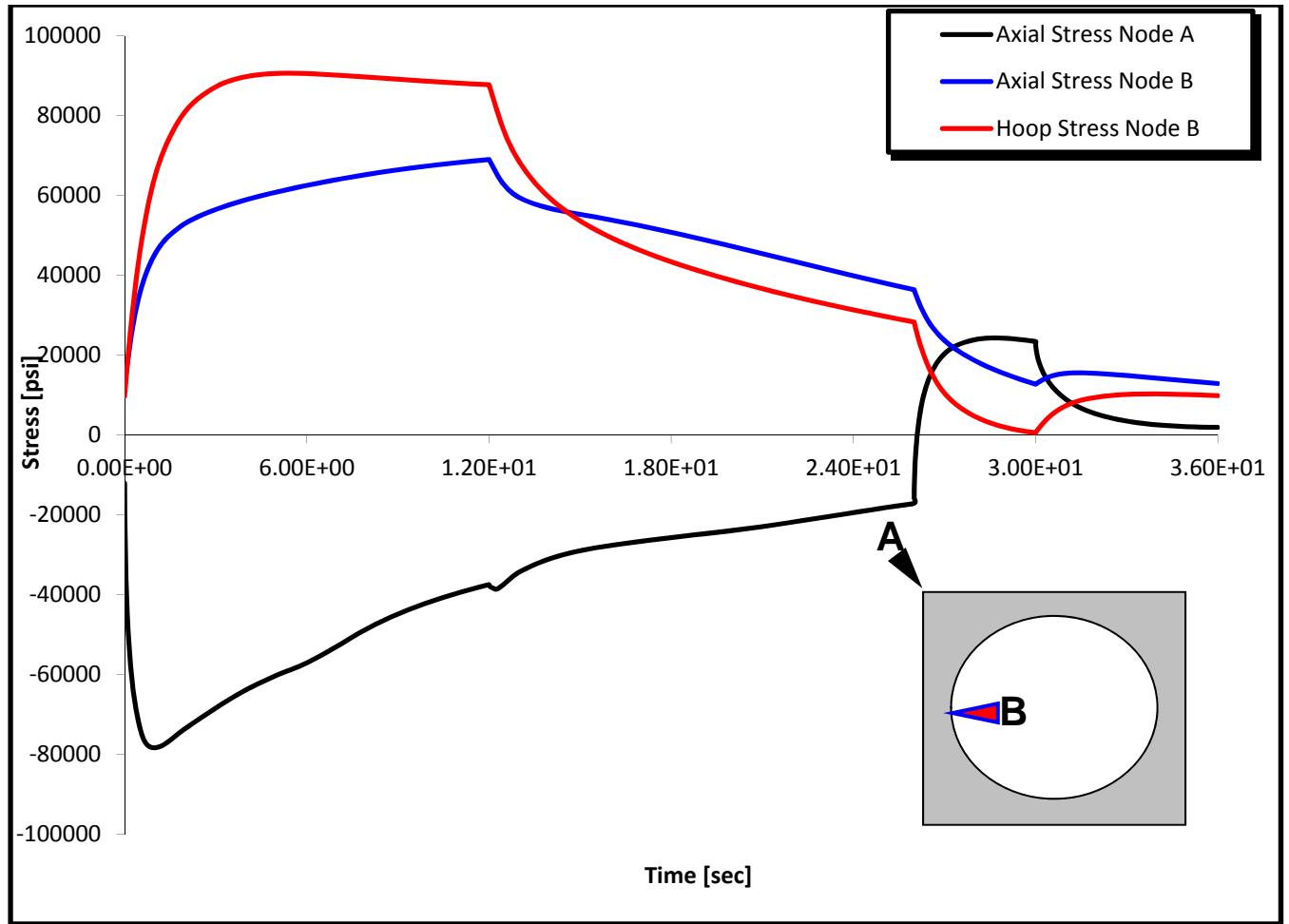
Figure 41 Cracks at the Corner of H13 Specimen

Figure 42 Crack at the Cooling Line of H13 Specimen

1.5" Cooling Line, 12 Seconds Immersion

Figure 43 Stress Modeling at the Corner and Cooling Line

3.3 Cooling Effect Evaluation for Bubblers

A uniform temperature distribution for a die is preferred. The existing problem in die-casting industry is that the core is always over heated more than other parts of the die, and the "hot spot" forms on the tip of the core, which is surrounded by the molten metal. Therefore it is more apt to be subjected to thermal fatigue cracking. The experiment used bubblers with different I.Ds and O.Ds to cool the specimen while it was heated in the air furnace. The lower temperature measured at the same point shows the better effect of the cooling.

Figure 44 shows the experimental temperature-flow rate curves for each bubbler. The temperature measuring point was on the central line of the specimen, 0.06" (1.5 mm) away from the bottom surface. It could be considered that for a cooling line with a given inner diameter, the thicker the bubbler, the better the cooling effect. However, the experiment result shows that evidently, when cooling water has the same flow rate, the bubbler whose I.D. is 0.17" can keep the specimen bottom the lowest temperature at steady state, compared with the bubblers whose I.D. are 0.214" and 0.307". Fluid jet velocity is an important factor in the heat transfer between coolant and the solid wall. The flow rate of cooling water can be used to determine the mean jet velocity of cooling water, $\overline{V}_j$ by:

$$\overline{V_j} = \frac{Q}{A}$$

(3-4)

where Q is the volumetric flow rate of cooling water and A is the cross-sectional area for flow. Figure 45 shows the strong effect of the jet velocity on the specimen bottom temperature.
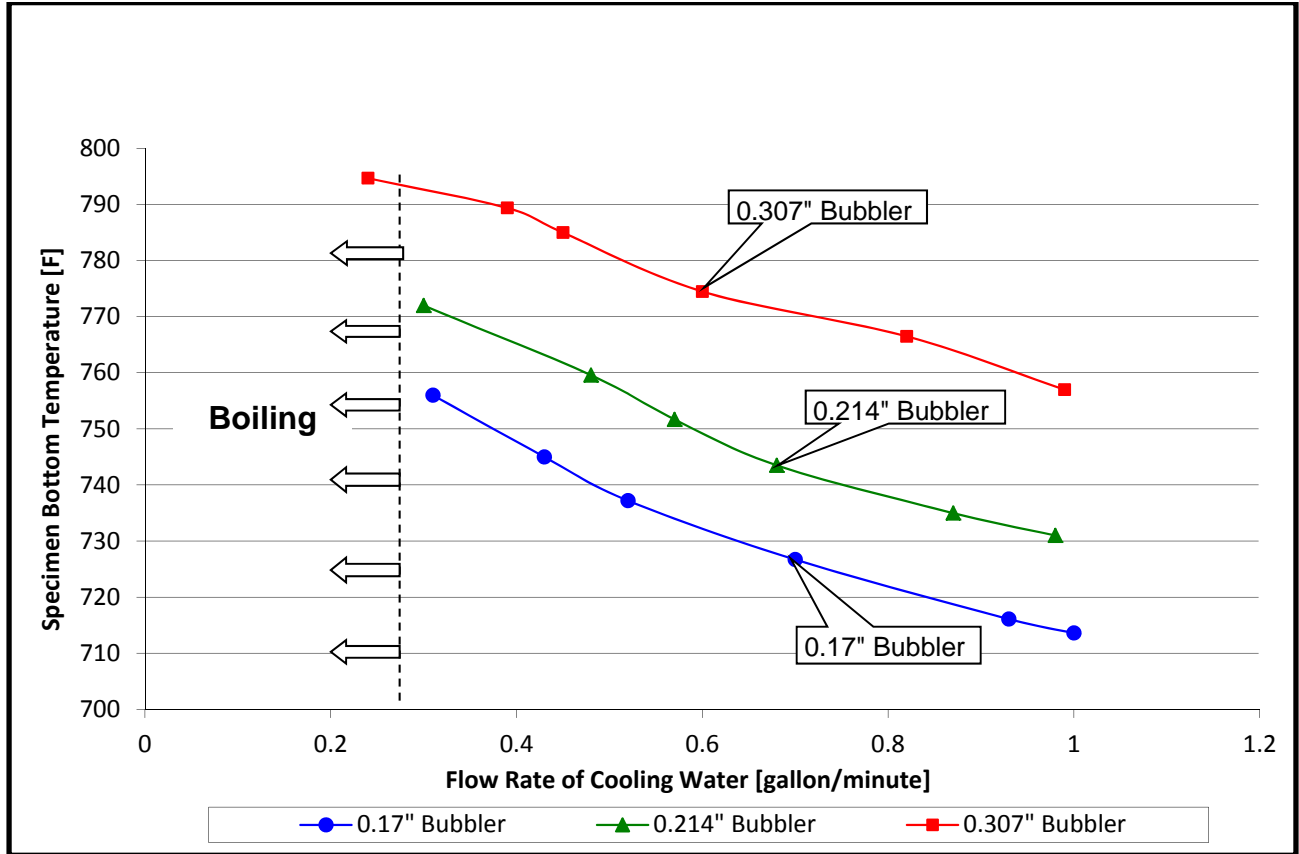

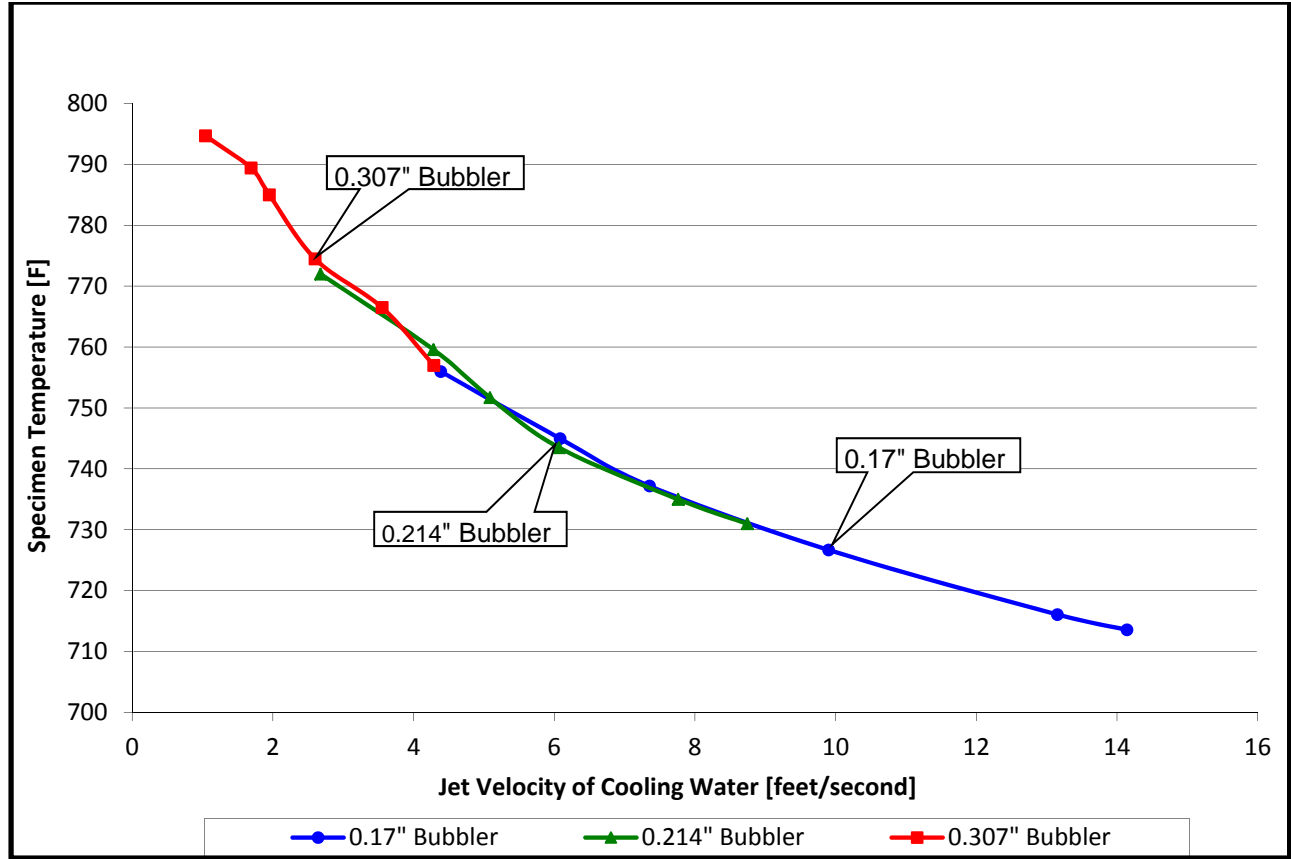**Figure 44 Specimen Bottom Temperature-Flow Rate of Cooling Water**

Figure 45 Specimen Bottom Temperature-Jet Velocity of Cooling Water

Since there is no well-developed theory about the heat transfer between fluid and sidewall at the tip of bubbler, we may have the aid of the heat transfer model between impinging jet flow and objective. Although in the model the jet flow is unconfined and the object is a flat surface, it is still applicable for the qualitative discussion since the considered point overlaps the stagnation point and geometry center in the research. According to the definition of parameters in equation (1-12), *r* gets the value of 0 in the research. Therefore, equation (1-12) is simplified to:

$$Nu = 1.122A \cdot \Pr^{1/3} \mathrm{Re}_j^{0.7} \text{ (3-5)}$$

Substitute the definitions of Nusselt number, Reynolds number and equation (3-4) into (3-5), the expression of local heat transfer *h* can be deducted as:

$$h = 1.122A \cdot \Pr^{\frac{1}{3}} \cdot \frac{k}{D} \left(\frac{4Q}{\pi D^2 v} \right)^{0.7} \text{ (3-6)}$$

where *A* is a constant; *k* is the thermal conductivity of cooling water; *D* is inner diameter of bubbler and v is the kinematic viscosity of cooling water. Equation (3-6) shows evidently that at the given flow rate, decrease the inner diameter of bubbler will increase the mean jet velocity, in turn will increase the local heat transfer coefficient at the stagnation point, if the effect of bubbler size to flow pattern is neglected. At the same flow rate, the bubbler with I.D. of 0.17" sets up a jet velocity 3 times higher than that of the bubbler with I.D. of 0.307". The different jet velocities at the same flow rate of 1.0 gallon per minute are listed in Table 5.

51

Table 5 Comparison of Water Jet Velocity of Three Bubblers

Flow Rate Velocity	1.0 gallon/minute	2.0 gallon/minute	3.0 gallon/minute
Water Jet Velocity of 0.17" Bubbler (Feet/Second)	14.0	28.1	42.2
Annulus Velocity of 0.17" Bubbler (Feet/Second)	1.6	3.2	4.8
Water Velocity through 0.09 inch^2 Baffle Gap (Feet/Second)	3.6	7.1	10.7
Water Velocity Parallel to Baffle Sidewall (Feet/Second)	2.9	5.8	8.7

3.4 Cooling Effect Evaluation for Baffles in Air Furnace

A baffle is another cooling device currently used in the industry. For a cooling line with a given I.D., the only controlling parameter for a baffle is its length, in particular, the gap area between the tip of the baffle and the bottom of the cooling line. The baffles with different lengths were used to cool the specimen while it was heated inside the air furnace at a temperature of 950°C/1742°F. Figure 46 shows the dependence of specimen bottom temperature on the flow rate of cooling water for different gap areas. Figure 47 indicates a general trend that the smaller the gap area, the better the cooling effect for the "hot spot". The gap area actually controls the average velocity of cooling water flowing through the gap. The flow rate can be translated into the average velocity, neglecting the leakage occurring at the clearance between the edge of baffle and the sidewall of the specimen. Figure 48 shows the relation between the specimen bottom temperature and the average velocity of cooling water through the gap. The theory about convection heat transfer for fluid flowing through a curved pipe is applicable for the qualitative heat transfer analysis for baffle-directed cooling water in the cooling line, as following:

$$\frac{h_{curved}}{h_{straight}} = 1 + 3.5\frac{D}{D_c} \qquad (3\text{-}7)$$

where h_{curved} is the local heat transfer coefficient in curved duct; $h_{straight}$ is the corresponding local heat transfer coefficient in straight duct; D is the inner diameter of the duct and D_c is the diameter of curvature. Obviously, for a given curvature, h_{curved} is proportional to $h_{straight}$. The dependence of h ($h=h_{straight}$, if not otherwise specified) on mean fluid velocity, $\overline{V}$, can be deducted from equation (1-7) as following:

$$Nu = \frac{hD}{k_c} = 0.023\,\mathrm{Re}^{0.8}\,\mathrm{Pr}^{0.4}$$

$$h = 0.023\left(\frac{4\rho Q}{\pi\mu D}\right)^{0.8}\left(\frac{c_p\mu}{k_c}\right)^{0.4}\frac{k_c}{D}$$

$$h = 0.023\left(\frac{\rho Q}{\frac{1}{4}\pi\mu D^2}\right)^{0.8}\left(\frac{c_p\mu}{k_c}\right)^{0.4}\frac{k_c}{D^{0.2}}$$

$$h = 0.023 \left(\frac{\rho \overline{V}}{\mu} \right)^{0.8} \left(\frac{c_p u}{k_c} \right)^{0.4} \frac{k_c}{D^{0.2}} \qquad (3\text{-}8)$$
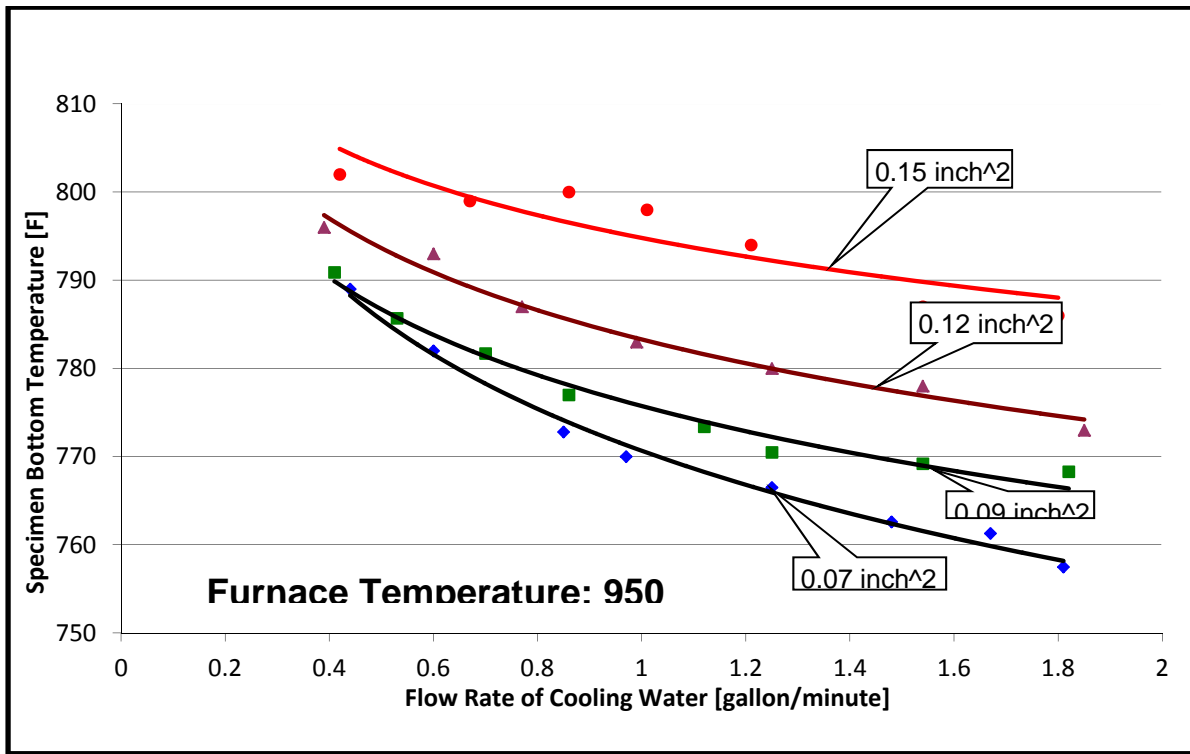

Figure 46 Effect of Gap Areas on Cooling Effect of Baffles
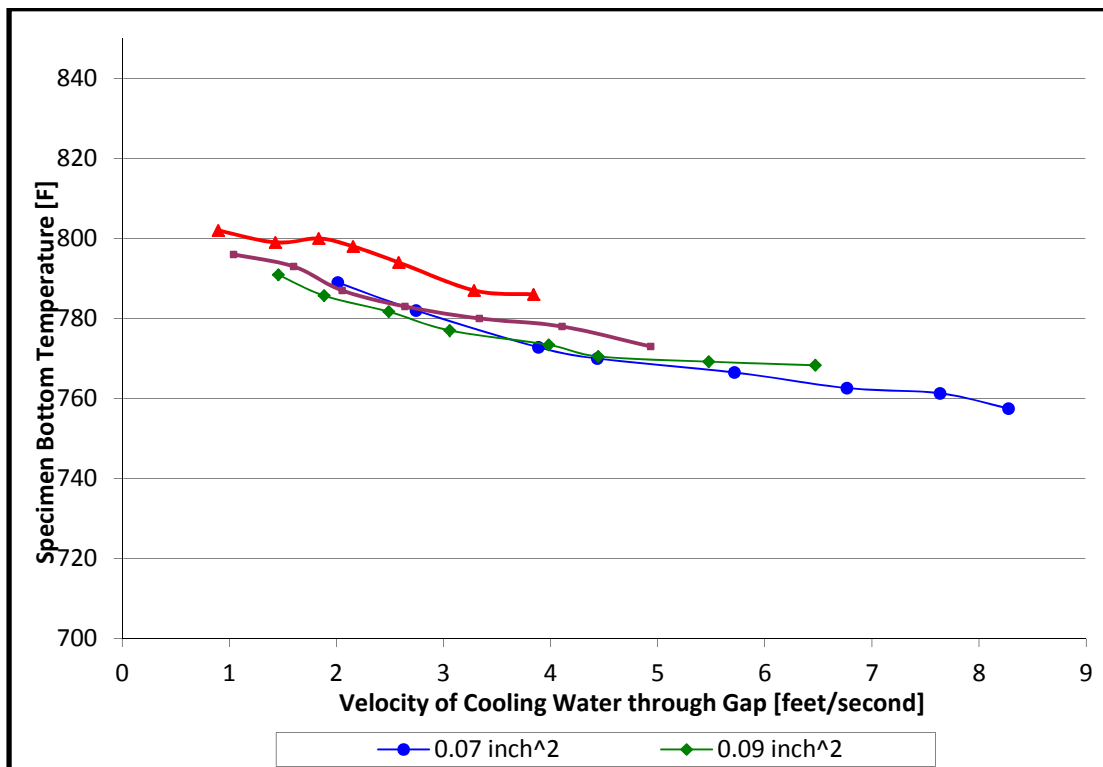

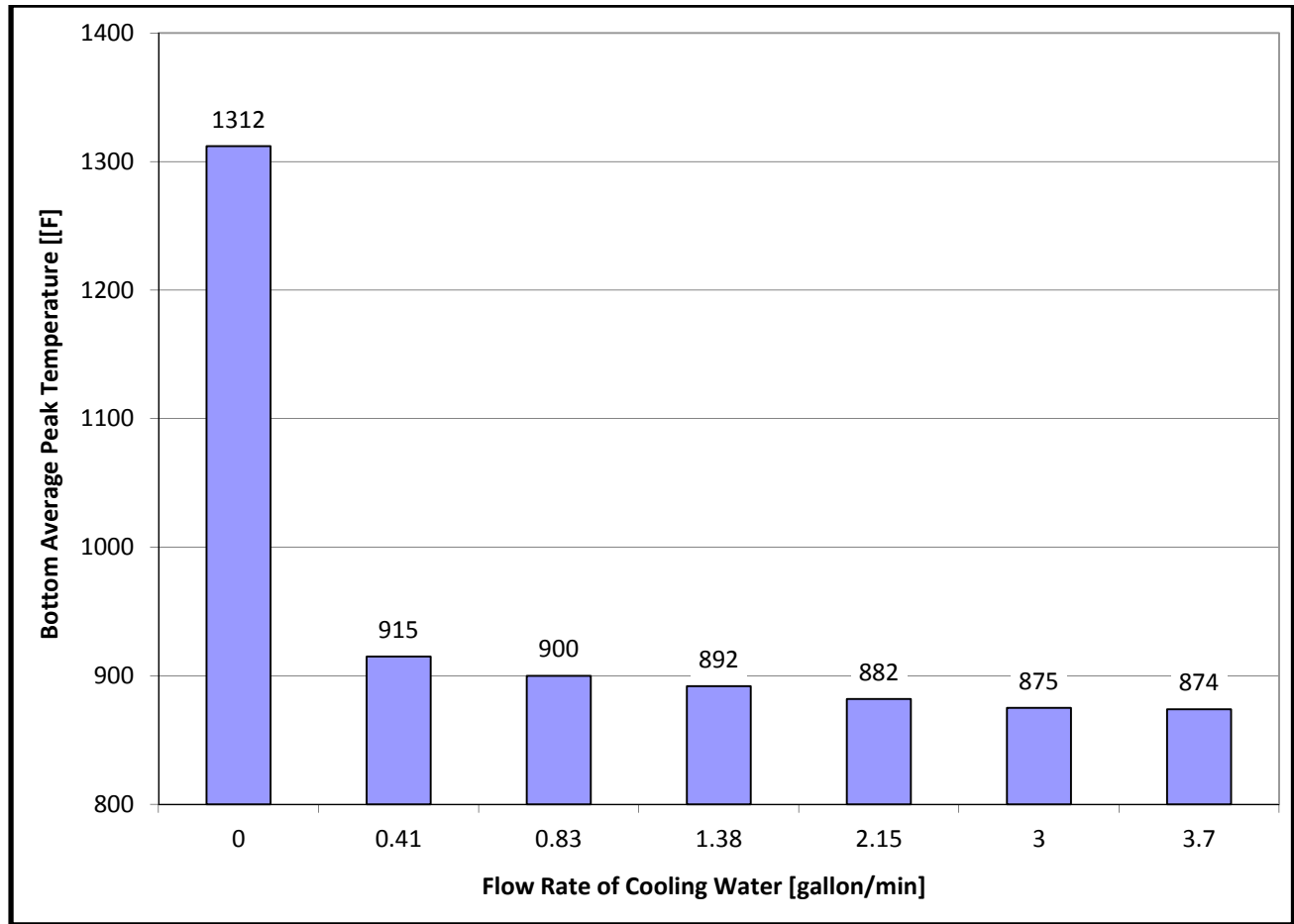**Figure 47 Effect of Velocity of Cooling Water on Specimen Bottom Temperature**

Figure 48 Comparison of Surface Temperature with/without Water-cooling

Equation (3-8) indicates that higher fluid velocity will enhance the local convection heat transfer in straight pipe. In turn, the higher fluid velocity will increase the local heat transfer coefficient in curved pipe. This is why the smallest gap has a relatively best cooling effect to the "hot spot" at the bottom of specimen.

Here, it should be noted that only heat transfer enhancement has been considered, and another important hydrodynamic parameter, pressure loss, was not in the scope of this work. However, the parameter is supposed to be taken into consideration for applications, which determines the flow rate of the cooling water at the given system pressure. Therefore, the results cannot be extended further because of the high pressure loss caused by smaller section area through which cooling water flows.

3.5 Dip In/Out Experiment in Molten Aluminum

The cooling effect evaluation experiments, run in an air furnace, indicated a general trend for bubbler and baffle that the velocity of cooling water plays an important role in the heat transfer between cooling water and the inner wall of the specimen. However, this is not directly applicable to the die-casting industry, due to the low heat transfer coefficient for interface of air and solid and the steady state condition. The purpose of the dip in and out experiment was to simulate the thermal shock that the die inserts withstand from the injection of molten metal, based on the principle of relative motion.

3.5.1 1" Immersion Depth

In order to simulate the "hot spot" existing at the tip of an insert, the immersion depth of the specimen was kept as 1". First, the specimen was tested without cooling water and the mean peak temperature calculated from the bottom temperature, measured at quasi-steady-state, was 1312°F. Then three bubblers, who's I.D. are 0.17", 0.214" and 0.307" respectively, were used to cool the specimen internally in the experiment. The comparison of specimen surface temperature with and without water-cooling is shown in Figure 49, which indicates how effectively the water cooling to the specimen bottom temperature. Figure 50 shows the comparison of average peak temperatures with respect to three bubblers. Then according to equation (3-4), the flow rate of the cooling water and the inner section area of the bubbler can be used to determine the water jet velocity. Figure 51 shows the effect of the jet velocity of cooling water on the average peak temperature of specimen bottom.
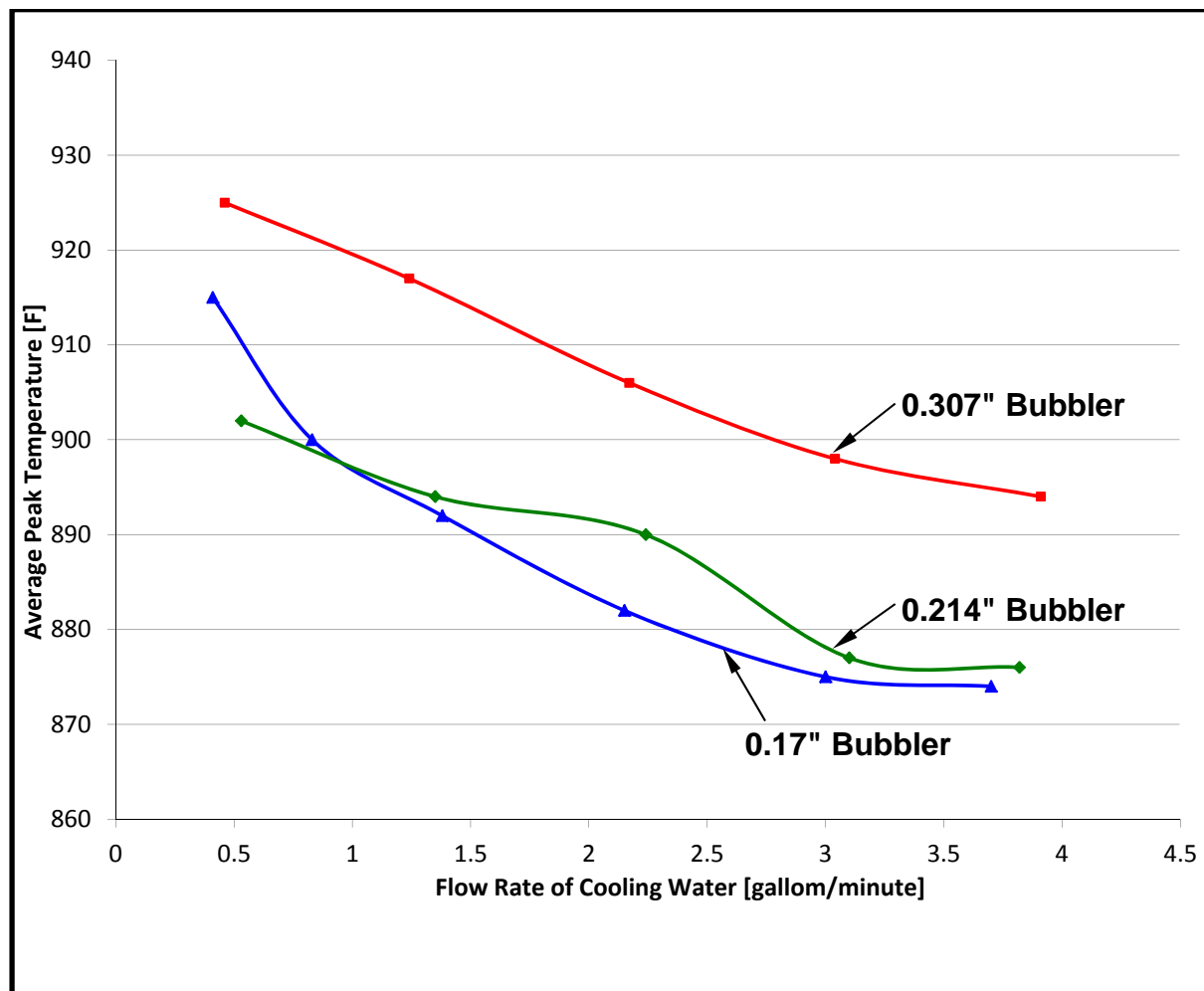
Figure 49 Specimen Bottom Temperature-Flow Rate of Cooling Water for 1" Immersion Depth
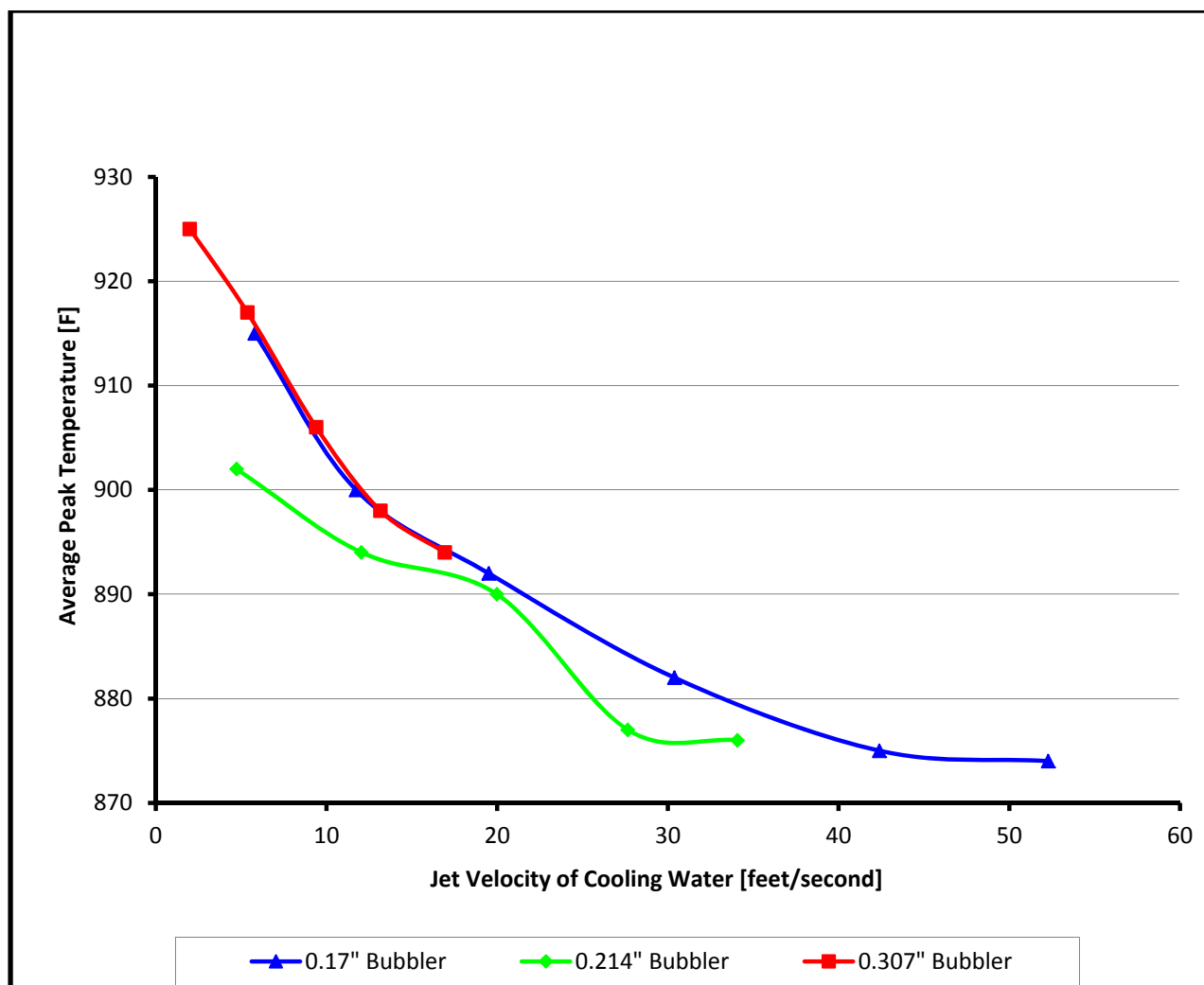
**Figure 50 Effect of Jet Velocity of Cooling Velocity on Peak Temperature of Specimen Bottom for 1"
Immersion**
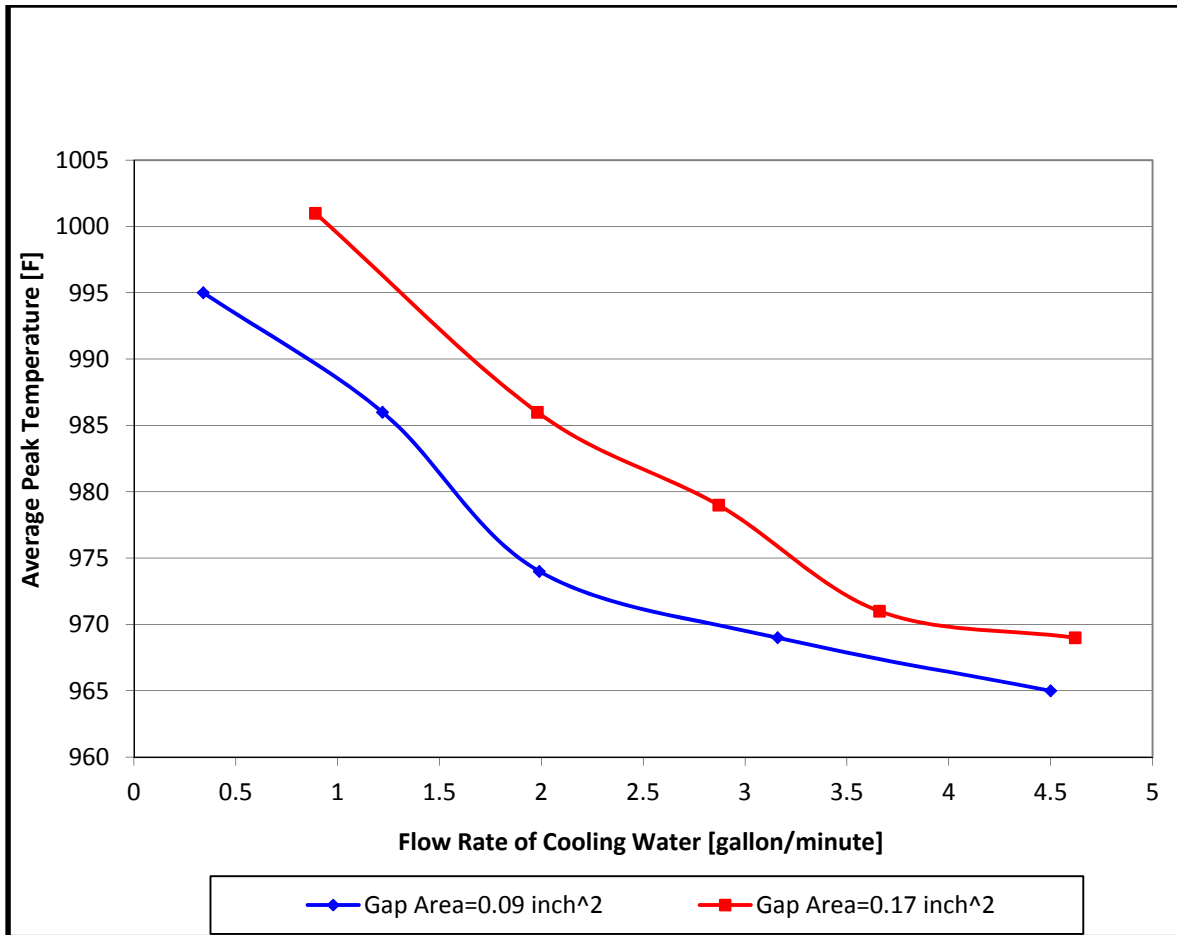
Figure 51 Effect of Gap Area on Specimen Bottom Average Peak Temperature for 1" Immersion

Some research was carried out regarding the failures of die casting die inserts, which initiated at the internal cooling line surface. The results show that repetitive vapor blanketing occurred within the cooling line. When an insulating vapor film covers the surface through which the heat must pass, the heat transfer coefficient is orders of magnitude lower than in the corresponding region before the critical heat flux was exceeded, due mainly to the lower thermal conductivity of the vapor. In this experiment, the vapor blanket is believed to form at the bottom of cooling line, which is close to the "hot spot". As mentioned before, for the smallest bubbler (I.D.=0.17"), the cooling water impinges against the bottom of the cooling line with high velocity. The impingement is believed to contribute to breaking away the vapor blanket. At the same time, the higher local velocity of cooling water at the interface of water and sidewall contributes to a decrease in the thickness of the vapor blanket, which in turn enhances the local heat transfer at the interface.

Two baffles with different lengths, which formed different gap areas, were also used to cool the specimen internally in the experiment. The results are shown in Figure 52 and Figure 53, with respect to the flow rate and the average velocity through the gap respectively. The figures demonstrate the same trend as the results of the experiments run in the air furnace, although the temperature differences in the figures are relatively small.
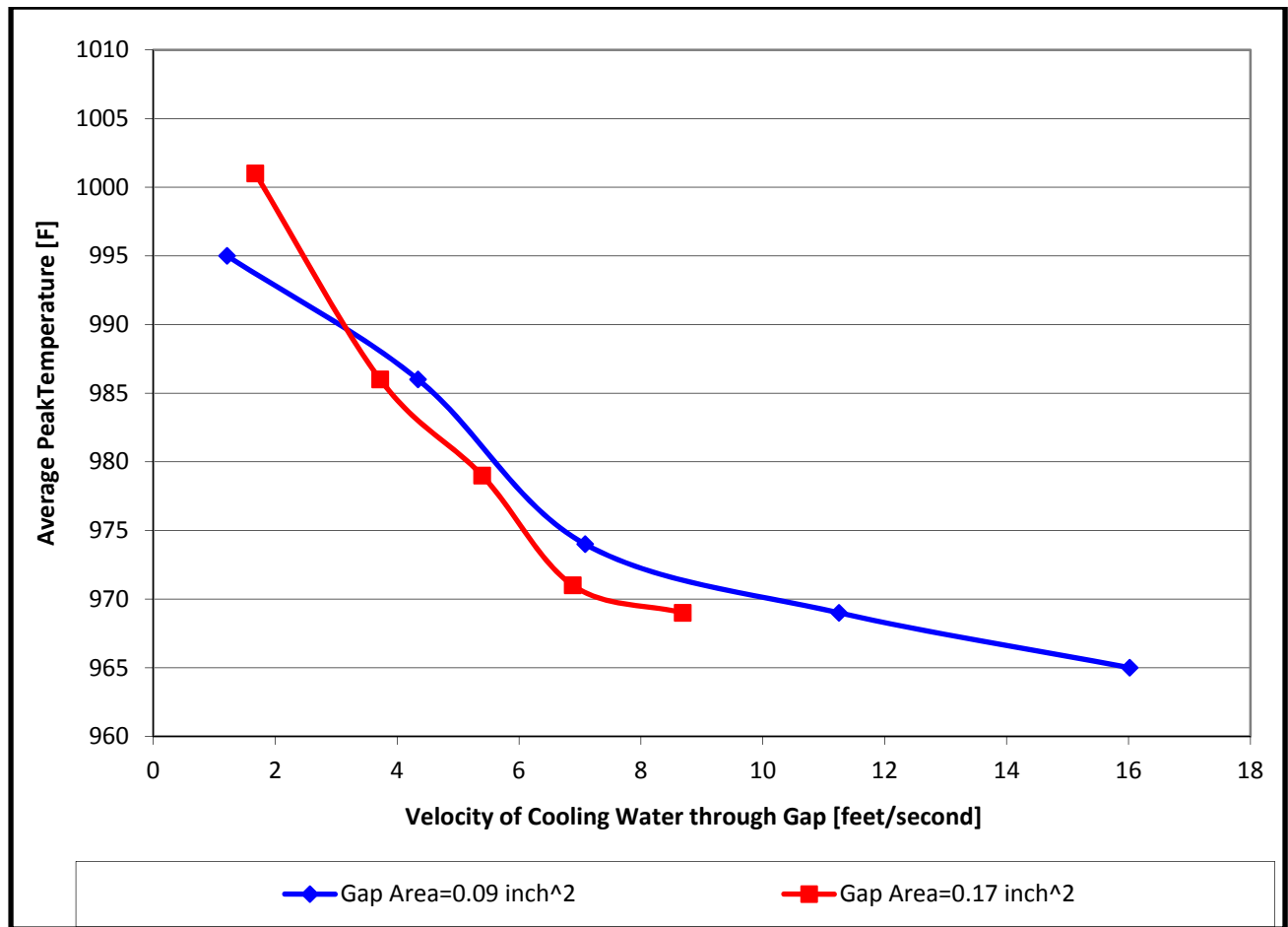
Figure 52 Specimen Bottom Average Temperature-Velocity of Cooling Water through Gap
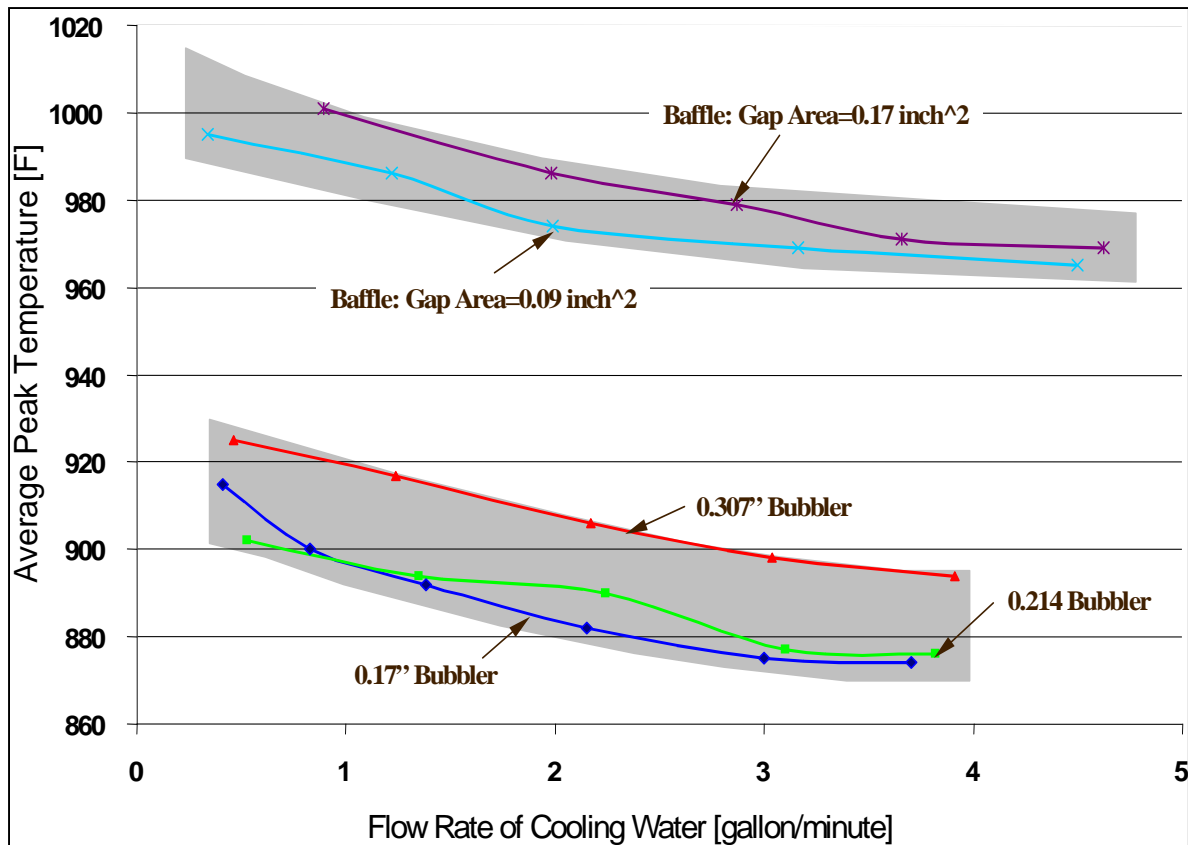
Figure 53 Cooling Effects of Bubblers and Baffles on "Hot Spot"

Both bubblers and baffles were used to cool the "hot spot" formed by 1" immersion into molten aluminum. Bubblers and Baffles have different performance, which is reflected by the specimen bottom average temperature, because of different flow patterns of the cooling water directed by bubblers and baffles. The comparison of the cooling effects of bubblers and baffles are shown in Figure 54, which indicates clearly that for the "hot spot", bubblers have better cooling performance than baffle.
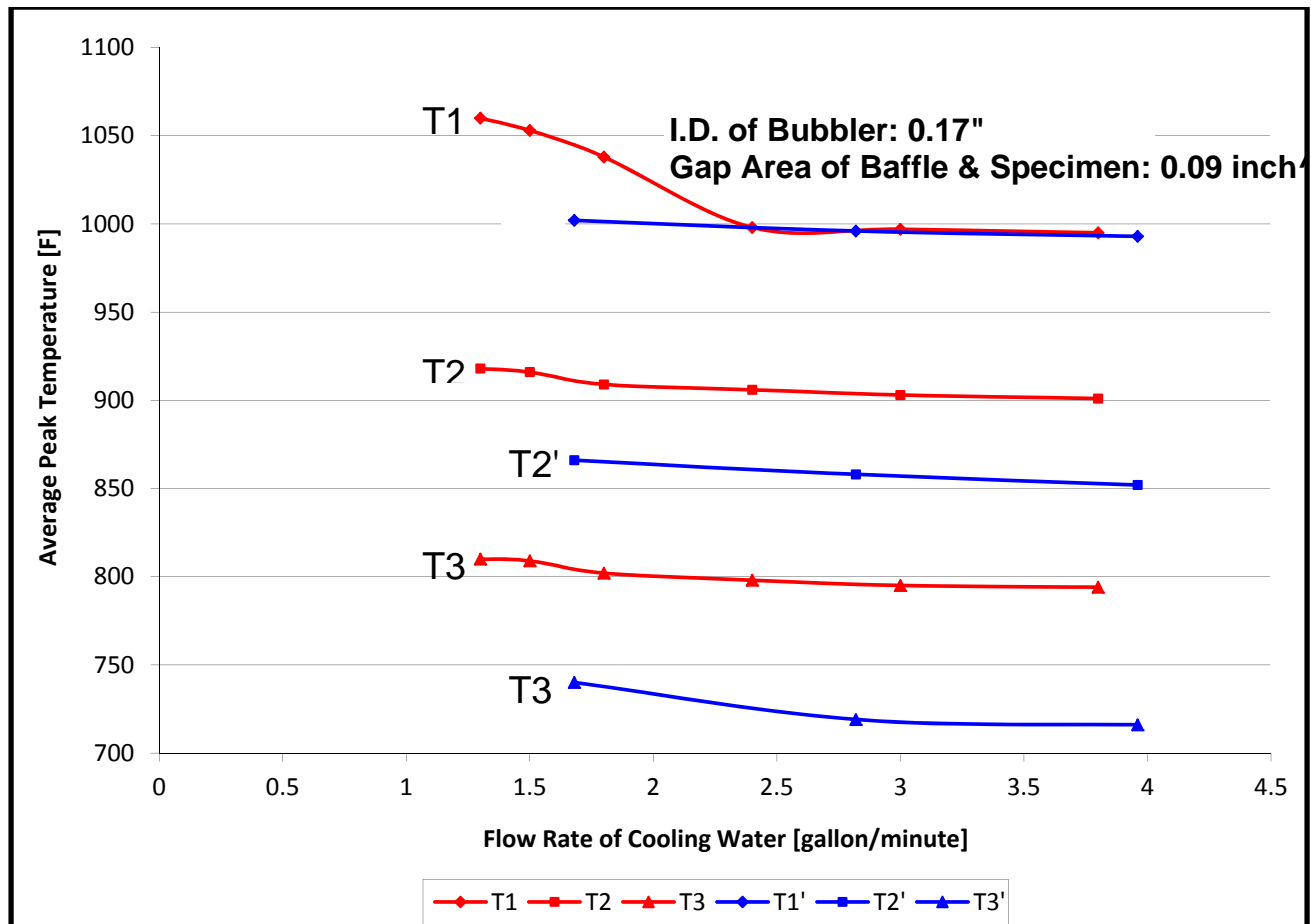
Figure 54 Cooling Effect of Bubbler and Baffle for 4.5" Immersion Depth

Also, attention should be paid to the higher pressure loss, caused by a smaller cross sectional area through which cooling water flows when several cooling lines are connected in series. The higher pressure loss will impose a limit for extending the trend.

3.5.2 .5" Immersion Depth

In order to evaluate the cooling effect of the bubbler and the baffle, the immersion depth of the specimen was increased to 4.5". Three temperatures, T1, T2 and T3, were measured at specified positions at different flow rates of cooling water. The result is shown in Figure 55, which indicates that for the sidewall of the specimen, a baffle has a better cooling effect than a bubbler.

Figure 55 H13 pins before coating

Because of the different configurations, the bubbler and baffle induced different flow patterns of cooling water and different velocity distribution of cooling water inside the cooling line. Table 6 lists velocities of cooling water directed by the bubbler and the baffle at different flow rates. It is evident that for a given flow rate, the velocity of baffle-directed cooling water flowing along the sidewall of the specimen was about 2 times higher than that of bubbler-directed water flowing along the sidewall of the specimen. A higher velocity of cooling water contributes to reduce the thickness of boundary layer, which accounts partially for the better cooling effect of the baffle than of the bubbler.

Table 6 Comparison of Cooling Water Velocity for Dip In/Out Experiment with 4.5" Immersion

Flow Rate Reynolds Number	2.0 gallon/minute	3.0 gallon/minute	4.0 gallon/minute
Approximate Average Water Temp.	90 ˚F	80 ˚F	70 ˚F
ν [feet^2/hour]	0.029	0.033	0.038
Re^{Bub} for 0.17" Bubbler	10.3×10^3	13.6×10^3	15.8×10^3
Re^{Baf}	18.4×10^3	24.2×10^3	28.1×10^3

Another reason is that baffle-directed cooling water has different turbulence along the sidewall of specimen with that of bubbler-directed cooling water flowing through the annulus channel, even though the average velocities are same. The turbulence of fluid is reflected by the Reynolds number. For turbulent flow in smooth noncircular pipe, equation (1-9) can be used to predict heat transfer coefficient, provided that the pipe diameter D is replaced by the equivalent diameter D_{eq}, defined by equation (1-10). Therefore, for baffle directed cooling water, the equivalent diameter D_{eq}^{Baf} can be figured out as:

$$D_{eq}^{Baf} = \frac{4 \times \frac{1}{2} \times \frac{1}{4}\pi \cdot D^2}{D + \frac{1}{2}\pi \cdot D} = \frac{\pi}{\pi + 2} \cdot D$$

(3-10)

where D is the inner diameter of cooling line. While for bubbler directed cooling water, the equivalent diameter D_{eq}^{Bub} can be figured out as:

$$D_{eq}^{Bub} = \frac{4 \times \pi \cdot \left(D^2 - d_o^2\right)}{\pi \cdot \left(D + d_o\right)} = D - d_o$$

(3-11)

where d_o is the O.D. of bubbler. Correspondingly, the Reynolds numbers for baffle directed cooling water, Re^{Baf}, and bubbler directed cooling water, Re^{Bub}, can be figured out respectively as following:

$$\mathrm{Re}^{Baf} = \frac{\overline{V} \cdot D_{eq}^{Baf}}{v} = \frac{Q \cdot D_{eq}^{Baf}}{A \cdot v} = \frac{Q \cdot \left(\dfrac{\pi}{\pi+2}\right)D}{\dfrac{1}{2} \times \dfrac{1}{4}\pi \cdot D^2 \cdot v} \approx 2.77\frac{Q}{v}$$

$$\mathrm{Re}^{Bub} = \frac{\overline{V} \cdot D_{eq}^{Bub}}{v} = \frac{Q \cdot D_{eq}^{Bub}}{A \cdot v} = \frac{Q \cdot \left(D - d_o\right)}{\dfrac{1}{4}\pi \cdot \left(D^2 - d_o^2\right) \cdot v} \approx 1.56\frac{Q}{v}$$

where D gets the value of 9/16" and d_o gets the value of 0.25". Table 7 lists the values of Re^{Baf} and Re^{Bub} at given cooling water flow rate. At the same flow rate, Re^{Baf} has a bigger value than that of Re^{Bub}, which enhances the heat transfer between baffle-directed cooling and the side-wall of the cooling line.

Table 7 Comparison of Re^{Bub} and Re^{Baf} of Cooling Water at Given Flow Rate

I.D. of Bubbler [inch]	0.170	0.214	0.307
Inner Section Area of Bubbler [inch^2]	0.023	0.036	0.074
Jet Velocity of Cooling Water at the Flow Rate of 1 gallon/minute [Feet/Second]	14.0	8.9	4.3

3.6 The Effect of Die Lubricants and Additives on Soldering

Experiments were carried out to evaluate the effectiveness of a range of die lubricants and die lubricant ingredients tabulated in Table 8, in preventing soldering of aluminum to H13 steels.

Table 8 List of soldering evaluation samples

Sample number #	
23	USDC-12-23
24	USDC-12-24
25	USDC-12-25
26	USDC-12-26
27	USDC-12-27
28	USDC-12-28
29	USDC-12-29
30	USDC-12-30
31	USDC-12-31
32	USDC-12-32
33	DI-H2O
34	Graphite*

35	Boron nitride*
36	No coating*

3.6.1 Procedure

- H13 steel core pins were cut into 4.5 inch long pieces (see Figure 56)
- The surface of these bars was thoroughly cleaned with alcohol.
- Each test bar was placed in a furnace, heated up to 437°C and held for 15 minutes.
- The bar was dipped into the coating suspension for 30 seconds.
- The bar was returned into the furnace for another 5 minutes at 437°C.
- The bar was dipped in the coating materials for another 30 seconds.
- Finally, the bar was placed in the furnace and held at 437°C for 10 minutes.
- The test bar is attached to the end of a sample holder (Figure 57).

Figure 56 Sample holder for rotating pin experiment
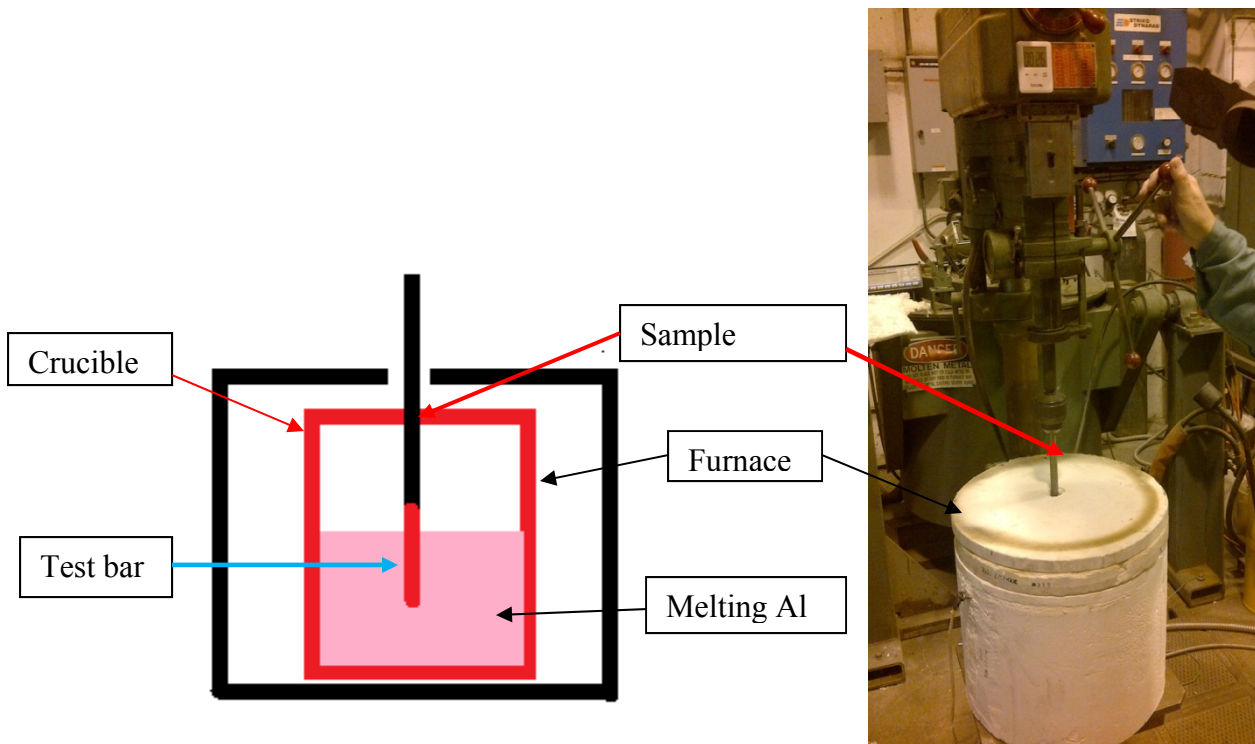
Figure 57 Experimental set-up for rotating pin experiment

The exposed samples are shown in Figures 58-71. Three samples, 34 (coated with graphite), 35 (coated with boron nitride), 36 (uncoated), were added as benchmarks. The perimeter of the samples was divided into four quadrants. Each quadrant 0-90, 90-180, 180-270 and 270-360 is shown separately. The two benchmark samples 34, 35 coated with graphite and BN show no soldering. The uncoated sample shows extensive soldering. The samples coated with Chemtrend die lubricants and additives show varying degrees of soldering: #24 shows no soldering, Sample#29 shows some. #27, 30, and 33 more but not complete soldering. The rest of the samples, including the control, uncoated #35 show complete soldering. No attempt has been made so far to measure how adherent the aluminum layer is to the substrate.

0-90°	
90°-180°	
180°-270°	
270°-360°	
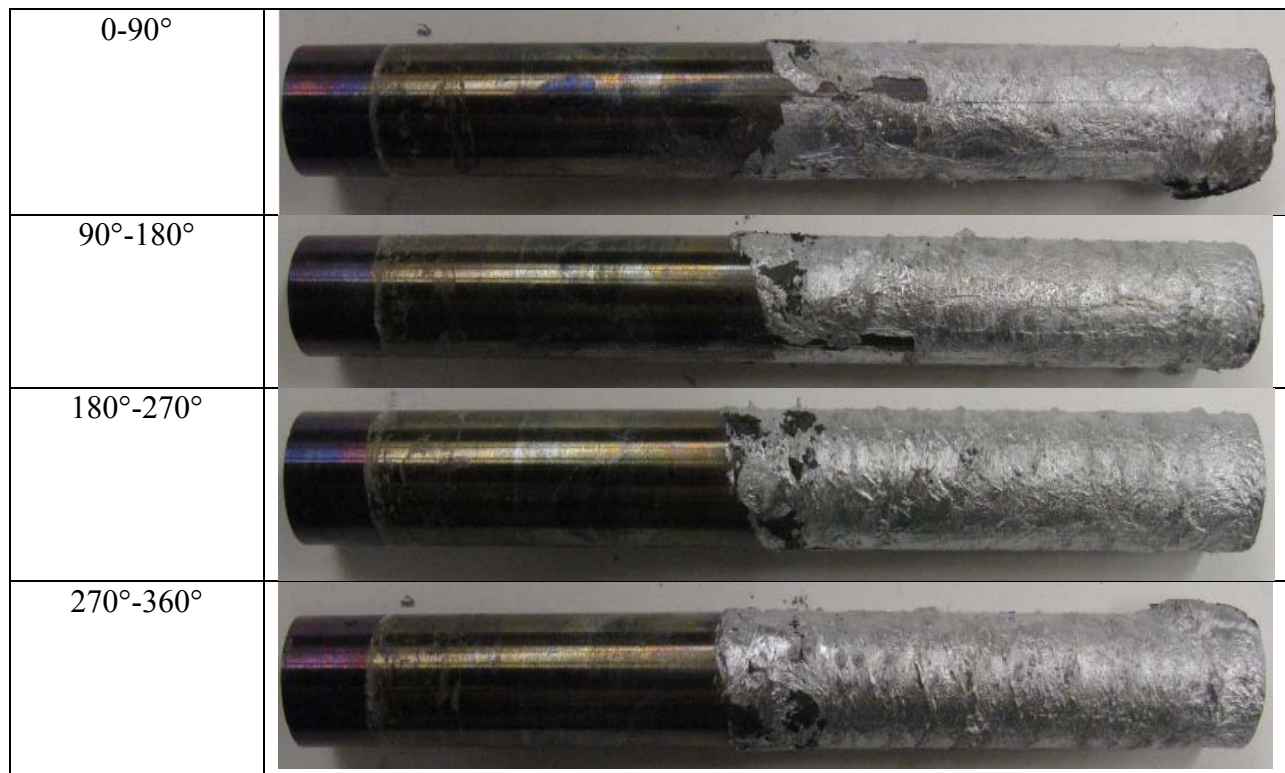
Figure 58 Sample after rotating pin testing (#23)

0-90°	
90°-180°	
180°-270°	
270°-360°	
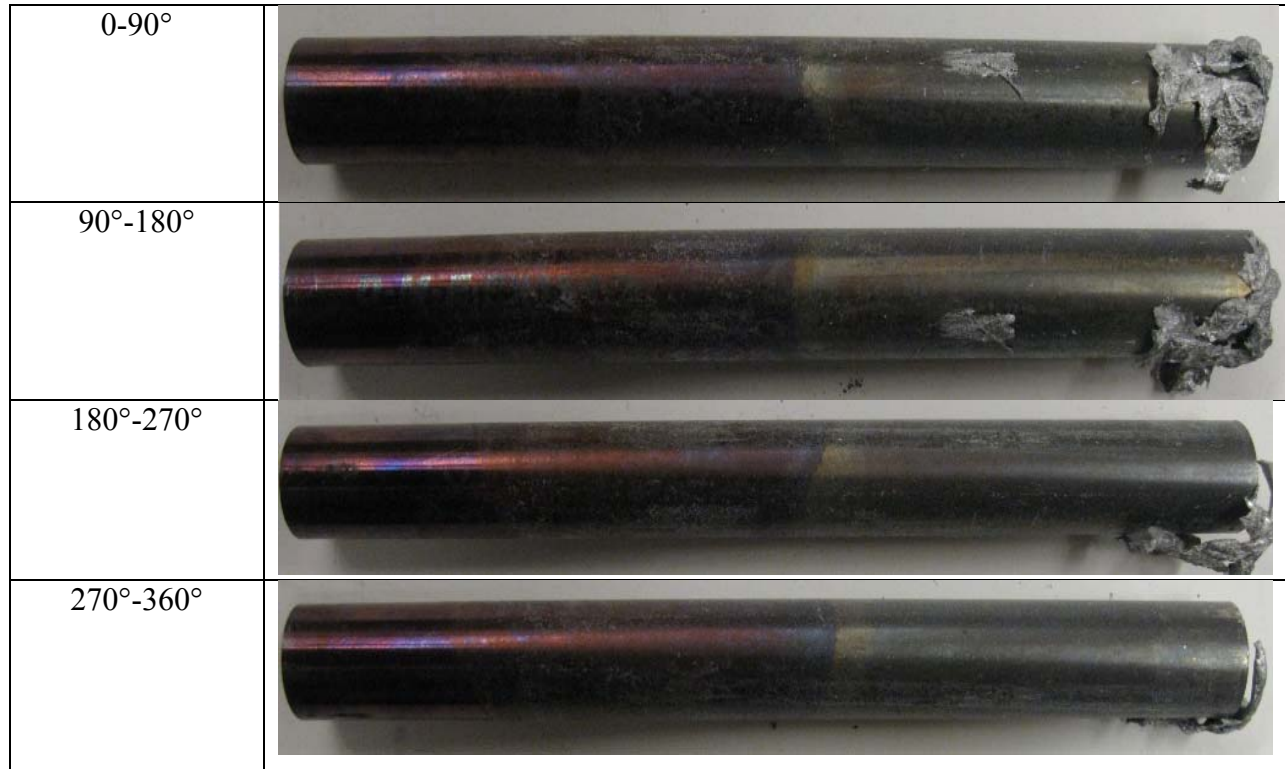
Figure 59 Sample after testing (#24)
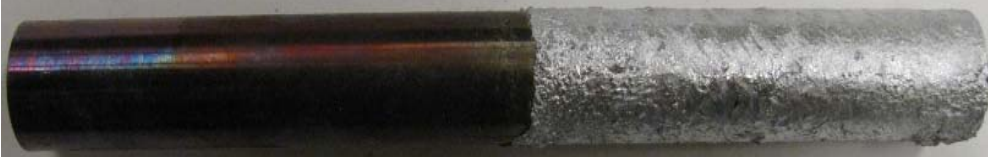
0-90°	
90°-180°	
180°-270°	
270°-360°	

Figure 60 Sample after testing (#25)

0-90°	
90°-180°	
180°-270°	
270°-360°	

Figure 61 Sample after testing (#26)

0-90°	
90°-180°	
180°-270°	
270°-360°	

Figure 62 Sample after testing (#27)
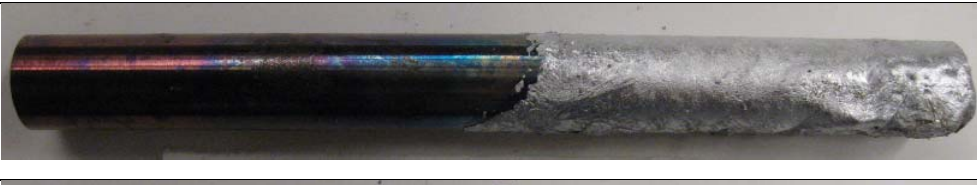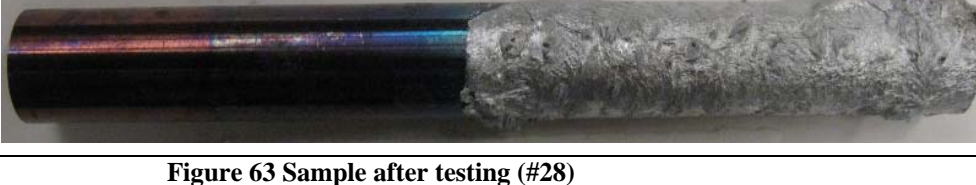
0-90°	
90°-180°	
180°-270°	
270°-360°	

Figure 63 Sample after testing (#28)

0-90°	
90°-180°	
180°-270°	
270°-360°	

Figure 64 Sample after testing (#29)

0-90°	
90°-180°	
180°-270°	
270°-360°	

Figure 65 Sample after testing (#30)

0-90°	
90°-180°	
180°-270°	
270°-360°	

Figure 66 Sample after testing (#31)

0-90°	
90°-180°	
180°-270°	
270°-360°	

Figure 67 Sample after testing (#32)

0-90°	
90°-180°	
180°-270°	
270°-360°	

Figure 68 Sample after testing (#33)

0-90°	
90°-180°	
180°-270°	
270°-360°	

Figure 69 Sample after testing (#34)

0-90°	
90°-180°	
180°-270°	
270°-360°	

Figure 70 Sample after testing (#35)

0-90°	
90°-180°	
180°-270°	
270°-360°	

Figure 71 Sample after testing (#36)

4. Benefits Assessment

In addition to improved part quality and higher production rates, improving die casting processes to preserve the life of the inserts will result in energy savings and a reduction in environmental

wastes. Improving die life by means of optimized cooling line placement, baffles and bubblers in the die will allow for reduced die temperatures during processing, saving energy associated with production. The utilization of optimized die lubricants will also reduce heat requirements in addition to reducing waste associated with soldering and washout.

This new technology was predicted to result in an average energy savings of 1.1 trillion BTU's/year over a 10 year period. Current (2012) annual energy saving estimates, based on commercial introduction in 2010, a market penetration of 70% by 2020 is 1.26 trillion BTU's/year.

Along with these energy savings, reduction of scrap and improvement in casting yield will result in a reduction of the environmental emissions associated with the melting and pouring of the metal which will be saved as a result of this technology. The average annual estimate of CO_2 reduction per year through 2020 is 0.025 Million Metric Tons of Carbon Equivalent (MM TCE).

5. Commercialization

Die casting is a conservative and risk adverse industry that expects compelling evidence before applying experimental research findings to production. This risk adversity is understandable when considering the high cost of a prematurely failed tool. Not only is the high cost of a new tool at stake, sometime in the hundreds of thousands of dollars, but also the costly downtime associated with replacing the dies.

This being said, findings of this study have been incorporated in tooling design at multiple die casting outfits. For example, St. Clair Die Casting has build Dievar inserts for die casting heat sinks for tank tracks. The cooling lines in these inserts have been moved from 0.75" to 0.5" from the cavity, to facilitate shorter cycle time and longer die life. Dievar is a modified H11 steel with superior Charpy V-notch toughness of over 20 ft*lb at room temperature. These inserts lasted over 200,000 shots, compared to 50,000 shots for standard H13 inserts. The cycle time was shortened by 12% from 57 seconds to 50 seconds. Empire Die Casting has modified bubblers to reach as close as 0.25" from the surface of cores, thus lowering the surface temperature enough to eliminate soldering issues with this application. More applications are underway at General Metal Die Casters and Twin City Die Casting.

The results of this project were also incorporated into the North American Die Casting Association (NADCA) website. This was accomplished through the development of an electronic tool incorporating the design guidance for the placement of cooling lines within dies. The dissemination and use of the tool, as well as direct support from NADCA, has assisted in the rapid deployment of the results developed under this project into industry.

6. Accomplishments

This research demonstrates the potential for significant improvements in the productivity of the die casting process. The fundamental premise tested and proven by the study is that softening of the die surface is the primary mechanism that leads to thermal fatigue cracking. Understanding the relationship between softening, strength, toughness and thermal fatigue allows the die caster to make good decisions in maximizing die life and increasing productivity.

Softening occurs when the sample is exposed to excessive temperature, and is accelerated in the presence of high stresses. Lowering the maximum surface temperature can slow the softening process and delay or eliminate thermal fatigue damage. For this reason, dies used in die casting magnesium or zinc last much longer than equivalent dies used in die casting aluminum alloys.

For the same reason, samples with cooling lines placed closer to the surface show less thermal fatigue cracking. This finding was clearly demonstrated in the study and has important practical implications.

Another accomplishment of the project is the design of an experimental set-up for the evaluation of die lubricants. This setup allows will compare soldering resistance of commercial die lubricants to graphite and boron nitride coatings in a closely controlled environment.

7. Conclusions

1) In the context of thermal fatigue damage, softening of the steel is the most important factor in the crack initiation. Less thermal fatigue damage has been observed when the conditions promoted lower temperature at the surface, which preserved the hardness and hence the strength of the die steel. A high value of yield strength means higher material resistance to plastic deformation. At the same time, elevated temperature at the surface will induce a deeper softening. It appears that a condition for the extension of the thermal fatigue cracking damage is the decrease in strength ahead the crack front.

2) In die-casting applications, the highest maximum temperature will occur in thin sections where the material capacity to absorb and transfer the heat from the surface is very different. From another point of view, high temperature - long resident time conditions are important, because of the similarity with the die casting of large components, when the die is subjected to elevated temperature for longer periods of time. The experimental results have shown an important decrease of the cracking when the cooling line is positioned closer to the surface. Moreover, the experimental data indicates the existence of a temperature threshold, below which the thermal fatigue damage is minimal. A cooling line closer to the surface will shift the maximum temperature towards lower values, and keep at the same time the stresses at a relative constant value. However, decreasing the maximum temperature at the surface by placing the cooling lines too close to the surface may be limited by the high level of hoop stresses created at the cooling line.

3) The use of a bubbler or a baffle to direct cooling water flowing through a cooling line can effectively lower the surface temperature of a core of the die, where a drilled waterline circuit is not possible because of the confinement of the space available and the fabrication.

4) To select the proper cooling mode for a given hot section to be cooled, a baffle is suitable to cool a certain area, while a bubbler is suitable to cool a specific spot, the so-called "hot spot".

5) For a given core and given cooling mode, higher flow rate has a better cooling effect, and the core has a lower surface temperature during thermal shock.

6) For a given cooling line, to some extent, the bubbler with smaller I.D. has a better cooling effect to "hot spot" than a bubbler with a larger I.D.

7) At same flow rate of cooling water, high velocity of cooling water enhances the heat transfer between the cooling water and the sidewall of a cooling line. For design and application, it is preferable to set up a high velocity of cooling water in a cooling line in order to prolong the service life of the core.

8) Graphite and Boron Nitride coatings are very effective in preventing soldering. Some commercial water-based lubricants are just as effective in preventing soldering.

8. Recommendations

- When using superior die steels with high toughness, cooling lines can be placed closer to the cavity surface. Depending on the configuration, cooling lines can be drilled as close as 0.5" from the cavity. Such a change in design should be implemented gradually, to ensure the increase in temperature gradients and respective thermal stresses is acceptable.
- In cases where cooling lines are drilled closer to the surface, the hardness of the tooling should be kept in the 44-46HRC range to lower the risk of gross cracking.
- Bubblers and baffles can also be drilled closer to the surface when high toughness superior steels are utilized. As with cooling lines, the hardness of the tooling should be kept in the 44-46HRC range.
- Well formulated water-based die lubricants can effectively eliminate or significantly reduce soldering. While environmentally objectionable, graphite base die lubricants provide excellent protection from soldering. Same is true for boron nitride. Such die lubricants can be used to establish a baseline for desired die lubricant protection.

9. Bibliography

1. Yan, M.; Fan, Z. "Durability of Materials in Molten Aluminum Alloys", Journal of Materials Science 36 (2001)
2. Stern, M. Die-Casting Practice, McGraw-Hill Book Company (1930)
3. Kaye, A. Die Casting Metallurgy, Butterworth Scientific (1978)
4. Wang, Y. Effect of Composition and Processing on the Thermal Fatigue and Toughness of High Performance Die Steels, Ph.D. Thesis, Case Western Reserve University (1997)
5. Failure Analysis and Prevention, ASM Handbook Vol. 11, 9th Edition, American Society for Materials Publications, pp. 266-267
6. Bertolo, R.B. Fracture Toughness of Aluminum Die Casting Die Steels, Ph.D. Thesis, Case Western Reserve University, 1976
7. Toyoda, H. et al. "Thermal Fatigue Properties and Their Evaluation", Transactions ISIJ 25 (1985)
8. Dieter, G. Mechanical Metallurgy, McGraw-Hill (1986), pp. 430
9. Zuchovski, R. "Analysis of the Thermal Fatigue Process", Journal of Materials Testing and Technology 106 (2000)
10. , R.P. "Introduction to Thermal Shock", High Temperature Technology 8 No. 2 (1990)
11. Zhou, Q. Master Thesis, Case Western Reserve University (2001)
12. Wallace, J.F. "Thermal Conditions in the Die", Foundry 96 (1968) [12]
13. Seth, B.B. "A Review of Die Casting Dies", Die Casting Engineer 16 (1972)
14. Bethge, K.; Munz, D.; Neumann, J. "Crack Initiation and Propagation Under Thermal Cyclic Loading", High Temperature Technology Vol. 8 No. 2 (1990)
15. Graham, R.R. Thermal Fatigue Mechanisms in Aluminum Die Casting Die Steel, Ph.D. Thesis, Case Western Reserve University (1978)
16. Das, S. K. Effect of Heat Treatment on the Thermal Fatigue Behavior and Fatigue Toughness of H13 Steel for Aluminum Die Casting Dies, Ph.D. Thesis, Case Western Reserve University (1981)
17. Sharp, H.J. "Aluminum Pressure Die Casting Dies-Their Failure by Surface Cracking", Metal Industry 51 (1953)
18. Roberts, G.A.; Grobe, A.H. "Service Failure of Aluminum Die Casting Dies", Metal Progress, 69 (1956)

19. Lu, T.J.; Fleck, N.A. "The Thermal Shock Resistance of Solids", Acta Materialia, Vol. 46, No. 13 (1998)
20. Manson, S.S. Thermal Stress and Low Cycle Fatigue, McGraw-Hill (1966), pp. 21-22, 303
21. Campbell, I.E. (Editor- in-Chief) High Temperature Technology, John Wiley and Sons (1957), pp. 460-476
22. Weronski, A.; Hejwowski, T. Thermal Fatigue of Metals, Marcel Dekker, Inc. (1991), pp.118-124
23. Birceanu, S. Master Thesis, Case Western Reserve University (2002)
24. Smith, W.E. Design and fabrication of quality die cast dies
25. Kaye A.; Street A. Die Casting Metallurgy, p256
26. DME Technical Catalog
27. Street A. The Die Casting Book, Portcullis Press Ltd. (1977), pp. 311-312
28. Brown, A.I.; Marco, S.M. Introduction to Heat Transfer, Third Edition,McGraw-Hill Book Company, Inc. (1958), pp. 125-133
29. Haupin, W "Understanding Boundarylayers", Light Metals 1997, 126th TMS Annual Meeting (1997)
30. Truelove, R.L. "Die Casting Temperature Control: A New Science", Die Casting Engineer, Vol. 26, No.1 (1982), pp. 28-31
31. Flynn, E.W.; Berger, C.M. "Corrosion fatigue: an anatomy of die-cast die insert failure", .Modern Casting, March (2001), pp.46-49
32. Collier, J.G. Convective Boiling and Condensation, 2nd Edition, McGraw-Hill International Book Company (1981), p.139
33. Fletcher, A.J.; Griffiths, W.D. "Heat Transfer during Vapour Blanket Stage of Quench", Materials Science and Technology, Vol.9 (1993), pp. 958-96
34. Fletcher, A.J.; Griffiths, W.D. "Heat Transfer during Vapour Blanket Stage of Quench", Materials Science and Technology, Vol.9 (1993), pp. 958-96
35. Fletcher, A.J.; Griffiths, W.D. "Heat Transfer during Vapour Blanket Stage of Quench", Materials Science and Technology, Vol.9 (1993), pp. 958-962
36. Minhas H.; Lock G.S.H. "Estimating the Influence of Prandtl Number on Heat Transfer in A Bayonet Tube", Int. Comm. Heat Mass Transfer, Vol. 23, No. 7 (1996), pp1011-1017
37. Li, C.H. "Analytical Solution of the Heat Transfer Equation for a Bayonet Tube Heat Exchanger"
38. Levenspiel, O. Engineering Flow and Heat Exchange, Revised Edition, pp. 272-274